AD-A072 740 NAVAL POSTGRADUATE SCHOOL MONTEREY CA F/G 8/3
AN INVESTIGATION INTO THE USE OF CEPSTRAL ANALYSIS IN THE DECOM--ETC(U)
APR 78 D E MORRIS

UNCLASSIFIED NL

1 OF 2
ADA 072740

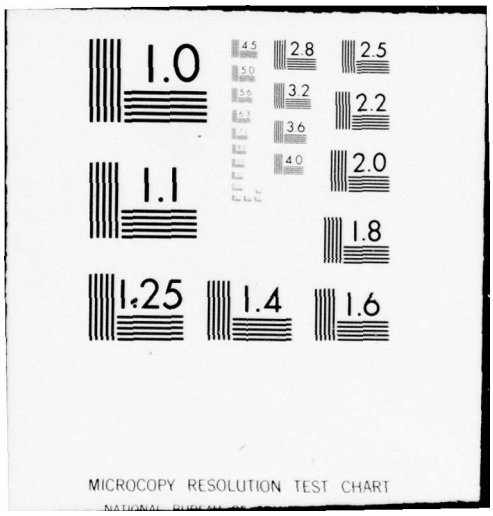
1.0
1.1
1.25
1.4
1.6
1.8
2.0
2.2
2.5
2.8
3.2
3.6
4.0
4.5
5.0
5.6
MICROCOPY RESOLUTION TEST CHART

SECURITY CLASSIFICATION OF THIS PAGE (When Data Entered)

REPORT DOCUMENTATION PAGE

READ INSTRUCTIONS BEFORE COMPLETING FORM

1. REPORT NUMBER	2. GOVT ACCESSION NO. / 3. RECIPIENT'S CATALOG NUMBER
4. TITLE (and Subtitle): AN INVESTIGATION INTO THE USE OF CEPSTRAL ANALYSIS IN THE DECOMPOSITION OF OCEAN WAVES.	5. TYPE OF REPORT & PERIOD COVERED: THESIS
	6. PERFORMING ORG. REPORT NUMBER
7. AUTHOR(s): MORRIS, DONALD EDWARD / Morris	8. CONTRACT OR GRANT NUMBER(s): Master's thesis
9. PERFORMING ORGANIZATION NAME AND ADDRESS: UNIVERSITY OF WASHINGTON, SEATTLE, WA	10. PROGRAM ELEMENT, PROJECT, TASK AREA & WORK UNIT NUMBERS
11. CONTROLLING OFFICE NAME AND ADDRESS: Code 031 NAVAL POSTGRADUATE SCHOOL MONTEREY, CALIFORNIA, 93940	12. REPORT DATE: APR 78
	13. NUMBER OF PAGES: 113
14. MONITORING AGENCY NAME & ADDRESS(if different from Controlling Office)	15. SECURITY CLASS. (of this report): UNCLASS
	15a. DECLASSIFICATION/ DOWNGRADING SCHEDULE

16. DISTRIBUTION STATEMENT (of this Report)

APPROVED FOR PUBLIC RELEASE; DISTRIBUTION UNLIMITED

12 126p.

17. DISTRIBUTION STATEMENT (of the abstract entered in Block 20, if different from Report)

18. SUPPLEMENTARY NOTES

19. KEY WORDS (Continue on reverse side if necessary and identify by block number)

CEPSTRAL ANALYSIS; OCEAN WAVES; DECOMPOSITION OF OCEAN WAVES.

20. ABSTRACT (Continue on reverse side if necessary and identify by block number)

NONE

251450 gn

DD FORM 1 JAN 73 1473 (Page 1)

EDITION OF 1 NOV 65 IS OBSOLETE S/N 0102-014-6601

UNCLASS

SECURITY CLASSIFICATION OF THIS PAGE (When Data Entered)

AN INVESTIGATION INTO THE USE OF CEPSTRAL ANALYSIS IN THE DECOMPOSITION OF OCEAN WAVES

BY

DONALD EDWARD MORRIS

A thesis submitted in partial fulfillment
of the requirements for the degree of

Master of Science in Civil Engineering

University of Washington

1978

Approved by (original copies signed by Prof. E. F. Richey)
(Chairman of Supervisory Committee)

Program Authorized
to Offer Degree Civil Engineering

Date 5 April 78

In presenting this thesis in partial fulfillment of the requirements for a Master's degree at the University of Washington, I agree that the Library shall make its copies freely available for inspection. I further agree that extensive copying of this thesis is allowable only for scholarly purposes. It is understood, however, that any copying or publication of this thesis for commercial purposes, or for financial gain, shall not be allowed without my written permission.

Signature Donald Edward Morris

Date 5 April 78

TABLE OF CONTENTS

LIST OF FIGURES

LIST OF SYMBOLS

SYMBOL	
f	frequency, in Hz
f_m	mid-frequencies of equal-area increments of P-M spectral model
f_p	frequency of spectral peak in P-M spectral model
h	incremental count of sampled data points in digital frequency series
m	incremental count of sinusoidal wave forms summed together to produce simulated ocean wave
M	Total number of sinusoidal wave shapes summed together to produce simulated ocean wave
n	incremental count of sampled data points in digital time series
N	Total number of sampled data points in a digital time series
$S(f)$	P-M spectral model amplitudes as a function of frequency
$S(f_p)$	P-M spectral model peak amplitude
t	time, in seconds
U	wind speed
x	distance
$x(n)$	value of data point in digital time series identified by incremental sample count
$x(t)$	value of time series data identified by elapsed time, t
$x_{PC}(t)$	value of power cepstrum of incident wave identified by elapsed time, t
$\hat{x}(t)$	value of complex cepstrum of incident wave identified by elapsed time, t
$X(f)$	Fourier transform value of time series data identified by frequency count
$X(h)$	value of data point in digital frequency series identified by incremental sample count

SYMBOL	
$X(s)$	Laplace transform value of time series data
$X(z)$	Z-transform value of time series data
$\|X(f)\|$	Amplitude value of Fourier transform of incident wave time series data, identified by frequency count
$\|X(f)\|^2$	Power Spectrum value of incident wave data identified by frequency count
$\hat{y}(n)$	value of complex cepstrum of combined incident/reflected wave identified by incremental sample count, represents positive portion of the continuous complex cepstrum
$\hat{y}(-n)$	value of complex cepstrum of combined incident/reflected wave identified by negative incremental sample count, represents negative portion of the continuous complex cepstrum
$y_{PC}(n)$	value of power cepstrum of combined incident/reflected wave data points identified by incremental sample count
$y_{PhC}(n)$	value of phase cepstrum of combined incident/reflected wave data points identified by incremental sample count
$y(t)$	value of combined incident/reflected wave time series data points identified by elapsed time, t
$y_{PC}(t)$	value of combined incident/reflected wave power cepstrum identified by elapsed time, t
$\hat{y}(t)$	value of combined incident/reflected wave complex cepstrum identified by elapsed time, t
$Y(f)$	Fourier transform value of combined incident/reflected wave data, identified by frequency count
$\|Y(f)\|$	Amplitude value of Fourier transform of combined incident/reflected wave time series data, identified by frequency count
$\|Y(f)\|^2$	Power Spectrum value of combined incident/reflected wave data, identified by frequency count
α	reflection coefficient in P-M spectral model, represents an empirical constant for fully arisen seas and a calculated value for limited fetch conditions

SYMBOL	
α_1	reflection coefficient for first of two incident/reflected wave combinations where more than one reflection is present
α_2	reflection coefficient for second of two incident/reflected wave combinations where more than one reflection is present
β	a constant in P-M spectral model for fully arisen seas, a calculated value for limited fetch conditions
δ	impulse or delta function operator
Δt	sampling rate or time between samples (sometimes written by others as T in digital time series expressions)
σ^2	variance of spectrum - represented by area under spectral curve - directly related to total energy of time series
τ	delay time between incident and reflected waves
τ_1	delay time between first of two incident/reflected wave combinations where more than one reflection is present
τ_2	delay time between second of two incident/reflected wave combinations where more than one reflection is present
ϕ	phase value of Fourier transform of time series data
ϕ_m	random phase shift value of sinusoid summed to other sinusoids to simulate ocean wave and identified by incremental count of sinusoid being computed
ω	frequency in radians, $=2\pi f$

ACKNOWLEDGEMENTS

Many individuals have inspired me throughout my work here at the University of Washington. In general, all those professors with whom I have come in contact in the Ocean Engineering program have demonstrated excellence in their respective fields and by their example have instilled in me a desire to learn. Specifically, I would like to thank Derald Christensen for his prolific guidance and advice on many questions related to time series analysis and for leading me into this specific branch of research. I would like to thank Professors Richey and Nece for assisting me prior to my arrival and throughout my stay at the University of Washington as well as offering encouragement and useful suggestions related to this work.

Most importantly, I would like to thank my wife, Gerry, and my children, Tina and Eddie, for adapting so well to my frequent absence from family activities and for their indefatigable support throughout this project. I would like to thank my parents for instilling in me at a very early age a desire to learn and for nurturing that desire throughout my growth. The fine example set by my brother, Bill, in his Master's work and his constant encouragement to do well is also greatly appreciated.

Finally, I would like to thank fellow ocean engineering students Norm, Harv, Mike, and Dave for giving both solicited and unsolicited peer group feedback related to this research and especially Bill Nelson who has prodigiously assisted me as interlocutor, advisor, instructor of diving and friend extraordinaire throughout my stay at the University of Washington.

CHAPTER I

INTRODUCTION

Many types of structures are designed for use below and/or above the surface or on the shoreline of oceans and various large inland water areas. They can be floating and/or structurally supported to withstand gravitational forces. These structures are constructed to withstand wave forces to the extent present day knowledge of water wave mechanics, standard of practice, and appropriate factor of safety allow. A criterion used in design may be the "design wave", a statistical culmination of known wave heights recorded in the area combined with an appropriate crest length which is used to compute the largest horizontal forces which the structure will be required to withstand.

An important design assumption used for many structures built to withstand water wave forces is the reflection coefficient. Defined as the ratio of the height of the wave reflected from the structure to the height of the incident wave coming in contact with the structure {1}*, it is an indicator of wave energy reflected from the structure as the square root of wave energy is directly proportional to wave height or amplitude. This reflected energy is an indicator of the direct effect the structure will have on any neighboring structure or shoreline. Combined with knowledge of the transmitted energy which passes through the structure and possible motion of the structure itself, it can be used to determine energy absorbed by the structure and forces which the structure will be required to withstand to perform properly.

*Numbers shown in brackets refer to the References listed on pp. 39-40.

Specifically, breakwaters, floating bridges, piers, wharves, and other structures designed to withstand and even modify water wave forces have a particular requirement for knowledge of reflection coefficients both in their design and for follow-up monitoring of true effects after construction is completed. Determination of reflection coefficients either from model study during design or from study of the finished structure itself is not always simple, even if the situation allows measurement of both the incident wave sea state alone and the combined reflected and incident wave sea state. These measurements are highly dependent on angle of attack of the incident wave train, local conditions (water depth, etc.), and the particular frequencies and amplitudes associated with different incident wave trains found at different times. The problem is particularly difficult when one is working with a structure such as a floating bridge where it is impossible to measure the incident wave sea state prior to its combination with reflected wave components.

Morden {2, 3}, Thornton and Calhoun {4} and others have developed deterministic approaches to computing reflection coefficients from the combined incident/reflected sea state based on linear deep water wave theory. Their methods require the use of two or more wave measurement devices in the combined wave field.

In contrast, the thrust of the current investigation is the separation of incident and reflected wave energy from the combined sea state using only one wave measurement device and cepstral analysis techniques. The present use of cepstral analysis is primarily in

seismic epicenter estimation, speech parameter estimation, photographic image enhancement, radar, sonar, and other fields where one desires separation or identification of the reflected signal from the original signal or the time of delay between the two signals. The literature contains several references to recent cepstral analysis work performed in the speech and seismic arenas but apparently no one has ever attempted application of this process to water waves.

Cepstral analysis wave recovery and decomposition techniques assume neither the reflection coefficient nor the delay time are functions of frequency. As this is not an absolutely correct assumption with water waves, it is probably understandable why this technique has not been actually attempted with water waves. However, cepstral analysis decomposition would allow determination of reflection coefficients using only one wave measurement device collecting data from the combined incident/reflected wave field. It, therefore, would be of great benefit if this method could be reliably applied with respect to ocean waves.

Chapter Two discusses very briefly some of the general mathematical concepts employed in this work and directs the reader to other references if one whishes to delve into discrete time series analysis in more detail. It by no means is an exhaustive explanation of background material but is instead a hint at what the field involves.

Chapter Three contains a description of cepstral analysis in general. Starting with a description of the power cepstrum, it

then discusses the complex cepstrum and the process of incident wave recovery. The chapter closes with limitations anticipated when applying cepstral analysis to ocean waves.

Chapters Four and Five discuss the test models used in applying cepstral analysis to simulated water waves and the results of this application. The first model is a finite summation of sinusoid signals containing random phase components keeping both delay time and reflection coefficient constant for all frequencies. The second model is the same summation of sinusoid signals as the first but the delay time of the reflected wave is allowed to vary with frequency. The third model is a summation of sinusoid signals allowing the reflection coefficient as well as the delay time of the reflected wave to vary with frequency.

Chapter Six is a brief look at some real world ocean data using cepstral analysis. A hint is given of problems remaining to be solved before this technique can be easily applied in the field.

Chapter Seven lists the conclusions from this work including recommendations for further study. Overall, the process shows promise and with more research could become a valuable tool in the decomposition of combined incident/reflected sea states.

CHAPTER II

BACKGROUND INFORMATION

The work throughout this study is based on use of the discrete Fourier Transform, specifically the FFT or Fast Fourier Transform. Reference will be made for illustrative purposes to other transform methods but all analysis was actually performed using the FFT. For a general review of the FFT and what it means and can do, the reader is referred to Bergland's article "A Guided Tour of the Fast Fourier Transform" {5}.

Although for simplicity some examples may be written in terminology more akin to continuous transform analysis, all work in this study is specifically digital time series analysis and is sometimes only possible in a sampled time series sense. Since Digital Signal Processing or Digital Time Series Analysis is an independent field of study usually couched in the realm of Electrical Engineering, strict adherence to digital analysis terminology would possibly thwart the main thrust of this paper which is to explain the cepstral analysis process in terms an engineer or scientist who is not thoroughly familiar with time series analysis may still understand. For a detailed description of the Discrete Fourier Transform, the reader is referred to Chapter 9 of Stanley {6}, Chapters 3 and 6 of Oppenheim and Schafer {7}, Chapters 6-9 of Brigham {8}, and/or Chapter 5 of Childers and Durling {9}.

All computer modeling and testing was performed using CSAP (Cepstral and Spectral Analysis Program) which was developed by the

author from TSAPC, an instructional program developed by Christensen at the University of Washington used in teaching spectral analysis. Some subroutines for CSAP were obtained from NSAP (Numerical Spectral Analysis Program) also developed by Christensen and were modified by the author as appropriate to meet the needs of this particular research. The FFT subroutine used was originally called NLOGN developed by Thompson and is described by Paniker {10}. Spectral computation is performed using this FFT subroutine and decimation by frequency. The cepstral computations were performed using a subroutine developed by the author based heavily on work presented by Skinner {11}.

Most signal processing people address cepstral analysis in the literature in terms of the Z-transform. In this study, use is made of the Fourier Transform which is exactly the same operation as computing the Z-transform on the unit circle. In brief, the Z-transform is merely a discrete version of the Laplace transform.

The Laplace transform (one-sided) can be expressed by

$$X(s) = \int_0^\infty x(t)e^{-st}dt$$

whose inverse is

$$x(t) = \frac{1}{2\pi i}\int_c X(s)e^{st}ds$$

It can be seen that if $s = i\omega$ where $\omega = 2\pi f$ the above relationships become the familiar continuous Fourier transform pair.

The Z-transform is

$$X(z) = \sum_{n=0}^{\infty} x(n)z^{-n}$$

where $z = e^{s\Delta t}$.

If $s = i\omega$, then the Z-transform is computed on the unit circle which yields the discrete Fourier transform,

$$X(f) = \sum_{n=o}^{\infty} x(n)e^{-i\omega n\Delta t}$$

or more correctly as the finite sum

$$X(h) = \sum_{n=o}^{N-1} x(n)e^{\frac{-i2\pi hn}{N}}$$

(where N = total number of sampled points and h represents digitized frequency in the same way that n represents digitized time) whose inverse is

$$x(n) = \frac{1}{N} \sum_{n=o}^{N-1} X(h)e^{\frac{i2\pi hn}{N}}$$

In this way, data points representing digital or discrete time series operated on by the Fourier transform become data points representing a digital frequency series, and the digital frequency series operated on by the inverse Fourier transform becomes a digital time series.

For our purposes this relationship between the Z-transform and the Fourier transform is sufficient. The Z-transform is extensively used in the literature as it is a more general mathematical principle that includes the Fourier transform as only a specific part of its domain. For a detailed background on the Z-transform the reader is referred to Chapter 4 of Stanley {6}, Chapter 2 of Oppenheim and Schafer {7}, Chapter 2 of Childers and Durling {9}, and/or Chapter 2 of Gold and Rader {12}.

CHAPTER III

DESCRIPTION OF CEPSTRAL ANALYSIS

A. Power Cepstrum and Determination of Delay Times.

In 1963, Bogert, Healy, and Tukey published their classic article {13} on power cepstral analysis which describes the cepstrum (pronounced Kĕṕ-strŭm, which violates a few rules of English, but sounds better than Sĕṕ-strŭm) as a tool for determining delay times between reflected wave components and incident wave components when recording both simultaneously as a combined wave field. The simplest model for the combined time series, y(t), containing only one reflected wave component or echo is

$$y(t) = x(t)+\alpha \cdot x(t-\tau)$$

where x(t) represents the original or incident wave and τ represents the delay time between the beginning of the incident wave to the beginning of the reflected wave. The α term in the above expression is the reflection coefficient, which is the ratio of the reflected wave height to the incident wave height.

The Fourier transform of the reflected echo is obtained from the Fourier transform of the original wave time series by multiplying by $\alpha e^{-2\pi i f \tau}$ where f is in frequency dimensions (Hz). Therefore the Fourier transform of the combined wave time series is

$$Y(f) = X(f)\{1+\alpha e^{-2\pi i f \tau}\}$$

Since the magnitude squared of the Fourier transform represents the power spectrum, we have

$$|Y(f)|^2 = |X(f)|^2\{1+\alpha^2+2\alpha\cos 2\pi f\tau\}$$

which represents the power spectrum of the combined wave time series. Taking the log of this power spectrum yields

$$\log|Y(f)|^2 = \log|X(f)|^2+\log\{1+\alpha^2+2\alpha\cos 2\pi f\tau\}$$

$$\log|Y(f)|^2 = \log(1+\alpha^2)|X(f)|^2+\log\left(1+\frac{2\alpha}{1+\alpha^2}\cos 2\pi f\tau\right)$$

Using the log series expansion:

$$\log(1+x) = x-\frac{x^2}{2}+\frac{x^3}{3}-\cdots, \quad |x|<1$$

we can expand the second term into a convergent series thus:

$$\log\left(1+\frac{2\alpha}{1+\alpha^2}\cos 2\pi f\tau\right) = \sum_{k=1}^{\infty}\frac{(-1)^{k+1}}{k}\left(\frac{2\alpha}{1+\alpha^2}\cos 2\pi f\tau\right)^k$$

The log of the power spectrum of the combined wave time series then contains a cosinusoidal ripple associated with the reflected wave component. The "frequency" of this ripple can be found by again calculating a power spectrum. This second power spectrum of the log of the original power spectrum is called the power cepstrum. In the transformation process, a change is made from the time domain (sec) to a frequency domain (Hz) and then to another temporal domain called the quefrency domain (sec) which could be thought of as ripples/Hz.

If we consider $\alpha<<1$ then we can simplify such that

$$\log|Y(f)|^2 = \log(1+\alpha^2)|X(f)|^2+\sum_{k=1}^{\infty}\frac{(-1)^{k+1}}{k}\left(\frac{2\alpha}{1+\alpha^2}\cos 2\pi f\tau\right)^k$$

becomes

$$\log|Y(f)|^2 = \log|X(f)|^2+2\alpha\cos 2\pi f\tau$$

where the second term in this expression is represented by the first term in the convergent series. The power spectrum of this expression then yields the power cepstrum

$$y_{PC}(t) = x_{PC}(t)+\alpha\delta(t-\tau)$$

such that the power cepstrum of the combined wave series is the power cepstrum of the incident wave series plus a unit impulse function or spike at the delay time τ. In the more general case when α is not $<<1$, additional impulses occur at multiples of τ.

If the delay time is sufficiently long, these spikes can be observed separated from the incident wave power cepstrum. Thus this procedure can be followed for determining the delay time, τ, between incident and reflected wave. The next step is to try and filter out the reflected information found at τ and multiples of τ to attempt recovery of the incident wave.

B. Complex Cepstrum and Wave Recovery.

A different approach to cepstral analysis is seen with the investigation of Oppenheim and Schafer into homomorphic deconvolution and the complex cepstrum {14, 7 (chap. 10)}. Using the single reflection model again:

$$y(t) = x(t)+\alpha x(t-\tau)$$

The Fourier transform of this is

$$Y(f) = X(f)(1+\alpha e^{-2\pi i f\tau})$$

Noting that Y(f) and X(f) are usually complex quantities, for this analysis, the log is taken directly of the Fourier transform of the time series and not of the power spectrum as was done before. We then have

$$\log\{Y(f)\} = \log\{X(f)\}+\log\{1+\alpha e^{-2\pi i f\tau}\}$$

Using the log series expansion expressed previously the second term becomes

$$\log(1+\alpha e^{-2\pi i f\tau}) = \alpha e^{-i2\pi f\tau} - \frac{\alpha^2}{2} e^{-i2(2\pi f\tau)} + \frac{\alpha^3}{3} e^{-i3(2\pi f\tau)} - \cdots\cdots$$

The complete log expression then undergoes inverse Fourier transformation to yield the complex cepstrum for the combined wave as

$$\hat{y}(t) = \hat{x}(t) + \alpha\delta(t-\tau) - \frac{\alpha^2}{2}\delta(t-2\tau) + \frac{\alpha^3}{3}\delta(t-3\tau) - \cdots\cdots$$

Note that the complex cepstrum for the combined wave time series, $\hat{y}(t)$, consists of the complex cepstrum of the incident wave time series, $\hat{x}(t)$, plus impulse functions or spikes at multiples of τ which decay exponentially with α and also alternate signs. In all of the above α is considered less than 1.0 which is the normal characteristic of the reflection coefficient in the ocean. If α is somehow greater than 1.0, a similar examination reveals that the complex cepstrum becomes the inverse Fourier transform of the complex log of the echo, plus impulse functions or spikes which decay exponentially with α and alternate signs in negative time only {15}. Kemerait and Childers {15} also go through a similar process for the double reflection case which yields this complex cepstrum

$$\hat{y}(t) = \hat{x}(t) + \alpha_1\delta(t-\tau_1) + \alpha_2\delta(t-\tau_2) - \frac{\alpha_1^2}{2}\delta(t-2\tau_1) - \alpha_1\alpha_2\delta\{t-(\tau_1+\tau_2)\} - \frac{\alpha_2^2}{2}\delta(t-2\tau_2)$$

where α_1, α_2 and τ_1, τ_2 represent the different reflection coefficients and delay times for the two different reflections or echoes from the same incident wave. Here $|\alpha_1 e^{-2\pi i f\tau_1} + \alpha_2 e^{-2\pi i f\tau_2}|$ must be less than 1.0. This could be expanded further to higher numbers of multiple echoes from the same incident wave. In the

ocean this would be equivalent to recording reflected wave data from say two or more neighboring breakwaters simultaneously combined with incident wave data. The present effort is limited to the single reflection case only. The incident ocean wave can also be thought of as consisting of a summation of many different independent waves each with its own single reflection but more will be said on this later.

In taking this complex logarithm of a forward Fourier transform of a real time sequence, some important considerations are worthy of mention. First, since with ocean or water wave data, only real information is recorded, the Fourier transform of this real information yields complex numbered information. These complex numbers are manipulated to determine the phase and frequency amplitude associated with the sampled wave series, which becomes a sampled frequency series after transformation. This amplitude is found by computing the resultant of each complex vector and the phase, ϕ, is found by taking the inverse tangent of the imaginary part divided by the real part. In the x - iy plane this looks like

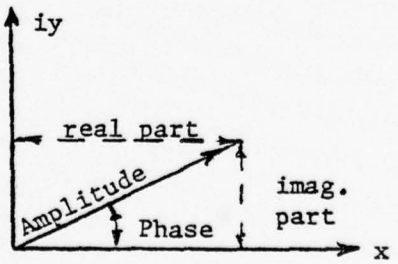

$$\text{Amplitude, } |X(f)| = \sqrt{(\text{Real})^2 + (\text{Imaginary})^2}$$

$$\text{Phase, } \phi = \tan^{-1}\left(\frac{\text{Imag.}}{\text{Real}}\right)$$

The log of these amplitudes (remembering that in discrete analysis each data point is acted upon individually) becomes the component in the complex cepstrum computation discussed above. For wave recovery, however, the phase information cannot be discarded. Additionally, since the phase thus computed from complex number algorithims is discontinuously varying between $-\pi$ and $+\pi$, it must be manipulated prior to taking the inverse transform as will be discussed later.

The cepstrum is a real valued quefrency (time) series. As such it has no imaginary part. To achieve this, the real part of the frequency series undergoing inverse transformation must be continuous and even and the imaginary part must be continuous and odd. The amplitude of the frequency series computed as shown above as well as the log amplitude will always yield a continuous and even function when the original time series is real. The phase, however, must be made continuous by "unwrapping" and its linear trend must be removed to avoid undesired shifting. When this happens the phase then becomes continuous and odd. The log amplitude becomes the real part and the unwrapped phase with linear trend removed becomes the imaginary part of a frequency series which undergoes inverse Fourier transformation to yield the real valued complex cepstrum.

To explain the phase unwrapping procedure further, Figures 1 & 2 show a sample raw phase and sample unwrapped phase. The unwrapped phase linear trend is removed by adjusting data points so that they fall above and below a zero-mean line the proportional dis-

tance they occur from a line drawn through the first and last points of the unwrapped phase plot. The heavy dotted line on Figure 2 indicates the line from which these distances from a zero-mean are computed. More examples of phase unwrapping and linear trend removal will be presented later.

Skinner {11} has shown that the power cepstrum can be computed from the complex cepstrum quite easily as

$$y_{PC}(n) = (\hat{y}(n)+\hat{y}(-n))^2$$

That is, the power cepstrum is merely 4 times the square of the even part of the complex cepstrum. He also defines a phase cepstrum that is related to the phase in the same way that the power cepstrum is related to the log magnitude. The phase cepstrum is four times the square of the odd part of the complex cepstrum and looks like

$$y_{PhC}(n) = (\hat{y}(n)-\hat{y}(-n))^2$$

The phase cepstrum is presented only for curiosity as the power cepstrum is still a better indicator of the delay time, τ. The phase cepstrum does, however, give some indication as to whether the phase unwrapping procedure was successful. That is, if the phase cepstrum is very weak or non existant, the phase unwrapping may not have been complete. This could happen if the phase differed by more than 2π between any two sample points.

The procedure for recovery of the incident wave first involves finding the delay time, τ, by either the complex or power cepstrum. Then the impulse functions or spikes which contain the reflected wave information found in the complex cepstrum at τ and

multiples of τ are filtered out and smoothed over by averaging neighboring points on either side of the spikes. The resulting filtered complex cepstrum then contains information pertaining solely to the incident wave. By reversing the process for computing the complex cepstrum the original incident wave time series is obtained. The algorithim for this process as obtained from Skinner {16} is described by Figure 3.

To demonstrate the wave recovery process, two models are taken from Skinner {11} and results plotted using a Calcomp Plotter. The first model is of a 256-point time series consisting of two 64-point long exponential signals with the second one reduced in amplitude by one half and delayed 30 points. Using a sampling rate of .3333 sec, this means the combined signal is a decaying exponential pulse 21.33 sec long combined with its echo reduced in half and delayed 10 sec. Mathematically it looks like: $y(t) = x(t)+.5x(t-\tau)$ where $x(t) = te^{-t}$; t is actually the sample number n multiplied by the sampling rate Δt and $\tau=30\Delta t=30x.3333$ or $\tau=10$ sec.

Figure 4 shows the raw spectrum of this combined signal, and Figure 5 shows the log amplitude. Figures 6 - 8 show the raw phase, the unwrapped phase, and the phase with linear trend removed. Figure 9 shows the real-valued complex cepstrum. Figures 10 and 11 show the power and phase cepstrums as computed from the complex cepstrum. Note the large sharp impulse spikes at multiples of τ(10 sec) in all three cepstral plots and the alternating positive/

negative impulse peaks in the complex cepstrum. Figure 12 shows the true incident wave in the middle with the recovered incident wave above and the combined wave below. Recovery with this example is almost perfect with a Mean Squared Error (MSE) of only 4.44×10^{-9} between true incident and recovered incident waves.

The other signal observed by Skinner {11} was a 256-point combined time series containing two FM signals pulsed over 64 points of which one was reduced by ½ in amplitude and delayed by 30 points before being added to the incident wave signal. Mathematically this combined signal looks like $y(t) = x(t)+.5x(t-\tau)$ where $x(t) = \sin((.4+.11t)t)$. Using a Δt of .3333 sec, the incident FM signal pulse is 21.33 sec long, and τ=10sec. Figures 13 through 21 show the same sequence as for the exponential signal but the recovered wave similarity to the incident wave in Figure 21 is much more impressive here as the combined signal went through quite a bit of unravelling. Note the small aberrations on the recovered signal (top time series of Figure 21) where not quite all of the reflected wave component was taken out probably due to a bit of leakage, etc. associated with the FFT. Mean Square Error (MSE) between the recovered incident and true incident waves in this case was computed to be 1.91×10^{-5}, again indicating almost perfect recovery.

Both of these examples were run under basically noise free conditions. Much of the work to date in cepstral analysis has been associated with effects of noise added to the signal.

Since in the ocean environment wave measurements can be made without noise other than the usually negligable amount produced electronically during sampling and recording, these effects will not be examined here. Generally any noise added to the signal makes recovery that much more difficult.

C. Anticipated Limitations Related to Application with Ocean Waves

A basic assumption in our original model used to define cepstral analysis is that the delay time, τ, and the reflection coefficient, α, are constant and not functions of frequency. With water waves this is not a correct assumption. Both τ and α may vary with frequency even in areas where the water depth is constant. When water depth varies and particularly if the waves under study are moving into shallower waters, the problem is even more complex due to wave celerity varying with depth by different amounts for different wave frequencies. It is hoped that the amount of differing τ's and α's with different frequencies will be small enough that this will not cause an insurmountable problem. In this regard results should probably be better for single peak and narrow banded spectrums* than for double or multi-peaked spectrums with broader frequency components as the different individual τ's will hopefully join together to form one main τ value. The varying α could possibly cause the amplitudes of the impulse spikes in the cepstrum at multiples of τ to change differently than expected from theory. Both

*Although the literature shows about equal preference between the use of spectra or spectrums as the plural form of spectrum, the latter form is used throughout this work.

of these effects may require a wider filtering and smoothing of the reflected information spikes in the complex cepstrum to completely remove all reflected wave information and allow recovery of the incident wave.

Another problem that may be encountered using the ocean wave is the magnitude of α. Kemerait and Childers {15} found problems trying to recover the incident wave as the reflection coefficient exceeds 0.8 for various computer generated test signals. For the multiple reflection case they found that if the reflected signal amplitudes are less than the basic wave, recovery is possible. In the general wave case, if the reflected signal amplitudes are greater than the incident wave, but not equal, the largest reflected signal can be recovered. If two or more reflected signals have larger amplitude than that of the incident wave, recovery is not possible. Since ocean structures frequently may have reflection coefficients approaching 1.0, this real limitation will be examined for at least the single reflection case.

Cepstral analysis to date has been involved with pulsed and burst-type signals of relatively short duration similar to the recently discussed exponential and FM signal examples. A problem may arise from using combined incident/reflected wave data collected over the total sample length. Since the time series is in fact digitally sampled it is felt this should not be an insurmountable problem. It may mean zeroes will have to be added to the end of the sampled data which increases the frequency sampling rate to get results similar to that of the pulsed signal. More will be said about this in Chapter V.

CHAPTER IV

DESCRIPTION OF TEST MODELS

A. Summation of Finite Number of Sinusoids with Random Phase.

The first test model for ocean simulated waves maintains both α, the reflection coefficient, and τ, the delay time, as constants non-variant with respect to frequency. The incident wave model used in this test is that derived by Borgman {17} which simulates an ocean waveform based on an assumed spectral curve. This model can be described as the summation of a finite number of sinusoid components having random phase shift angles. Simplified mathematically it looks like:

$$x(t) = \sum_{m=1}^{M} \sqrt{\frac{2}{M}\sigma^2} \cos(2\pi f_m \Delta t + \phi_m)$$

where $x(t)$ represents the simulated ocean wave surface profile. As M, which represents the number of sinusoid components, gets larger, the more realistic the simulated wave becomes. The tradeoff for using larger and larger values of M is increased computer cost for "building" the simulated wave. For the testing in this work, an M value of 40 is used for a 256-point time series. The amplitude of each component is found by dividing the total assumed energy represented as the variance, σ^2, of the assumed spectrum (where σ^2 is the area under that spectral curve) by the number of sinusoids being summed and taking the square root of that result (remembering that the square root of energy is directly proportional to wave height). Therefore, the total energy in the simulated wave will equal the energy represented by the

initially assumed spectral curve. When the assumed spectral curve is divided into equal area increments, f_m values are chosen as the mid-frequency of each incremental frequency band. Δt is the time increment between samples, and ϕ_m is a uniformly distributed random variable between zero and 2π which represents the random phase shift or starting point of each sinusoid component being summed.

For example, with an M value of 5 the assumed spectrum would be divided as shown below to obtain the equal energy value for computing amplitudes and for determining f_m values or the mid-point frequencies.

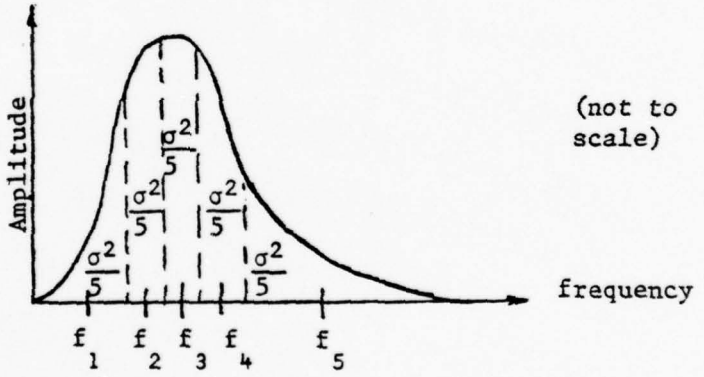

The assumed spectrum used in creating this wave form is that proposed by Pierson and Moskovitz {18} and modified for limited fetches by Mitsuyasu {19}, Barnett {20} and Sylvester and Vorgvisessomjai {21}. The general form of the P-M spectrum is

$$S(f) = \frac{\alpha g^2}{(2\pi)^4 f^5} \exp\left[-\beta\left(\frac{g}{2\pi U f}\right)^4\right]$$

where α (not to be confused with the reflection coefficient) and β are assumed to be constant for a fully arisen sea state. U

is the wind velocity, f the frequency, and g the gravitational constant. However, as derived by Christensen and described by Morden {2}, for limited fetches α and β become

$$\alpha = \frac{5(2\pi)^4\sigma^2 f_p^4}{g^2} = \frac{3.49(2\pi)^4 S(f_p) f_p^5}{g^2}$$

$$\beta = \frac{5}{4}\left(\frac{2\pi U f_p}{g}\right)^4$$

where f_p is the frequency of the spectral peak and $S(f_p)$ is the amplitude of the spectral peak. The variance σ^2 is then found from

$$\sigma^2 = 2\int_0^\infty S(f)df = \frac{\alpha U^2}{4\beta g^2}$$

A model wave then can be created based on the variables U, f_p, $S(f_p)$, and σ^2. Assuming U and f_p and either σ^2 or $S(f_p)$ will completely define the P-M spectrum.

Therefore, the simulated incident ocean wave is computed by first assuming values of $S(f_p)$ and f_p to compute the P-M spectral model and a value for σ^2. This spectral curve is divided into equal areas and mid-point frequencies for each equal area increment are computed. Using a suitable random number generator to compute random phase angles, each sinusoid is computed and summed to the previously computed sinusoid(s) as described previously. For simplicity, this simulated incident ocean wave will be called the P-M generated wave.

Taking the P-M generated wave and scaling it by a reflection coefficient α produces the simulated reflected wave. Delaying this reflected wave by τ and adding the two together yields the initial P-M generated combined wave test model. Note τ is

constant for the whole wave train in this initial model. In Chapter V, further description of model manipulation is described related to testing procedure.

B. Varying Delay Time with Respect to Frequency

In water waves, the delay time τ varies with respect to the wave celerity which varies as a function of wave length which in turn varies with frequency, so it follows that τ does in fact vary with frequency. For linear deep water wave theory this variation can be expressed in fps units by $\tau = \frac{xf}{2.56}$ where f is the frequency of the wave component and x is the distance from the wave measurement device to the reflecting surface. This relationship is derived from $\text{celerity} = \frac{\text{distance traveled}}{\text{time of travel}} = \sqrt{\frac{g}{2\pi}}\, T$ for deep-water wave theory where T is the wave period and g is the gravitational constant. Therefore $\text{celerity} = \frac{2x}{\tau} = 5.12\, \frac{1}{f}$ since distance x is traveled twice over the delay time, τ, so that $\tau = \frac{2xf}{5.12} = \frac{xf}{2.56}$

Using the P-M generated wave model previously described, the incident wave is generated in the same manner as before. However, the reflected wave components are delayed by their own τ values for their particular frequency before being summed together, scaled by α and combined with the incident wave. This is then a model where each separate reflected frequency component has its own delay time τ contributing to the overall resultant τ of the reflected wave time series. Results from using this model are discussed in the next chapter.

C. Varying Reflection Coefficient with Respect to Frequency.

To carry the P-M generated wave model one step closer to the real world reflected water wave, an attempt is made at varying the reflection coefficient as a function of frequency. This first-try variation is performed by merely making α a linear function varying from .4 to .6, .5 to .7, or .7 to .9 incremented by $\frac{.2}{M}$ for each sinusoidal component of the reflected wave where M is the total number of components. The results from using this test model are also discussed in Chapter V.

In reality, the reflection coefficient, α, probably varies as some non-linear function of frequency such that α would be higher for higher frequency waves than for lower frequency waves depending on the structure. That is, the lower frequency wave components are more likely to be absorbed or transmitted by most structures than are the higher frequency wave components making up the ocean wave. However, the simplified model described above and in Chapter V is sufficient for an initial test of effects from α varying as a function of frequency.

CHAPTER V

APPLICATION OF CEPSTRAL ANALYSIS TO TEST MODELS

As mentioned in Chapter III, cepstral analysis techniques are usually applied to "pulse" type signals where no signal information is contained between the incident wave and the reflected wave. Figure 22 shows a sample of incident and reflected pulse signals which would be added together to form such a combined incident/reflected signal. Note the lack of information over time, τ, at the end of the incident wave and over time, τ, at the beginning of the reflected wave. Both incident and reflected waves are of the same length. The exponential and FM signals discussed in Chapter III are examples of pulse waves.

When the incident wave extends the full length of the time series, the incident and reflected waves appear as shown in Figure 23. This combined wave is called a "pulse-shifted" wave as no information exists over time, τ, in the beginning of the reflected wave. Note the reflected wave is now not as long as the incident wave. This creates a situation known as "echo truncation" where the incident wave does not terminate τ seconds before the end of the reflected wave as in the pulse signal described above.

For a more realistic look at ocean wave data sampling, a "forward-shift" combined wave is created from incident and reflected waves following the pattern shown in Figure 24. The name "forward-shift" comes from the fact that a new incident wave is made from the previously created incident wave by extending the wave train and

figuratively shifting it forward. The important item here is that signal information exists from both the incident and reflected waves throughout the sampling period.

To test the first model described in Chapter IV where neither α nor τ are allowed to vary with frequency the combined wave is formed first using the "pulse-shift" combination and then using the "forward-shift" combination. In both cases, the incident and reflected waves are created and stored and each data point in the reflected wave is multiplied by a reflection coefficient before the two waves are added together to form the combined wave.

The P-M Spectral model used to create the P-M Generated Wave is shown as Figure 25. This spectrum is selected as most of the spectral energy is concentrated around a narrow frequency band. With later trials this should help produce one τ value for the total combined wave when τ is allowed to vary with frequency.

Using a rectangular window (no weighting of input data) as recommended by Skinner {11} for the pulse-shifted wave, results are somewhat discouraging. For a 256 data point time series, Δt=.3333 sec, τ=10 sec (30 data points) and α=.8, the Mean Squared Error (MSE) between the recovered incident wave and the true incident wave is .122 with the MSE between the true incident and combined wave equal to .285. The MSE (equal to the mean of the difference squared comparing parallel data points of two "side-by-side" time series) between recovered and true incident waves is an indicator of recovery results and the MSE between true incident and combined waves is an indicator of what the recovery process starts with. Comparing these two indicators, the MSE relation-

ships show that some recovery did occur but that the recovered incident wave and the true incident wave are still not very much alike.

Oppenheim and Shafer {7} state that using an exponential window (exponential weighting of input data) enhances the identification of delay time, τ, and improves the overall cepstral analysis recovery process. Skinner {11} found this not to be the case for the exponential and FM signals discussed in Chapter III. Using an exponential window on the pulse-shifted combined wave where each data point (n=1 to n=N) is "weighted" or multiplied by $(.99)^{n-1}$ before the cepstral decomposition process and dividing the resulting recovered wave by $(.99)^{n-1}$ to "unweight" the output lowers the MSE between original and recovered incident waves to .044. This indicates quite satisfactory recovery results as can be observed from Figure 34.

It should be pointed out here that although "one-sided" plots (representing only the positive half of the spectrum) of the raw spectrum and log amplitude are shown for the exponential and FM signals, all subsequent plotting of raw spectrum and log amplitude before the cepstrum is computed are shown as "two-sided" plots (noting that the negative half of the spectrum is reproduced to the right of the positive half since transformation was performed via the DFT). This is done to show that in fact the log amplitude is indeed continuous and even and the unwrapped phase with linear trend removed is continuous and odd which together produce a real valued cepstrum. Smoothed spectral curves to be seen later will still be shown as one-sided plots.

To discuss the positive results from exponential weighting further, it is seen that it helps reduce echo truncation error by plac-

ing greater emphasis on the beginning of the input combined wave time series than on the end. Different exponential "base" values from .900 to .999 were tried for different input conditions and a base value of .99 always seemed to produce the best results.

Figures 26 through 34 show the plots of the time series manipulation through the spectral and cepstral processes at the same stages as listed for the exponential and FM signals. An important observation when seeing these plots is that this more irregular wave form produces a more irregular cepstrum but the reflected information impulse spikes are still very obvious in all three cepstrums. When the spikes located at multiples of τ are filtered out of the complex cepstrum, wave recovery is quite good as is seen in Figure 34 when comparing the original incident time series located in the middle of this figure to the recovered incident time series located at the top.

A better indicator of how good the results are using this model is seen in Figures 35 through 38. These figures represent the smoothed spectrums (every 8 points averaged together for these particular plots) of the combined wave, the original incident wave, the recovered incident wave, and the reflected wave, respectively. The spectrums of the recovered and original incident waves are almost identical indicating good wave recovery. The reflected wave spectrum is obtained from the recovered reflected wave found by subtracting the recovered incident wave data points from the combined wave data points. Using the formula $\sigma_R^2 = \alpha^2\sigma_I^2$ which relates the variance, or area under the spectrum of the reflected wave to the variance or area under the spectrum of the incident wave times the reflection coefficient squared, an

attempt is made at determining the reflection coefficient used to create the combined wave. The resulting computation produces a reflection coefficient equal to .785, which is very close to the actual .8 value used.

The results of this first test of a P-M generated wave shape therefore are very encouraging. The next tests using the "forward-shift" model, however, are not so gratifying. Input parameters are the same as with the pulse-shift model. Figures 39 through 47 show the same plot sequence as before. The impulse spikes are not as readily noticable in the three cepstrums now and recovery attempts as seen from the time series comparisons in Figure 47 between the original incident wave (middle) and the recovered incident wave (top) show results poorer than with the pulse-shift test. The smoothed (averaged spectral value of every 10 data points) spectral plots of results shown in Figures 48 through 51 also show recovery as less than satisfactory. The recovered wave spectrum shows its energy level to be somewhere between that of the true incident and combined waves instead of equal to that of the true incident wave. The reflected wave spectrum is obviously too small such that the computed reflection coefficient is much lower than the value of .8 used in creating the combined wave. An encouraging observation in this, however, is that some energy is in fact removed from the combined wave so that the process at least attempted to perform some decomposition.

Following Skinner's {11} recommendation, a first step or try at improving results is to add N zeroes to the end of the input data (adding 256 zeroes for 256 data points) before performing the spectral

and cepstral computations. This effectively doubles the sampling rate in the frequency domain and hence the quefrency domain without changing the time series information whatsoever. When zeroes are added to the end of the pulse-shifted combined wave from before, no improvement is noted, probably due to the fact that results are already very good. Adding N zeroes to the end of the input data of the forward-shifted combined wave before performing decomposition yields the smoothed recovered incident and reflected wave spectral plots shown in Figures 52 and 53. It is seen that this technique helps produce a recovered incident wave spectrum that is slightly closer to the true incident wave spectrum, but results are still unsatisfactory as evidenced by the again small reflected wave spectrum and the obvious resulting incorrect calculation of the reflection coefficient.

Manipulation of data sampling methods is also employed in searching for better results. These methods include trying different time sampling rates, trying different τ values and increasing the total sample length to 1024 data points from the previous length of 256 data points. All attempts at data sampling manipulation seem to be ineffectual for improving results. When the reflection coefficient is reduced to .5, results improve only very slightly. Attempts at improving recovery using a rectangular window and an exponential window with differing base values above and below .99 show best results are still achieved with exponential weighting and un-weighting using the $(.99)^{n-1}$ factor described previously.

Therefore, a problem exists using the P-M Generated wave forward-shift model even when τ and α are constant and independent of

frequency. This problem appears to be centered around the fact that information is now contained in the beginning of the reflected wave. This information looks more like noise when comparing the incident and reflected waves' time series because the actual image reflection from the incident wave doesn't start until τ seconds later.

When the second model described in Chapter IV is employed, where τ is allowed to vary with frequency for each sinusoid making up the P-M generated combined wave, even less incident wave recovery is possible. The different attempts at improving results follow the same sequence as those tried with the forward shift wave. Figure 54 shows a typical complex cepstrum for this model where $\Delta t=.3333$, $\tau=10$ sec and $\alpha=.5$. It is readily obvious that identifying a τ, even when the input τ is known, is very difficult in this situation. Filtering the impulse spikes which should be present at multiples of τ yields the filtered complex cepstrum shown in Figure 55. Figures 56 and 57 demonstrate the same technique showing a complex cepstrum and a filtered complex cepstrum for $\Delta t=.7333$. Again it is quite difficult to identify a τ.

Since it appears initially that the τ peak in Figure 54 may be wider than just one point, five different filter variations are attempted filtering out more than one point. Some examples are shown in Figures 58 and 59 of the resulting filtered complex cepstrums. None of these different filter methods help and in fact all of them make the MSE even greater between the original and recovered incident waves. Some attempts even made the MSE between actual incident and recovered incident waves higher than between the incident and combined waves.

Therefore, it appears the impulse spike definition for location of τ is more accurate than a wider peak definition of τ even in the model where τ is allowed to vary with frequency.

When employing the third model described in Chapter IV, where reflection coefficient is also allowed to vary with frequency, very little difference is observed in the appearance of the complex cepstrum using the same input parameters as for the constant reflection coefficient model above. Wave recovery attempts for this model are not satisfactory. Again, no improvement is obtained by using different Δt's, different τ's, or different reflection coefficient ranges, including α varying from .7 to .9, .5 to .7, and .4 to .6. Example complex cepstrums for this model are shown in Figures 60 and 61. The difficulty in identifying a value for τ is also readily apparent for this model.

The problems with the latter two models cannot be readily identified until satisfactory results can first be obtained from the forward shift model where α and τ are non-variant with frequency. This requires some way of satisfactorily dealing with the "noise" or continuous wave section existing in front of the reflected wave contribution.

CHAPTER VI

APPLICATION OF CEPSTRAL ANALYSIS TO ACTUAL OCEAN DATA

Some time series data records recorded near a breakwater in Sitka, Alaska, in 1973 are run through this algorithm to determine if a value for τ can be identified. Figure 62 shows the breakwater plan and the location of instruments on this breakwater. The data points utilized are taken from the combined wave recorded at the Northernmost gage when wave action was predominately perpendicular to the short leg of the breakwater. This site has the advantage that any recovered incident wave obtained through the decomposition process can be compared for accuracy with the true incident wave recorded from the wave staff off the corner of the breakwater.

These data records had a major disadvantage, however, as the breakwater is only about two feet deep allowing some of the low frequency waves to transmit through the breakwater causing the reflected wave to be different in shape and frequency composition from the incident wave. Also, the frequency spectrum for this location is "double-peaked," that is, a low frequency swell condition exists as well as the waveform produced by local winds over a local fetch.

Looking at cepstrums generated from this data is informative, however, in that it reveals some of the other problems associated with using this process on real world data. Three records are selected and tested which are 2048 data points long recorded at a Δt of .44 sec. producing 15 minute long data records. An example of the complex cepstrum thus obtained using no weighting of the input data

(rectangular window) is shown in Figure 63. It is interesting to observe the unwrapped phase and unwrapped phase with linear trend removed for this data which are shown in Figures 64 and 65. The simularity between the two raises suspicion that phase unwrapping may not have been complete. A remedy for this problem is to add zeroes to the end of the original input data. This is tried using 1024 data points from the same record and adding 1024 zeroes before computing the spectrum and complex cepstrum.

Figures 66, 67, 68, and 69 show the raw spectrum, log amplitude, unwrapped phase, and unwrapped phase with linear trend removed for this new input. The linearity seen in the unwrapped phase plot shows phase unwrapping is indeed now more complete.

Figures 70 and 71 show the complex cepstrum and power cepstrums, respectively. Difficulty in obtaining a value for τ from these plots is readily apparent. Perhaps some help could be obtained by plotting the cepstrum over a longer quefrency axis for better plot visualization. Using deep water wave theory, the physical location of the wave staff and predominant frequency from the wave spectrum, τ is estimated to be about 18-20 seconds. This would probably be very hard to identify in a 15 minute record even if an impulse spike were located at this point.

The most important reason for failure to identify a τ for this situation is more probably due to the fact that the reflected wave is altered in shape and frequency and is not in fact a true replica of the original incident wave. It seems Cepstral Analysis

decomposition should work even if the reflected wave shape is different from the incident wave shape as long as the frequency information is not altered in the reflection process. Since the floating breakwater used here does in fact filter certain low frequency components out of the reflected wave by allowing them to pass through the breakwater, it is not surprising that an impulse spike is not observable in either the complex or power cepstrums at an identifiable location for τ.

The predominant spike at the beginning of these cepstrums is left over from the incident wave complex cepstrum which always produces an extremely large spike at zero quefrency in the cepstral plots. In fact, all of the cepstral plots seen in this thesis have their first 5 data points set to zero amplitude on either side of zero quefrency (more properly in the digital sense, points $n = 1, 2, 3, 4, 5, N, N-1, N-2, N-3$, and $N-4$ were set equal to zero) to allow easier identification of the smaller amplitude spikes containing the reflected wave information. Otherwise, plotting would be based on the large spike at zero quefrency and the smaller reflected information impulse spikes would be even more difficult to identify.

Even taking this into consideration, an actual τ value is practically impossible to identify from these cepstrums. The power cepstrum shown in Figure 71 offers many possible impulse spikes but at times which are totally unrealistic with the ocean wave data interacting with this breakwater. Obviously, better data and more

research are required to demonstrate any sort of positive results with cepstral analysis decomposition using ocean data.

CHAPTER VII

CONCLUSIONS AND RECOMMENDATIONS

Cepstral analysis decomposition techniques work extremely well with the pulse-shift P-M generated combined wave model and not so well with the forward-shift P-M generated combined wave model as described in Chapters IV and V. Problems exist with identification of delay time as well as with decomposition of the combined wave when cepstral analysis techniques are applied to P-M generated wave models which vary τ and/or the reflection coefficient, α, as a function of frequency. More research is required before this decomposition technique can be successfully applied to real-world ocean waves. It may never work for decomposition of combined waves for which the reflected wave frequency information is altered by the structure and no longer is the same as the incident wave, such as occurs with shorelines and many breakwaters.

Exponential windowing or weighting does help when using these decomposition techniques with P-M generated wave models. Adding zeroes to the end of the input data prior to application of cepstral analysis decomposition does improve phase unwrapping but helps only slightly to none at all with incident wave recovery.

Of the three cepstrum types examined, the power cepstrum is the best indicator of delay time between incident and reflected waves. The phase cepstrum does not seem to offer much information other than reinforcement or possible validation of the power cepstrum information.

It is recommended that this process be tested using real-world ocean data for which the reflected wave frequency information is identical to that of the incident wave such that all frequency components are reflected by the structure. Further experimentation should begin using real-world data with a "single-peaked" smoothed spectrum before going to data with a "two-peaked" or "multi-peaked" spectrum. When using data with more than one spectral peak, experimentation could be made into the effect of filtering out one or more peak(s) before going through the decomposition process. Of particular interest would be results obtained after filtering out the lower frequencies from the combined wave that would be transmitted through a structure like the floating breakwater investigated in Chapter VI.

Since the complex cepstrum consists of impulse spikes at multiples of τ which decay exponentially as a function of the reflection coefficient, investigation could be made into possible determination of reflection coefficients directly from the amplitudes of these peaks. This would save the inverse process presently necessary by not requiring actual determination of the incident wave to obtain the reflected wave before computing a reflection coefficient.

Research should be conducted towards improving results with the forward-shift. One possible alternative is to try reiterative techniques. Once a value for delay time is determined, the recovered wave could possibly be improved by putting it through

the decomposition process again. Another possibility to improve results is to somehow weight or alter the data points at the beginning of the combined wave time series so that the leading portion of the reflected wave will not have such a degrading effect on results.

It appears from attempts at adjusting the filtering of the impulse spikes from the complex cepstrum that the spikes do not join together to form a wider peak when τ varies with frequency. Perhaps what actually happens is impulse spikes occur separately at the different τ values produced by different frequency components making up the wave. This possibility could be investigated further.

Other windowing or weighting of input data prior to the decomposition process has generally not met with success when using cepstral analysis techniques. However, this could be investigated further for the ocean wave by experimenting with other data windows.

Generally, cepstral analysis decomposition methods do not appear at this time to be the final answer in recovery of the incident wave from combined incident/reflected ocean wave data. First, the τ value itself must be made reliably discernable in the cepstrum and then actual recovery must be made more efficient. However, with further research, it may yet prove to be a valuable tool in helping to determine delay times, reflection coefficients, and other parameters associated with wave decomposition when determining true wave forces acting on and/or from a structure.

REFERENCES

1 Ippen, et al., Estuary and Coastline Hydrodynamics, McGraw Hill Book Co., New York, 1966, pp. 382-385.

2 Morden, D.B. "The Decomposition of Co-Existing Random Incident and Reflected Wave Energy," PhD Dissertation, University of Washington, 1975.

3 Morden, D.B., Richey, E.P. & Christensen, D.R., "Decomposition of Co-Existing Random Wave Energy," Proceedings of the Fifteenth Coastal Engineering Conference, 1976, pp. 846-865.

4 Thornton, E.B., & Calhoun, R.J., "Spectral Resolution of Breakwater Reflected Waves," ASCE Proceedings, Journal of Waterways, Harbors, and Coastal Engineering Division, Vol. 98, November, 1972, pp. 443-460.

5 Bergland, G.D., "A Guided Tour of the Fast Fourier Transform," IEEE Spectrum, Vol. 6, No. 7, July 1969, pp. 41-52.

6 Stanley, W.D. Digital Signal Processing, Reston Publishing Co., Reston, Virginia, 1975.

7 Oppenheim, A.V., and Schafer, R.W., Digital Signal Processing, Prentice Hall, Englewood Cliffs, New Jersey, 1975.

8 Brigham, E.L., The Fast Fourier Transform, Prentice Hall, Inc., Englewood Cliffs, New Jersey, 1974.

9 Childers, D., and Durling, A., Digital Filtering and Signal Processing, West Publishing Co., St. Paul, Minn., 1975.

10 Paniker, N.N., "Determination of Directional Spectra of Ocean Waves from Gage Arrays," University of California Hydraulic Engineering Laboratory Research Report HEL 1-18, August, 1971.

11 Skinner, D., "Real Time Composite Signal Decomposition," PhD Dissertation, University of Florida, 1974.

12 Gold, B., and Rader, C.M., Digital Processing of Signals, McGraw Hill Book Co., New York, 1969.

13 Bogert, B., Healy, M., and Tukey, J., Quefrency Alanysis of Time Series for Echoes: Cepstrum, Pseudo-Autocovariance. Cross-Cepstrum and Saphe Cracking, M. Rosenblatt, Ed., New York, Wiley, 1963, Ch. 15, pp. 209-243.

14 Oppenheim, A.V., Schafer, R.W., and Stockham, J.G., "Nonlinear Filtering of Multiplied and Convolved Signals," Proceedings of the IEEE, Vol. 56, No. 8, August, 1968, pp. 1264-1291.

15 Kemerait, R.C., and Childers, D.G., "Signal Detection and Extraction by Cepstrum Techniques," IEEE Transactions on Information Theory, Vol. IT-18, No. 6, November, 1972.

16 Skinner, D.P. and Childers, D.G. "Real-Time Composite Signal Decomposition," IEEE Transactions on Acoustics, Speech, and Signal Processing, June, 1976, pp. 267-270.

17 Borgman, L., "Ocean Wave Simulation for Engineering Design", Journal of the Waterways and Harbors Division, Proceedings of the ASCE, November, 1969, pp. 557-583.

18 Pierson, W.J. and Moskovitz, L.I., "A Proposed Spectral Form for Fully Developed Seas Based on the Similarity Theory of S.A. Kitaigorodskii," Journal of Geophysical Research, Vol. 69, 1964, pp. 5181-5190.

19 Mitsuyasu, "One Dimensional Wave Spectra at Limited Fetch," Proceedings of the Thirteenth Coastal Engineering Conference, ASCE, New York, N.Y., 1972, pp. 351-360.

20 Barnett, T.P. "Observations of Wind Waves Generation and Dissipation in the North Sea: Implications for Offshore Industry," Offshore Technology Conference, Paper #OTC 1516, Dallas, Texas, 1972, p. 10.

21 Silvester, R. and Vorgvisessomjai, S., "Energy Distribution Curves of Developing and Fully Arisen Seas," Journal of Hydraulic Research, Vol. 8, No. 4, Delft, Netherlands, 1970, pp. 493-521.

BIBLIOGRAPHY

Barber, N.F., Experimental Correlograms and Fourier Transforms, Pergamon Press, New York, 1961.

Barnett, T.P. "Observations of Wind Waves Generation and Dissipation in the North Sea: Implications for Offshore Industry," Offshore Technology Conference, Paper #OTC 1516, Dallas, Texas, 1972, p. 10.

Bendat, Julius S. and Piersol, Allan G., Random Data Analysis and Measurement Procedures, Wiley-Interscience, a Division of John Wiley & Sons, Inc., N.Y., 1971.

Bergland, G.D., "A Guided Tour of the Fast Fourier Transform," IEEE Spectrum, Vol. 6, No. 7, July 1969, pp. 41-52.

Bloomfield, Peter, Fourier Analysis of Time Series: An Introduction, John Wiley & Sons, N.Y., 1976.

Bogert, B., Healy, M., and Tukey, J., Quefrency Alanysis of Time Series for Echoes: Cepstrum, Pseudo-Autocovariance, Cross-Cepstrum and Saphe Cracking, M. Rosenblatt, Ed., New York, Wiley, 1963, Ch. 15, pp. 209-243.

Borgman, L., "Ocean Wave Simulation for Engineering Design," Journal of the Waterways and Harbors Division, Proceedings of the ASCE, November, 1969, pp. 557-583.

Bracewell, Ron, The Fourier Transform and Its Applications, McGraw Hill Book Co., New York, 1965.

Brigham, E.L., The Fast Fourier Transform, Prentice Hall, Inc., Englewood Cliffs, New Jersey, 1974.

Brillinger, David R., Time Series Data Analysis and Theory, Holt, Rinehart and Winston, New York, 1975.

Carnahan, Brice, Luther, H.A., and Wilkes, James O., Applied Numerical Methods, John Wiley & Sons, Inc., New York, 1969.

Champeney, D.C., Fourier Transforms and Their Physical Applications, Academic Press, London and N.Y., 1973.

Childers, D., and Durling, A., Digital Filtering and Signal Processing, West Publishing Co., St. Paul, Minn., 1975.

Churchill, Ruel V., Fourier Series and Boundary Value Problems, McGraw-Hill Book Co., 1969.

Churchill, R.V., Brown, J.W., Verhey, R.F., Complex Variables and Applications, McGraw-Hill Book Co., New York, 1976.

Cooper, George R., and McGillen, Clare D., Methods of Signal and System Analysis, Holt, Rinehart and Winston, Inc., N.Y., 1967.

Enochson, Loren D., and Otnes, Robert K., Programming and Analysis for Digital Time Series Data, The Shock and Vibration Information Center, U.S. Dept. of Defense, 1968.

Gold, B., and Rader, C.M., Digital Processing of Signals, McGraw-Hill Book Co., New York, 1969.

Goldberg, Richard R., Fourier Transforms, Cambridge at the University Press, 1961.

Hannon, E.J., Multiple Time Series, John Wiley and Sons, Inc., New York, 1970.

Ippen, et al., Estuary and Coastline Hydrodynamics, McGraw-Hill Book Co., New York, 1966.

Jenkins, Gwilyn M., and Watts, Donald G., Spectral Analysis and its Applications, Holden-Day, San Francisco, 1969.

Kemerait, R.C., and Childers, D.G., "Signal Detection and Extraction by Cepstrum Techniques," IEEE Transactions on Information Theory, Vol. IT-18, No. 6, November, 1972.

Koopmans, L.H., The Spectral Analysis of Time Series, Academic Press, New York, 1974.

Lubkin, Y.J., Filter Systems and Design: Electrical, Microwave, and Digital, Addison-Wesley Pub. Co., Reading, Mass., 1970.

Mikhail, E.M., Ackermann, F., Observations and Least Squares, IEP-a Dun-Donnelley Publisher, N.Y., 1976.

Mitsuyasu, "One Dimensional Wave Spectra at Limited Fetch," Proceedings of the Thirteenth Coastal Engineering Conference, ASCE, New York, N.Y., 1972, pp. 351-360.

Morden, D.B. "The Decomposition of Co-Existing Random Incident and Reflected Wave Energy," PhD Dissertation, University of Washington, 1975.

Morden, D.B., Richey, E.P. & Christensen, D.R., "Decomposition of Co-Existing Random Wave Energy," Proceedings of the Fifteenth Coastal Engineering Conference, 1976, pp. 846-865.

Oppenheim, A.V., Schafer, R.W., and Stockham, J.G., "Nonlinear Filtering of Multiplied and Convolved Signals," Proceedings of the IEEE, Vol. 56, No. 8, August, 1968, pp. 1264-1291.

Oppenheim, Ed., A.V., Papers on Digital Signal Processing, The M.I.T. Press, Cambridge, Mass., 1969.

Oppenheim, A.V., and Schafer, R.W., Digital Signal Processing, Prentice Hall, Englewood Cliffs, New Jersey, 1975.

Otnes, R.K. and Enochson, Loren, Digital Time Series Analysis, A Wiley-Interscience Publication, John Wiley & Sons, New York, 1972.

Paley, R.E.A.C., Weiner, N., Fourier Transforms in the Complex Domain, American Mathematical Society, New York, 1934.

Paniker, N.N., "Determination of Directional Spectra of Ocean Waves from Gage Arrays," University of California Hydraulic Engineering Laboratory Research Report HEL 1-18, August, 1971.

Pierson, W.J. and Moskovitz, L.I., "A Proposed Spectral Form for Fully Developed Seas Based on the Similarity Theory of S.A. Kitaigorodskii, Journal of Geophysical Research, Vol. 69, 1964, pp. 5181-5190.

Rabiner, Lawrence R., and Rader, Charles M., editors, Digital Signal Processing, IEEE Press, Institute of Electrical and Electronic Engineers, Inc., N.Y., 1972.

Rosenblatt, M., Ed., Time Series Analysis, Wiley & Sons, N.Y., 1963.

Silvester, R. and Vorgvisessomjai, S., "Energy Distribution Curves of Developing and Fully Arisen Seas," Journal of Hydraulic Research, Vol. 8, No. 4, Delft, Netherlands, 1970, pp. 493-521.

Skinner, D., "Real Time Composite Signal Decomposition," PhD Dissertation, University of Florida, 1974.

Skinner, D.P. and Childers, D.G., "Real-Time Composite Signal Decomposition," IEEE Transactions on Acoustics, Speech, and Signal Processing, June, 1976, pp. 267-270.

Stanley, W.D., Digital Signal Processing, Reston Publishing Co., Reston, Virginia, 1975.

Thornton, E.B., & Calhoun, R.J., "Spectral Resolution of Breakwater Reflected Waves," ASCE Proceedings, Journal of Waterways, Harbors, and Coastal Engineering Division, Vol. 98, November, 1972, pp. 443-460.

U.S. Army Coastal Engineering Research Center, Shore Protection Manual, Volumes I, II, III, Superintendent of Documents, U. S. Government Printing Office, Washington, D.C., 1973.

Wason, M.T., Parametric Estimation, McGraw-Hill Book Co., N.Y., 1970.

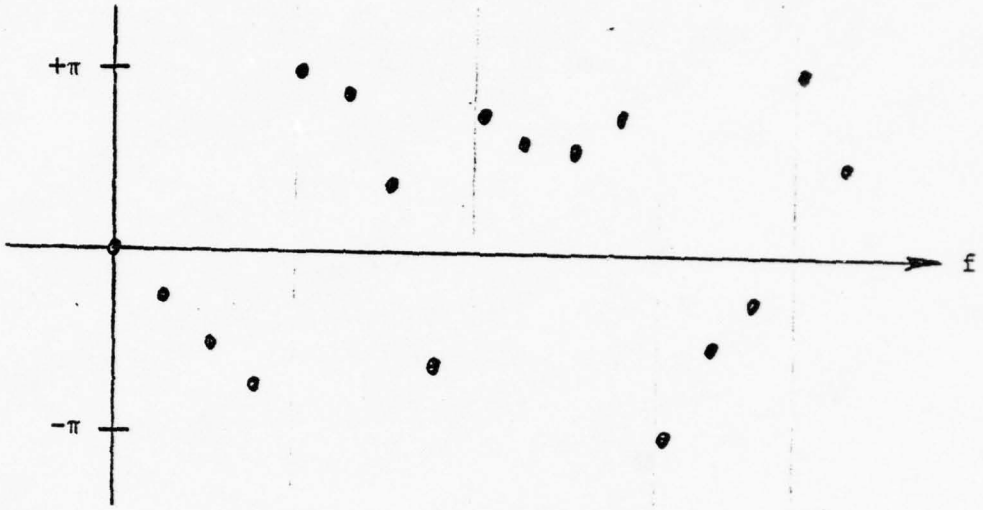

Figure 1. Sample Raw Phase Plot

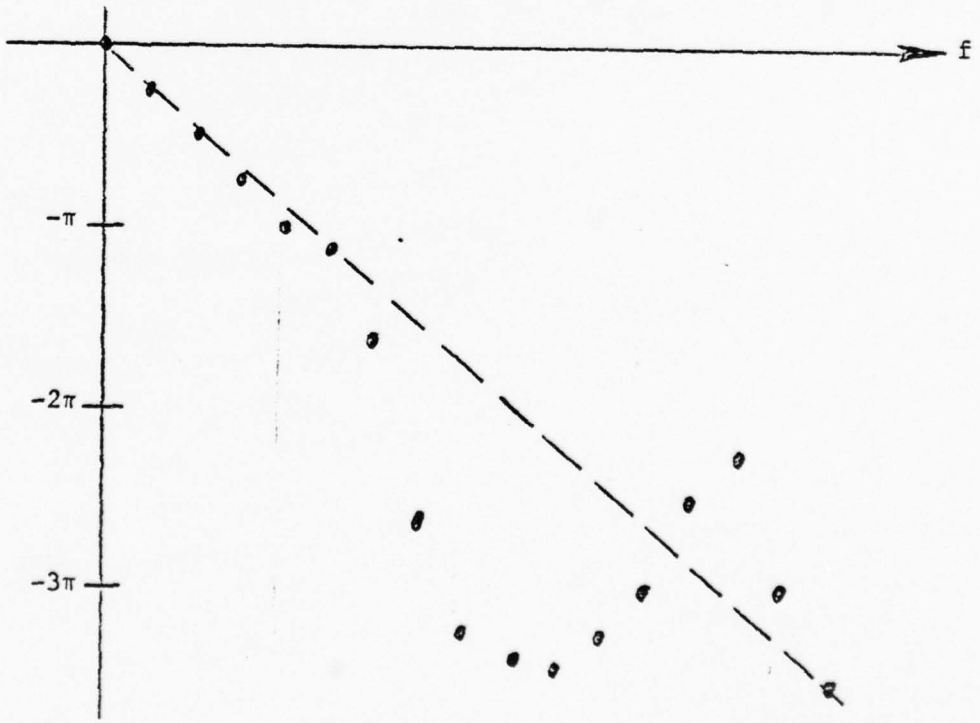

Figure 2. Sample Unwrapped Phase Plot

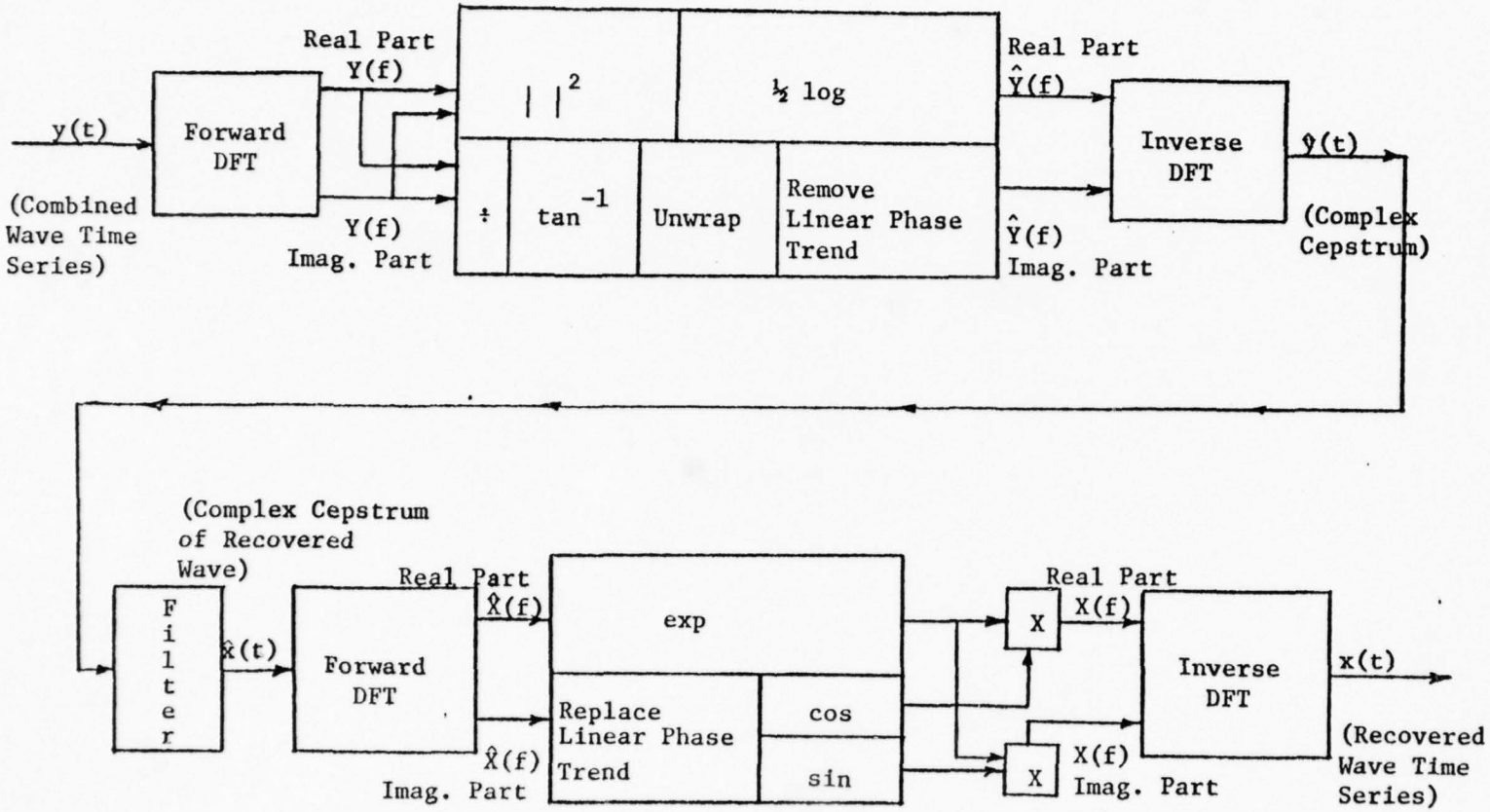

Figure 3. Wave Recovery Algorithm

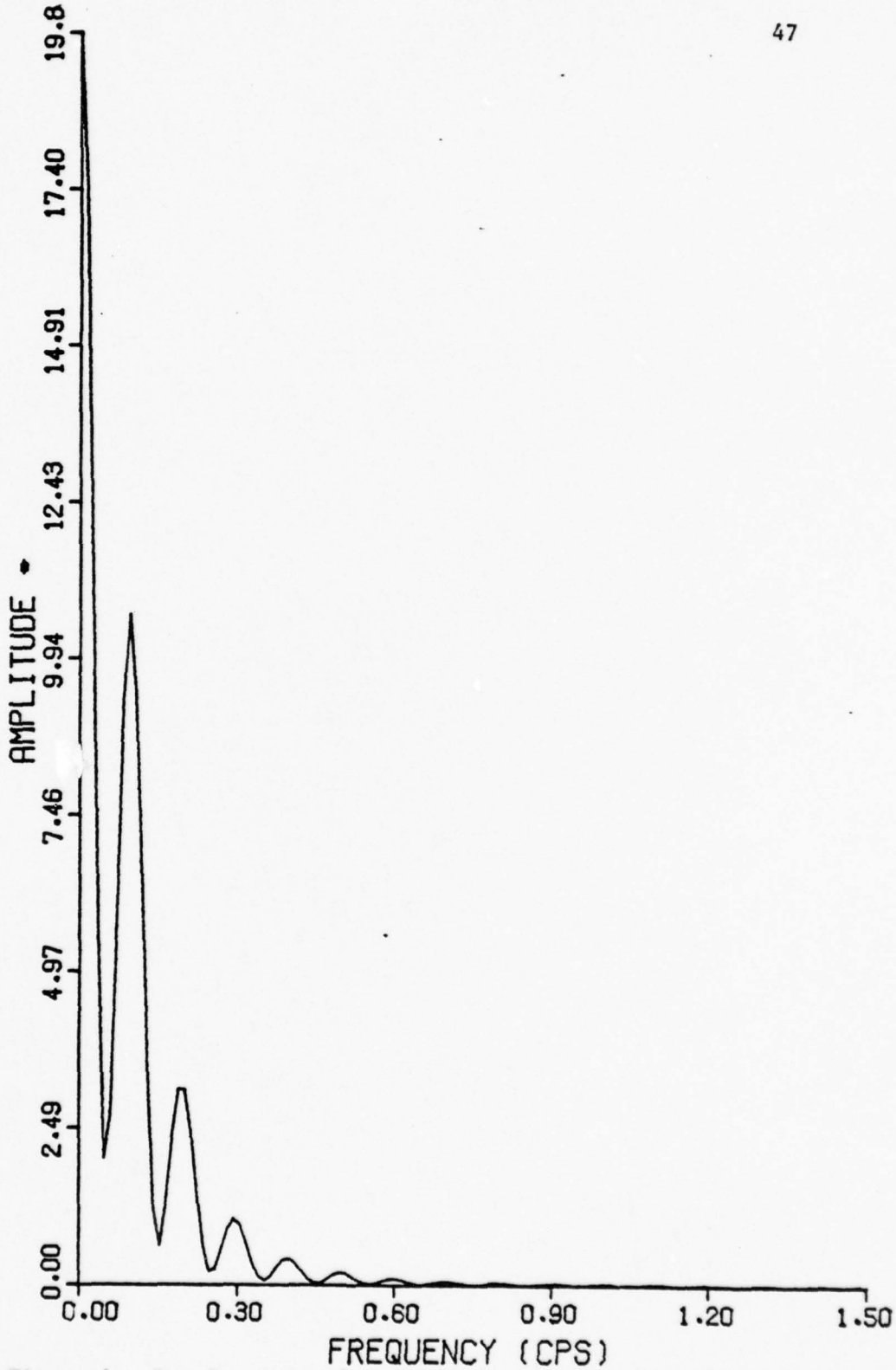

Figure 4. Raw Spectrum of Combined Exponential Signal

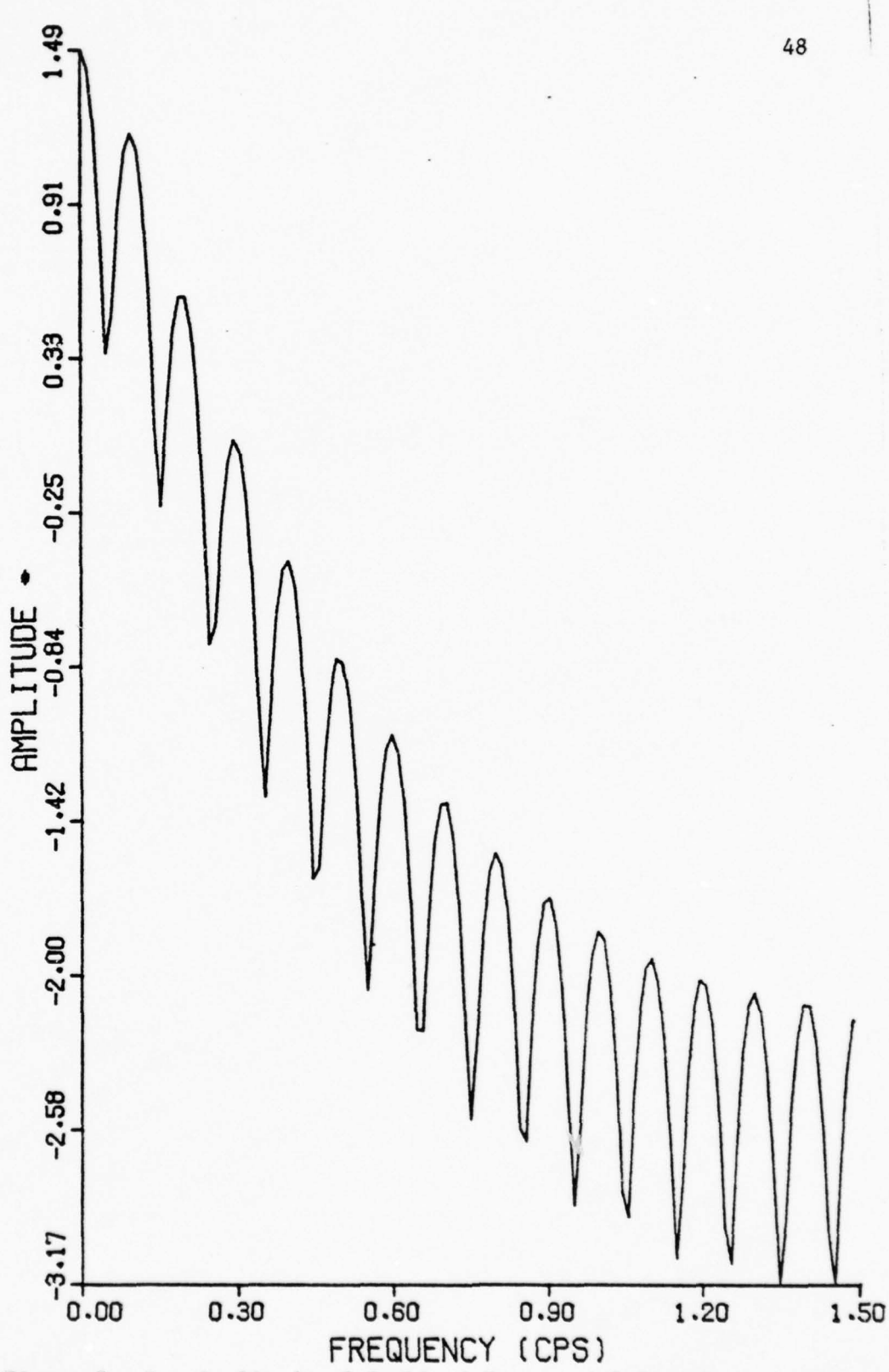

Figure 5. Log Amplitude of Combined Exponential Signal

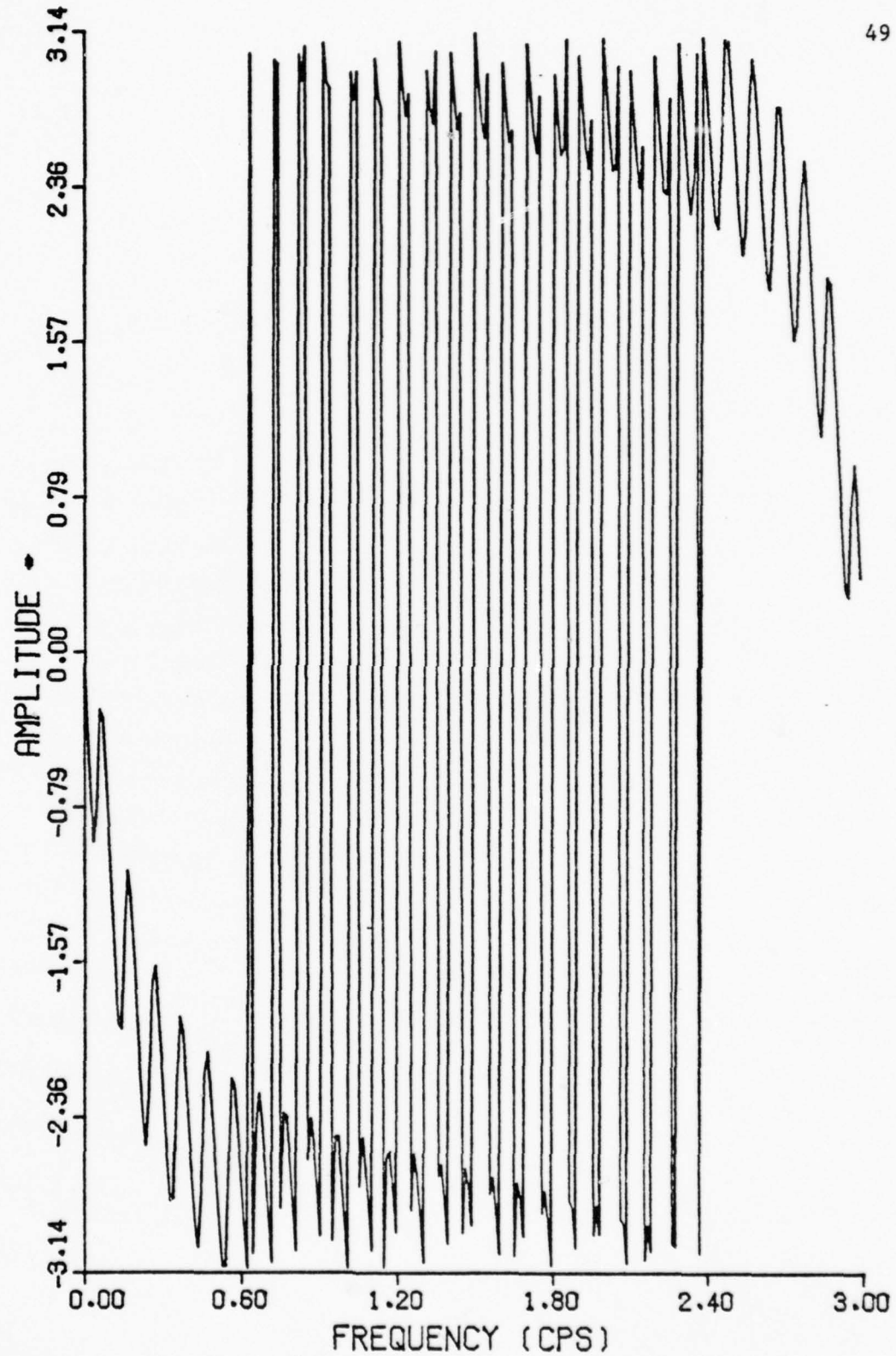

Figure 6. Raw Phase of Combined Exponential Signal

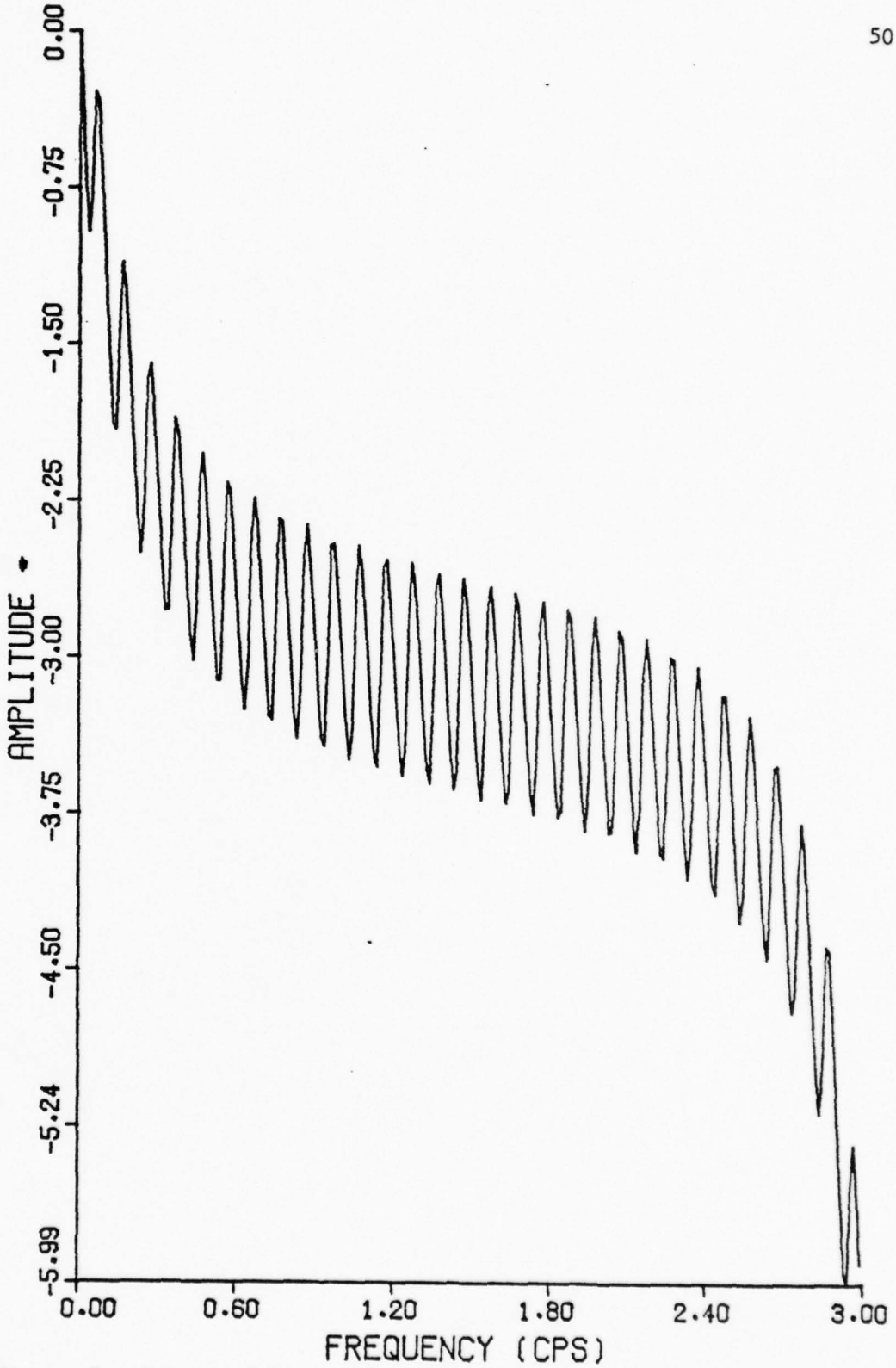

Figure 7. Unwrapped Phase of Combined Exponential Signal

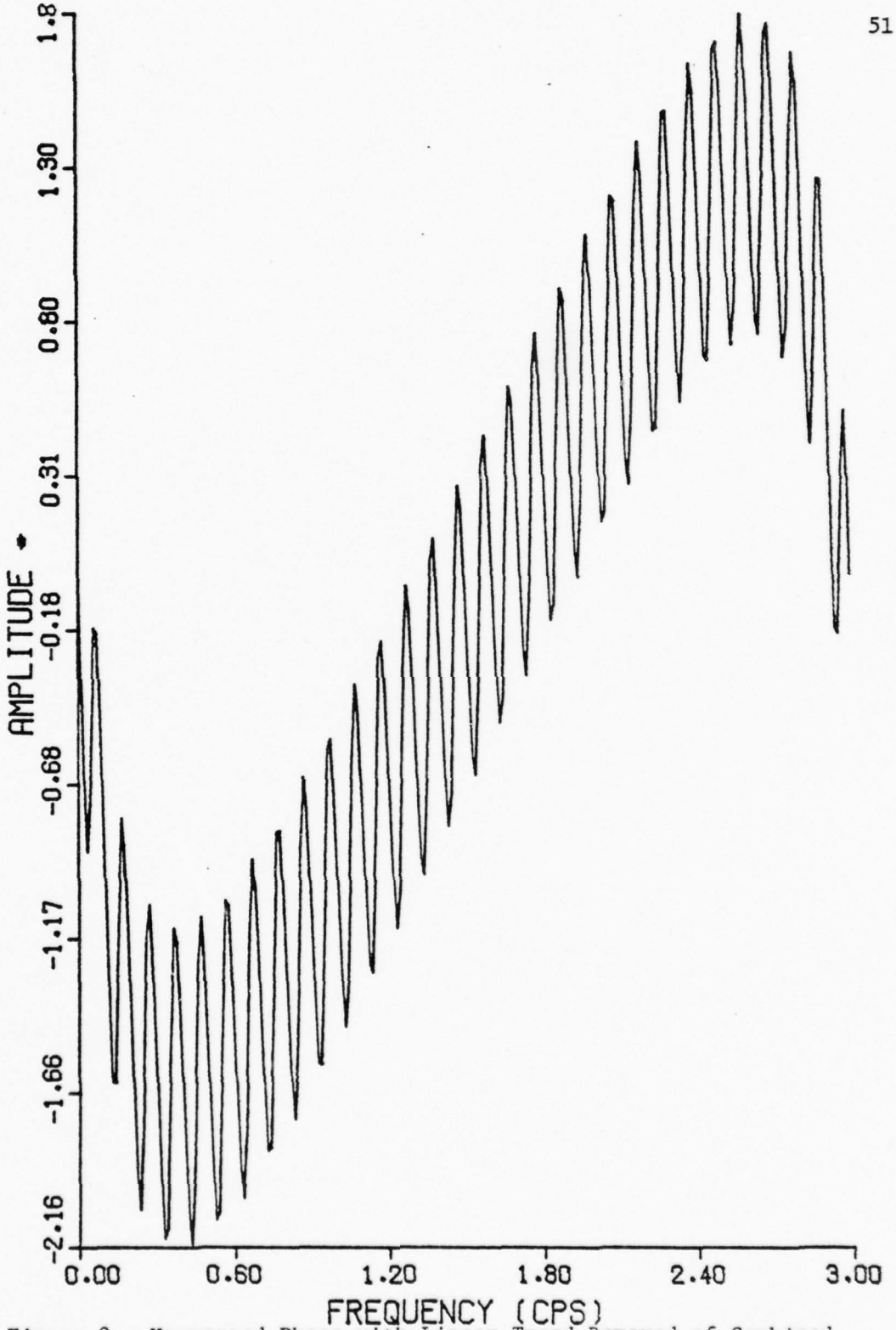

Figure 8. Unwrapped Phase with Linear Trend Removed of Combined Exponential Signal

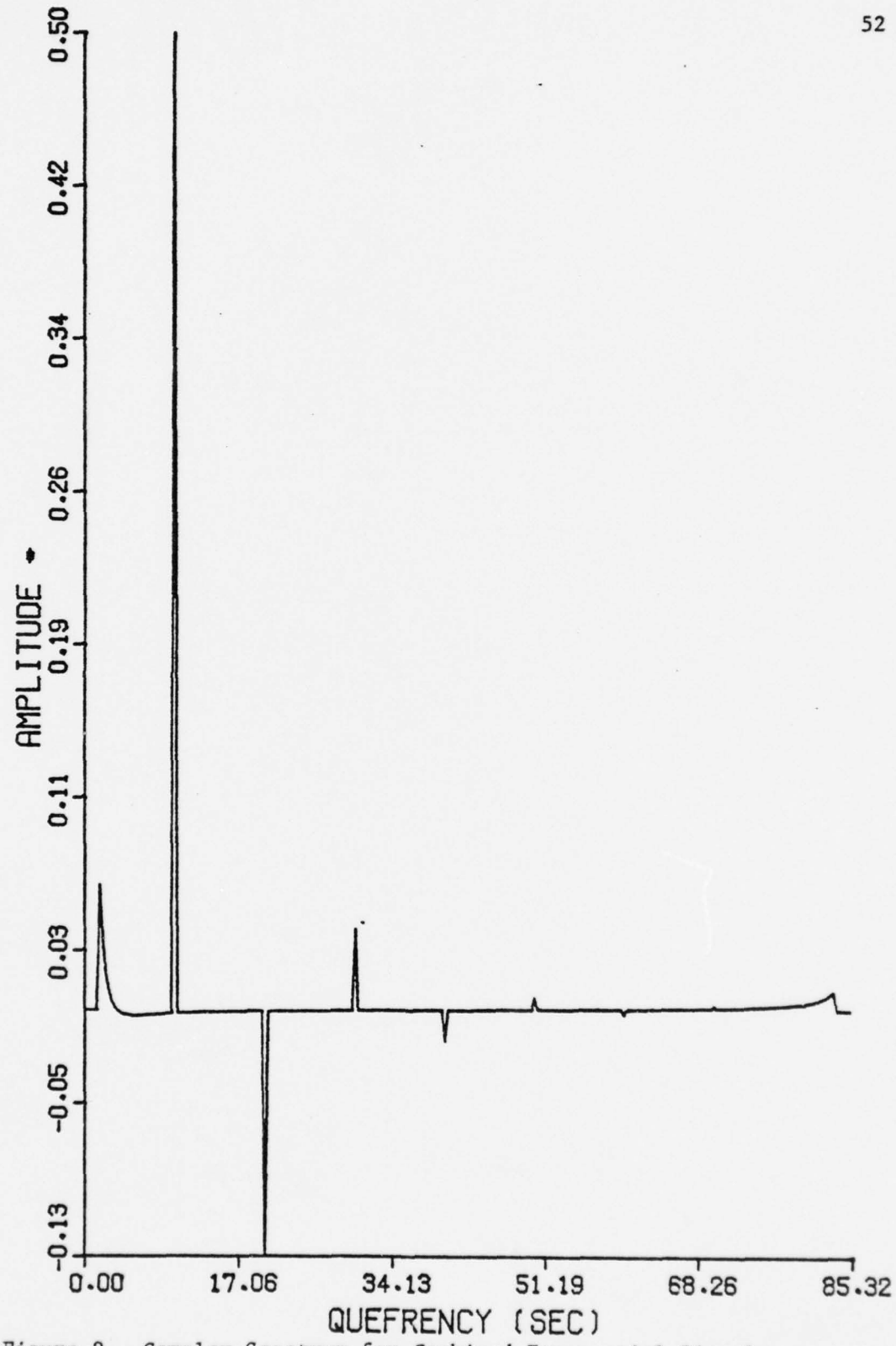

Figure 9. Complex Cepstrum for Combined Exponential Signal

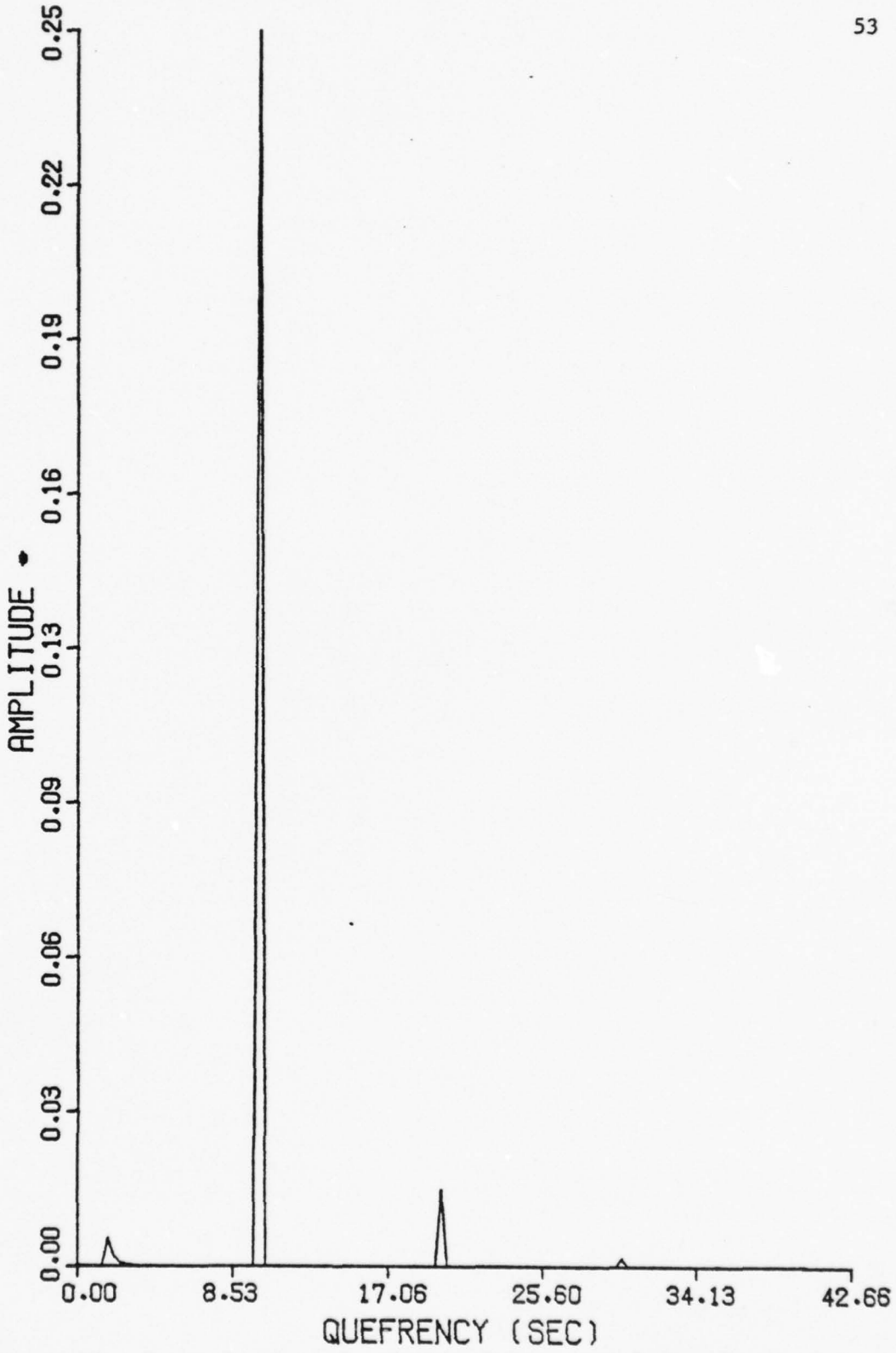

Figure 10. Power Cepstrum for Combined Exponential Signal

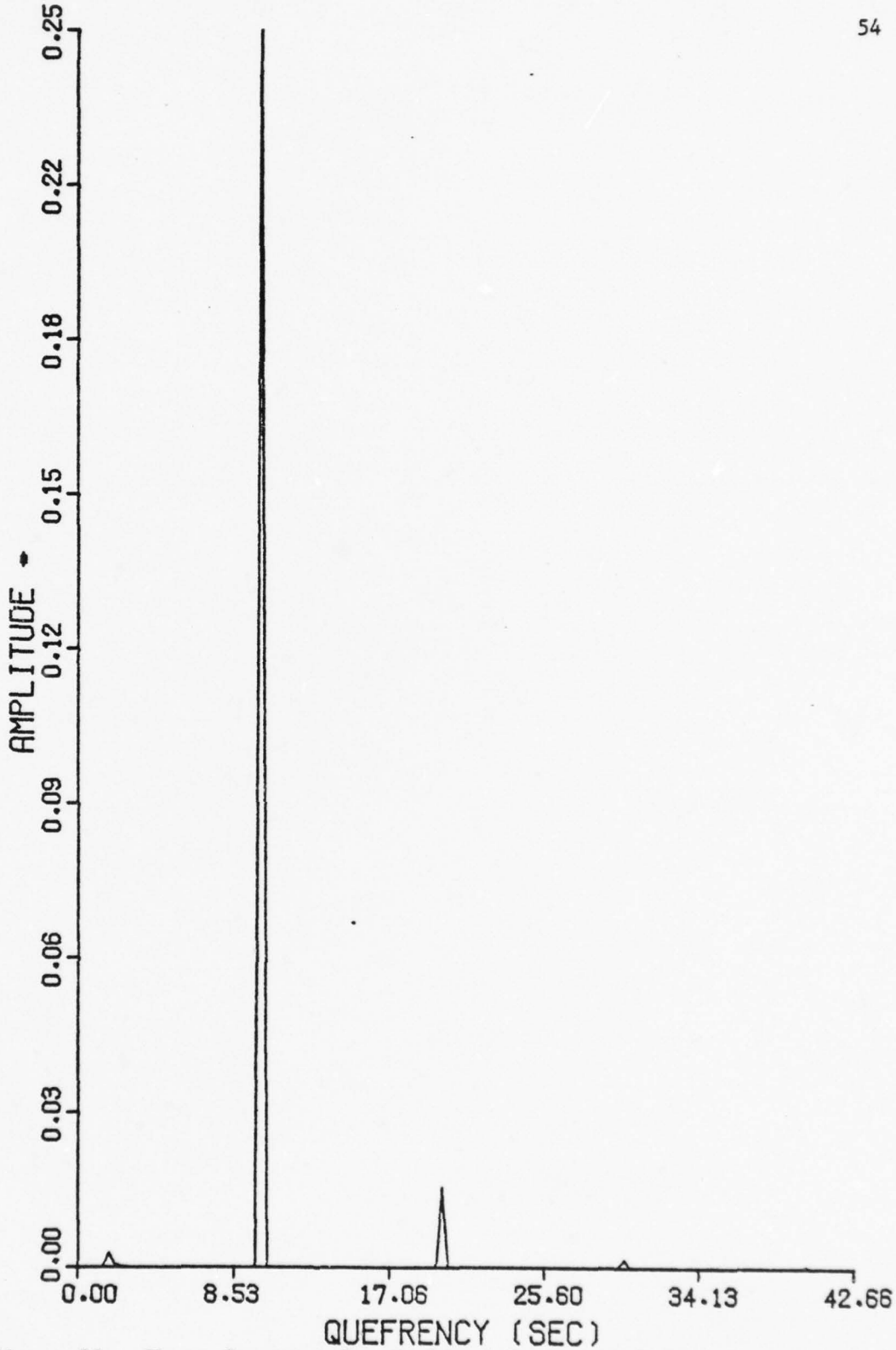

Figure 11. Phase Cepstrum for Combined Exponential Signal

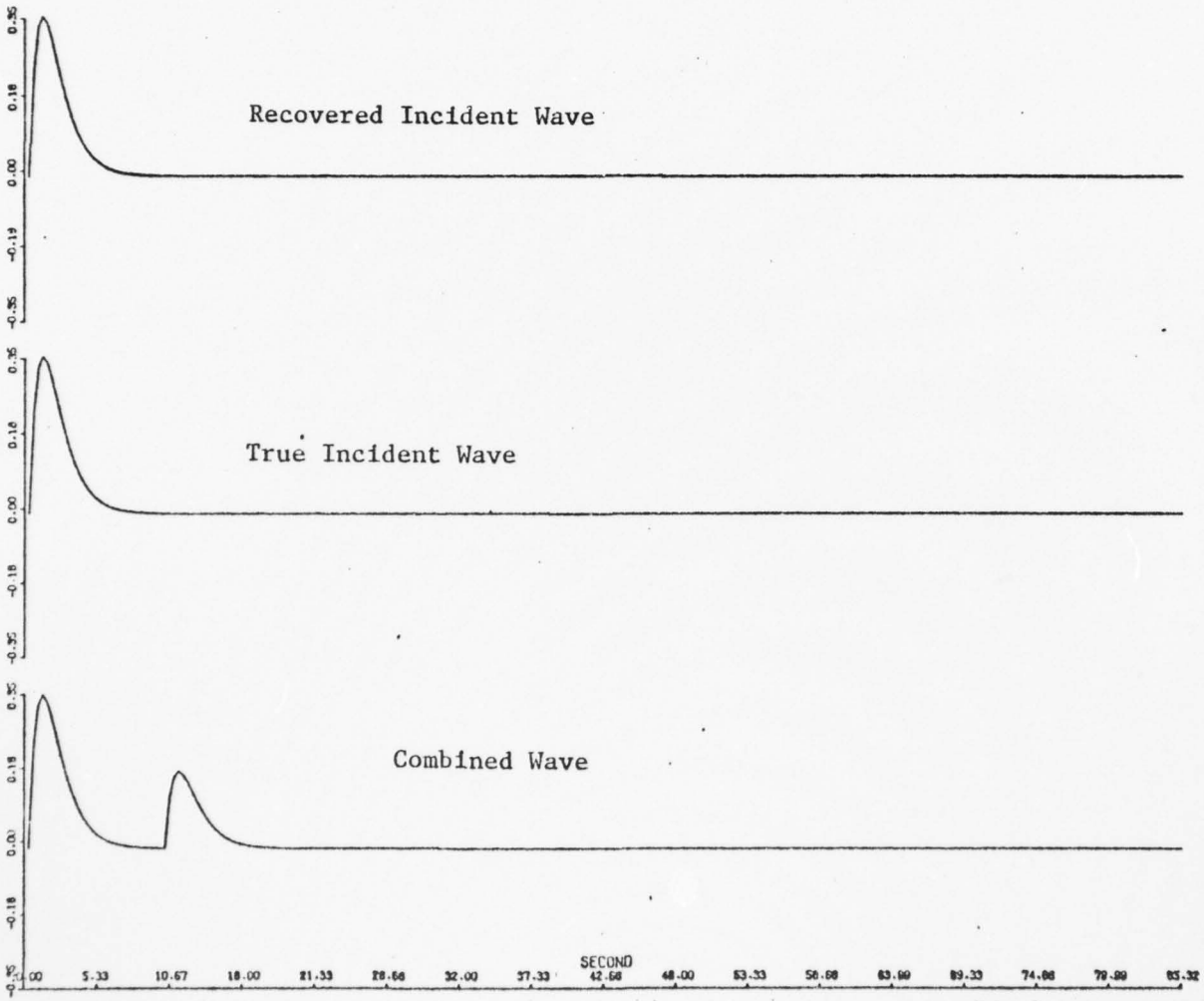

Figure 12. Recovered Incident, True Incident and Combined Wave Time Series for Exponential Signal

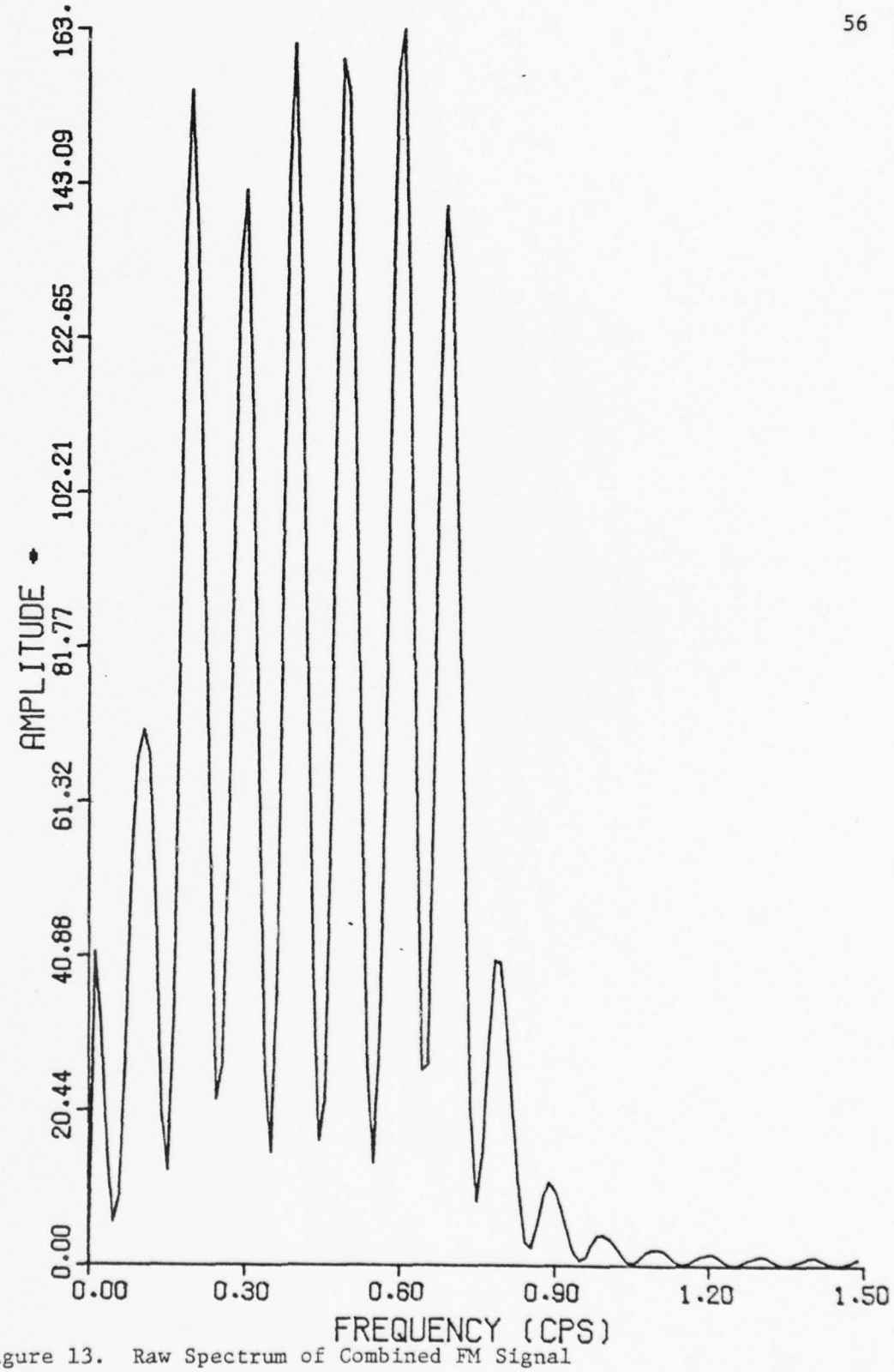

Figure 13. Raw Spectrum of Combined FM Signal

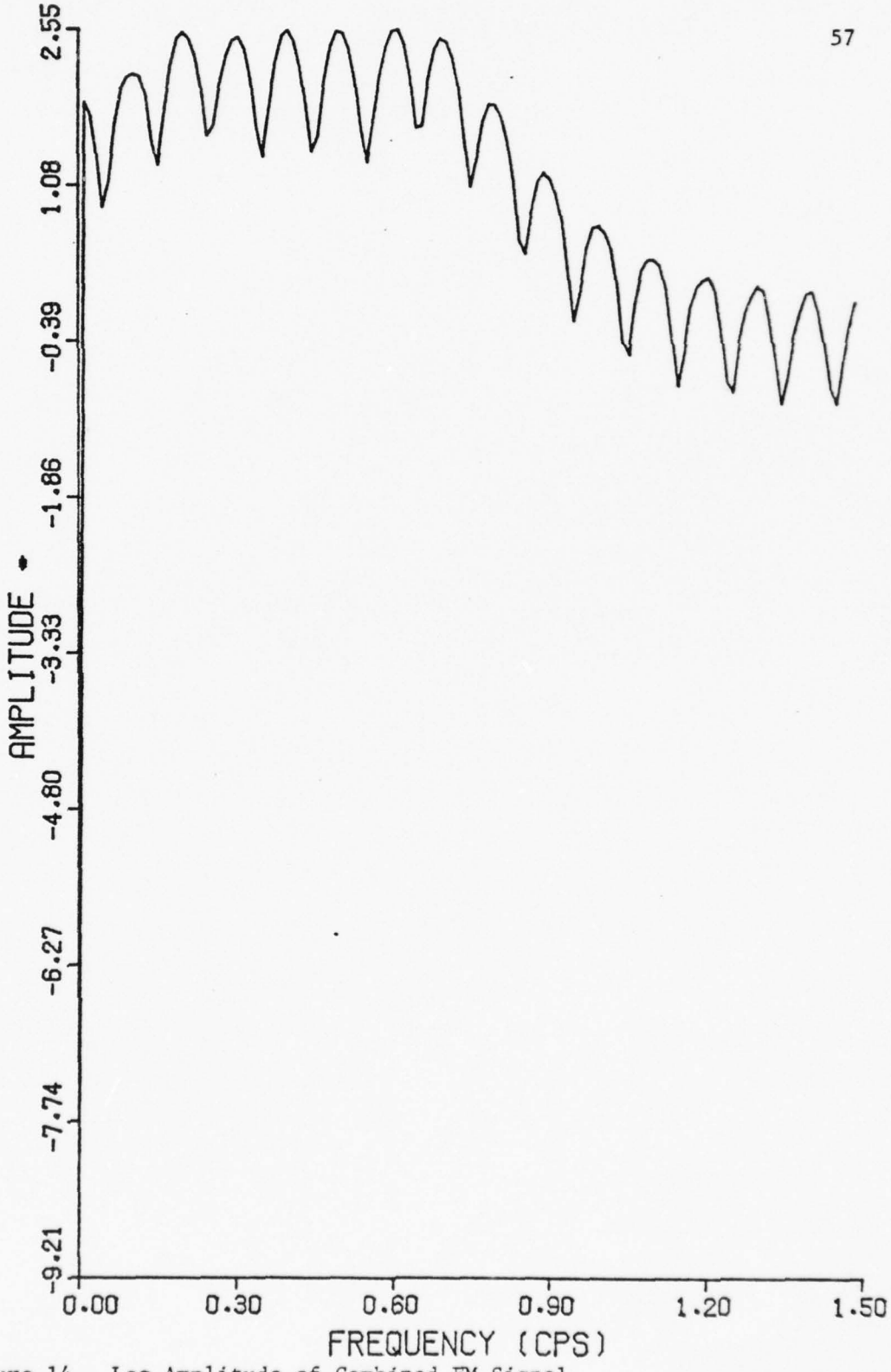

Figure 14. Log Amplitude of Combined FM Signal

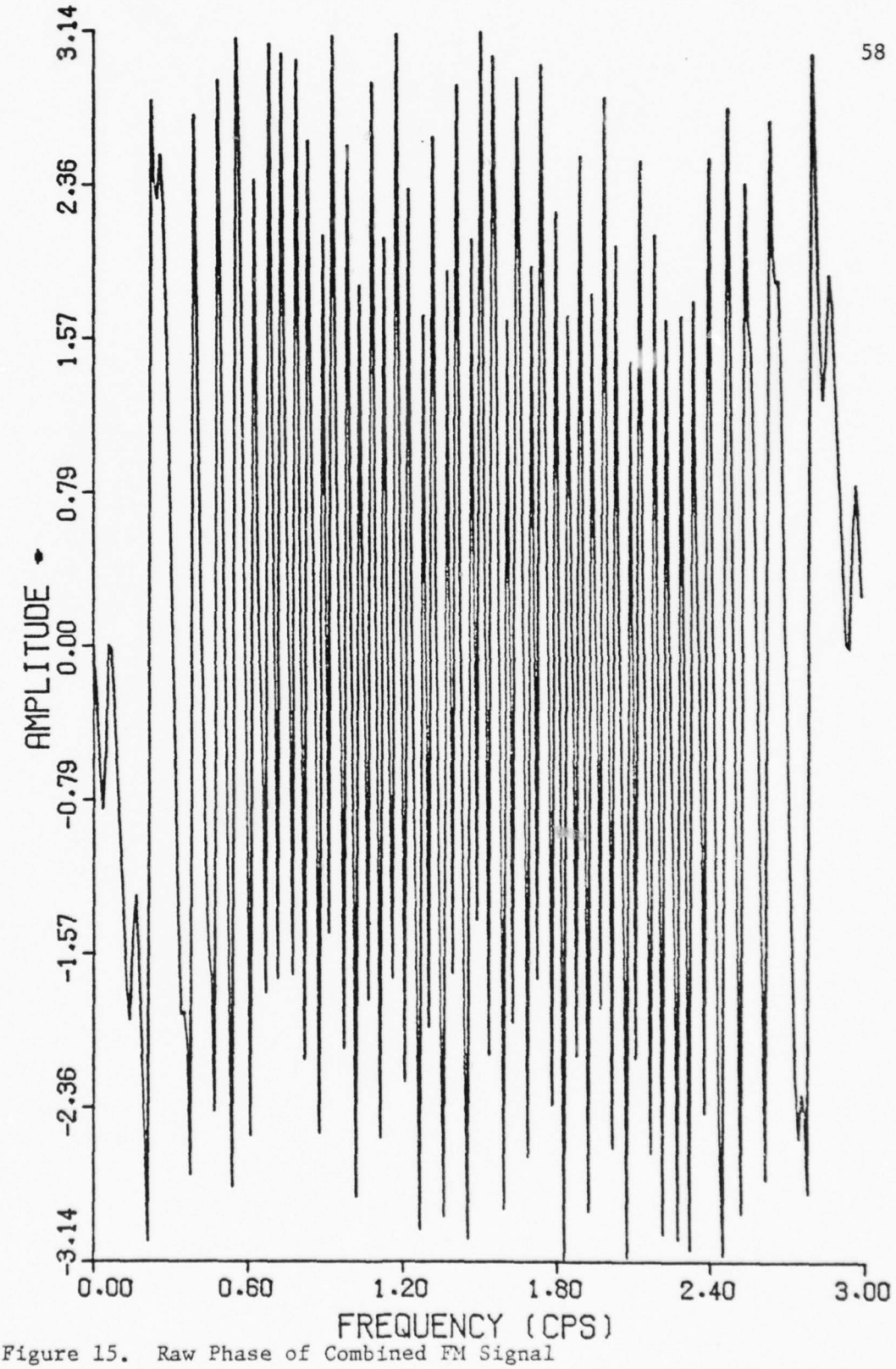

Figure 15. Raw Phase of Combined FM Signal

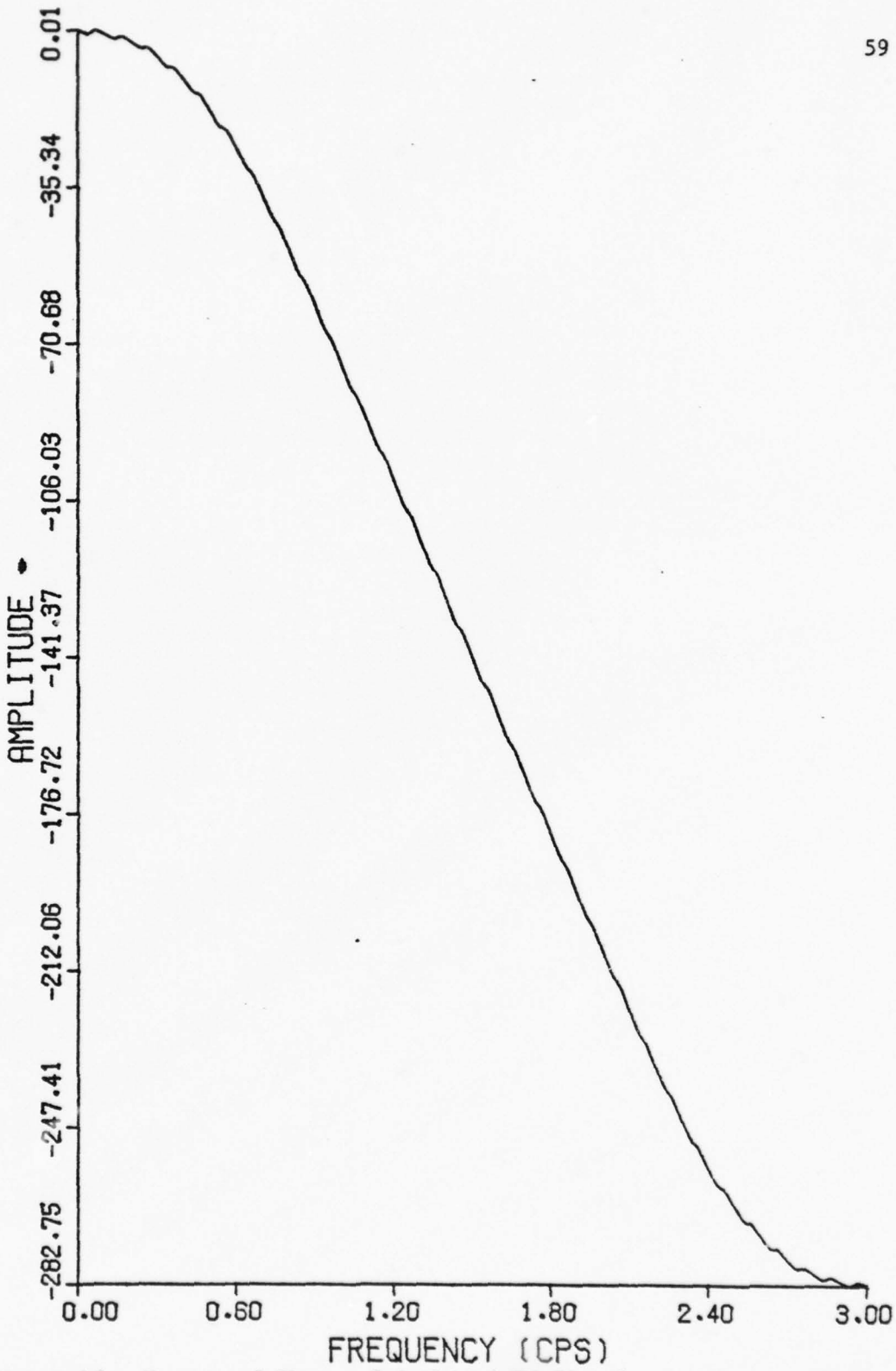

Figure 16. Unwrapped Phase of Combined FM Signal

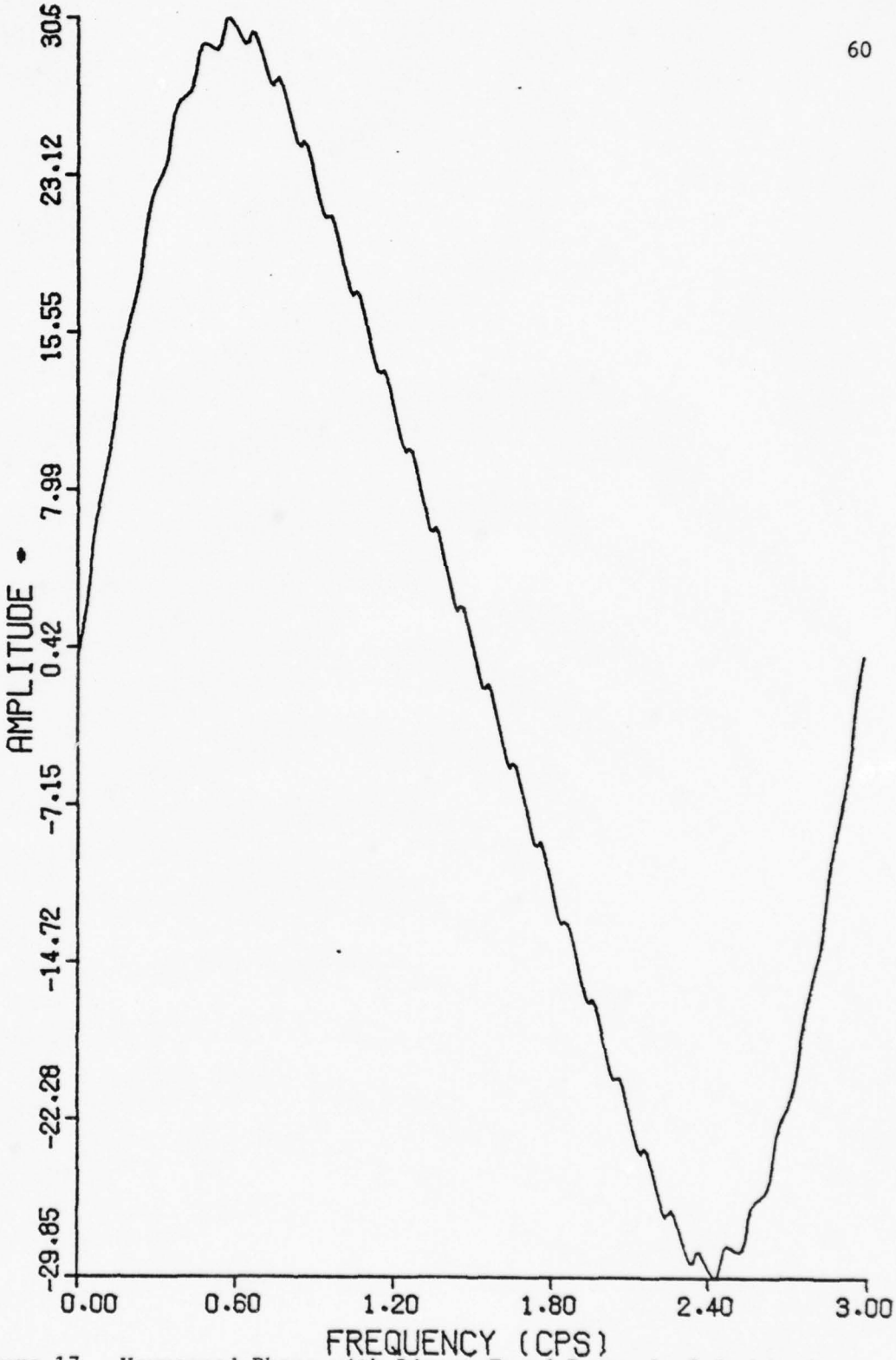

Figure 17. Unwrapped Phase with Linear Trend Removed of Combined FM Signal

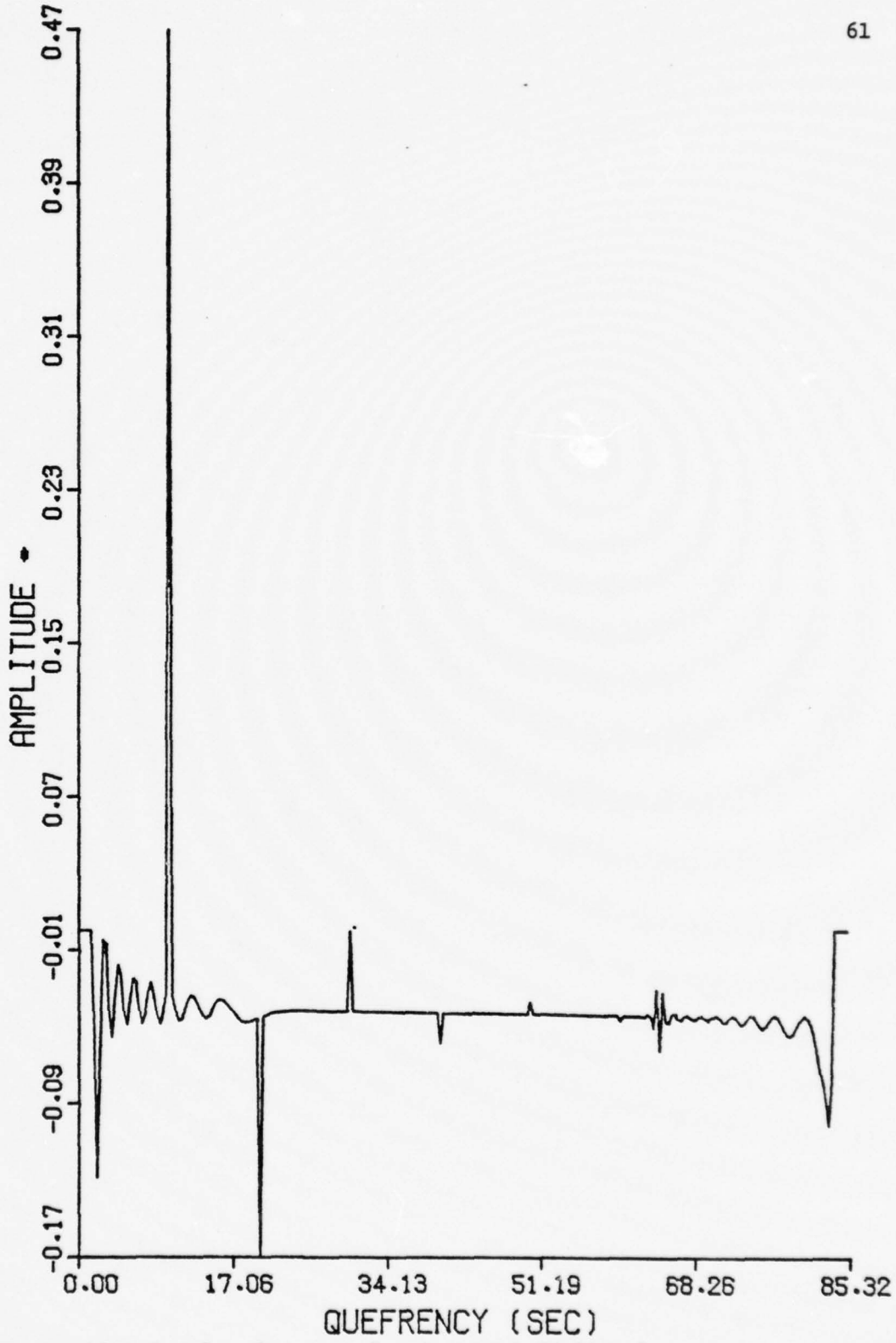

Figure 18. Complex Cepstrum for Combined FM Signal

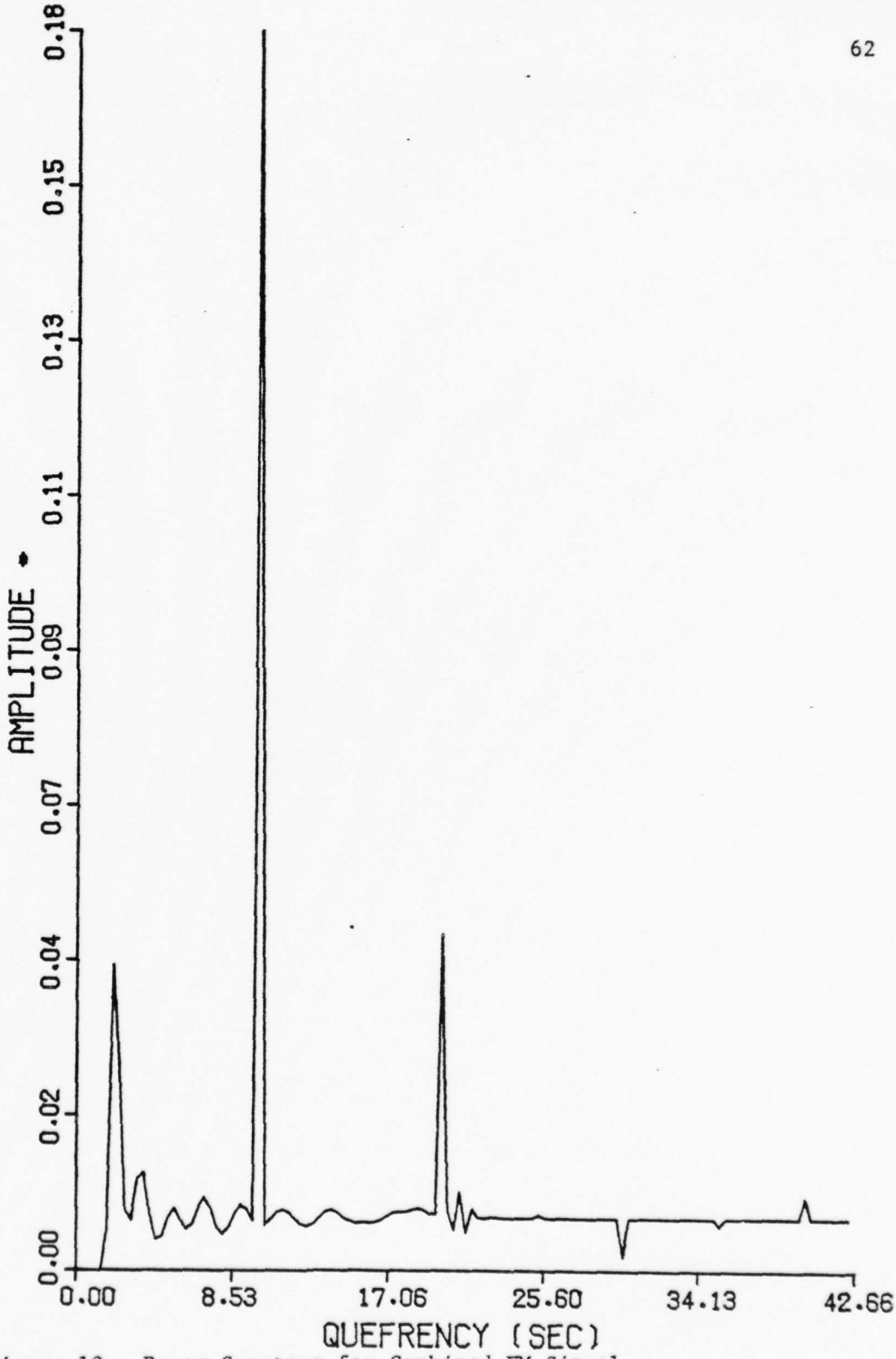

Figure 19. Power Cepstrum for Combined FM Signal

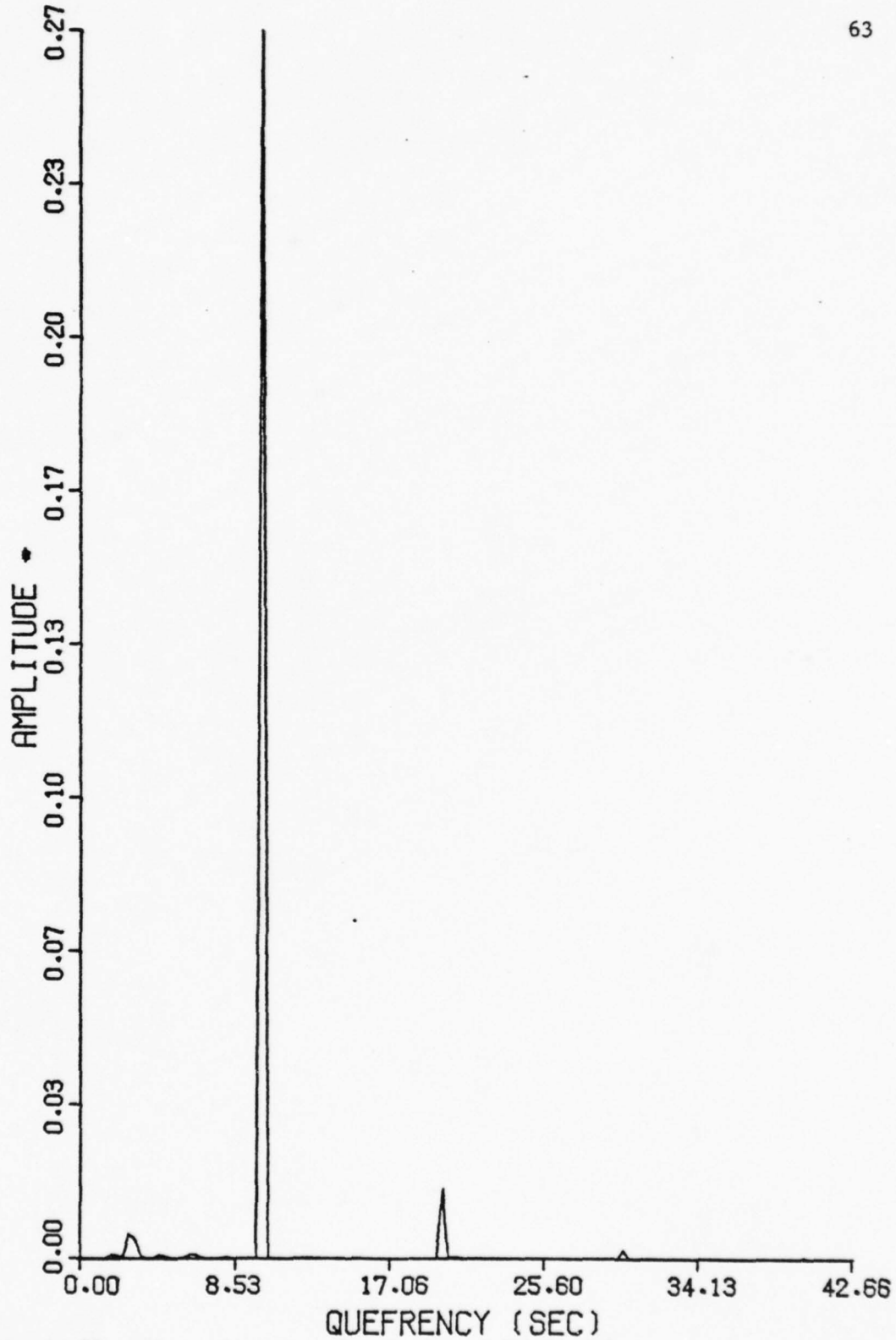

Figure 20. Phase Cepstrum for Combined FM Signal

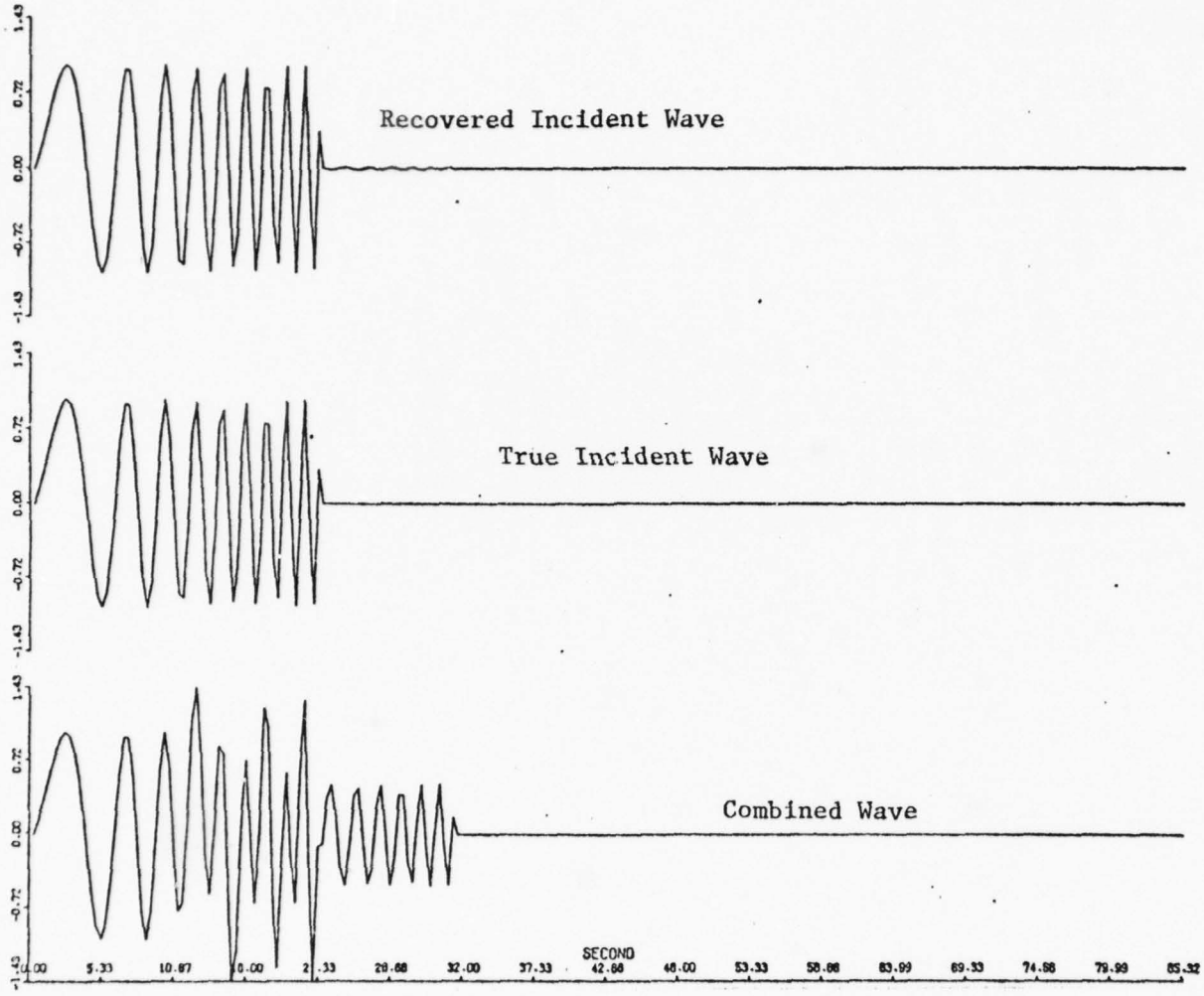

Figure 21. Recovered Incident, True Incident and Combined Wave Time Series for FM Signal

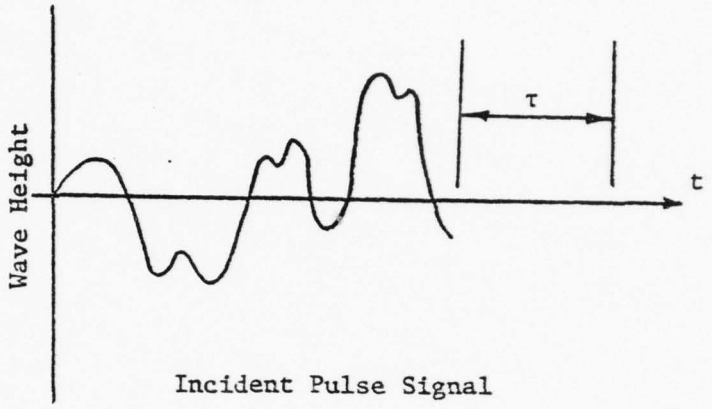

Incident Pulse Signal

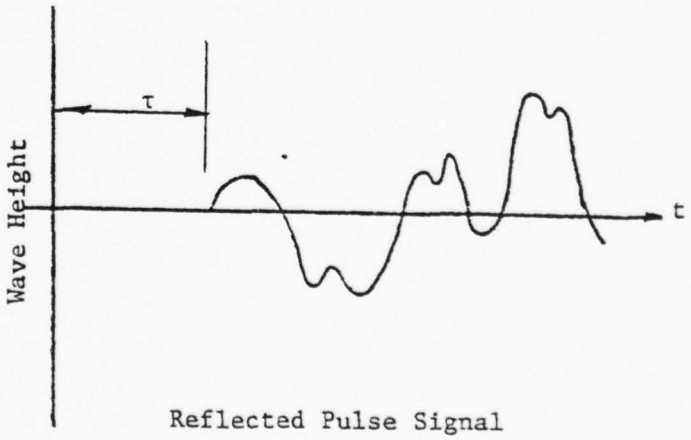

Reflected Pulse Signal

Figure 22. Sample Pulse Incident and Reflected Signal

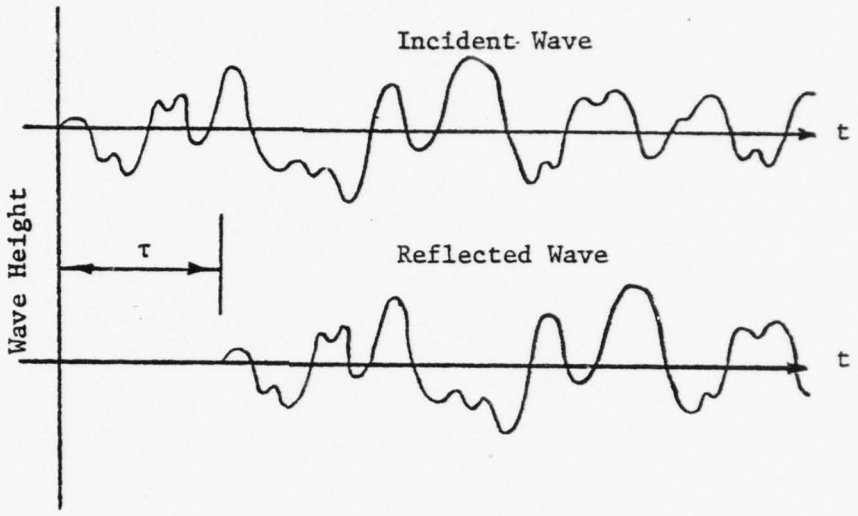

Figure 23. Sample Pulse-Shifted P-M Generated Incident and Reflected Wave

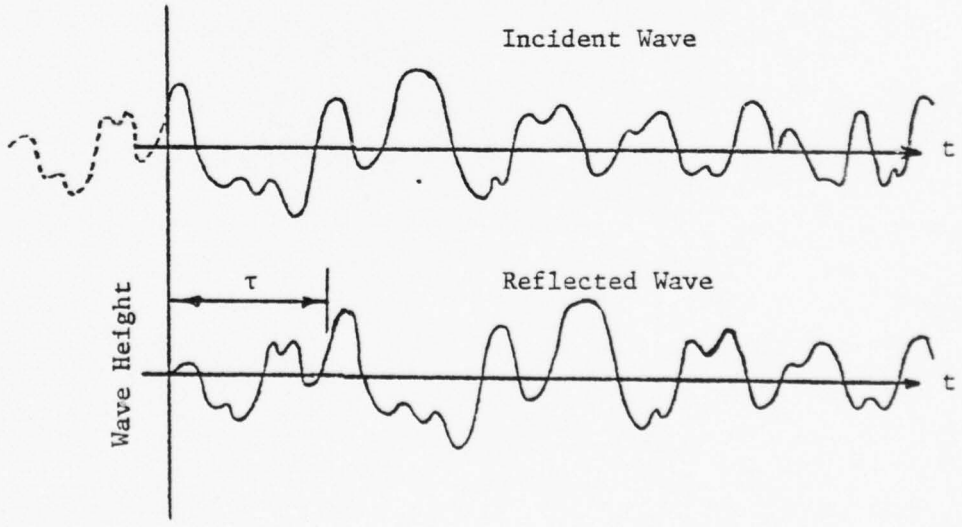

Figure 24. Sample Forward-Shifted P-M Generated Incident and Reflected Wave

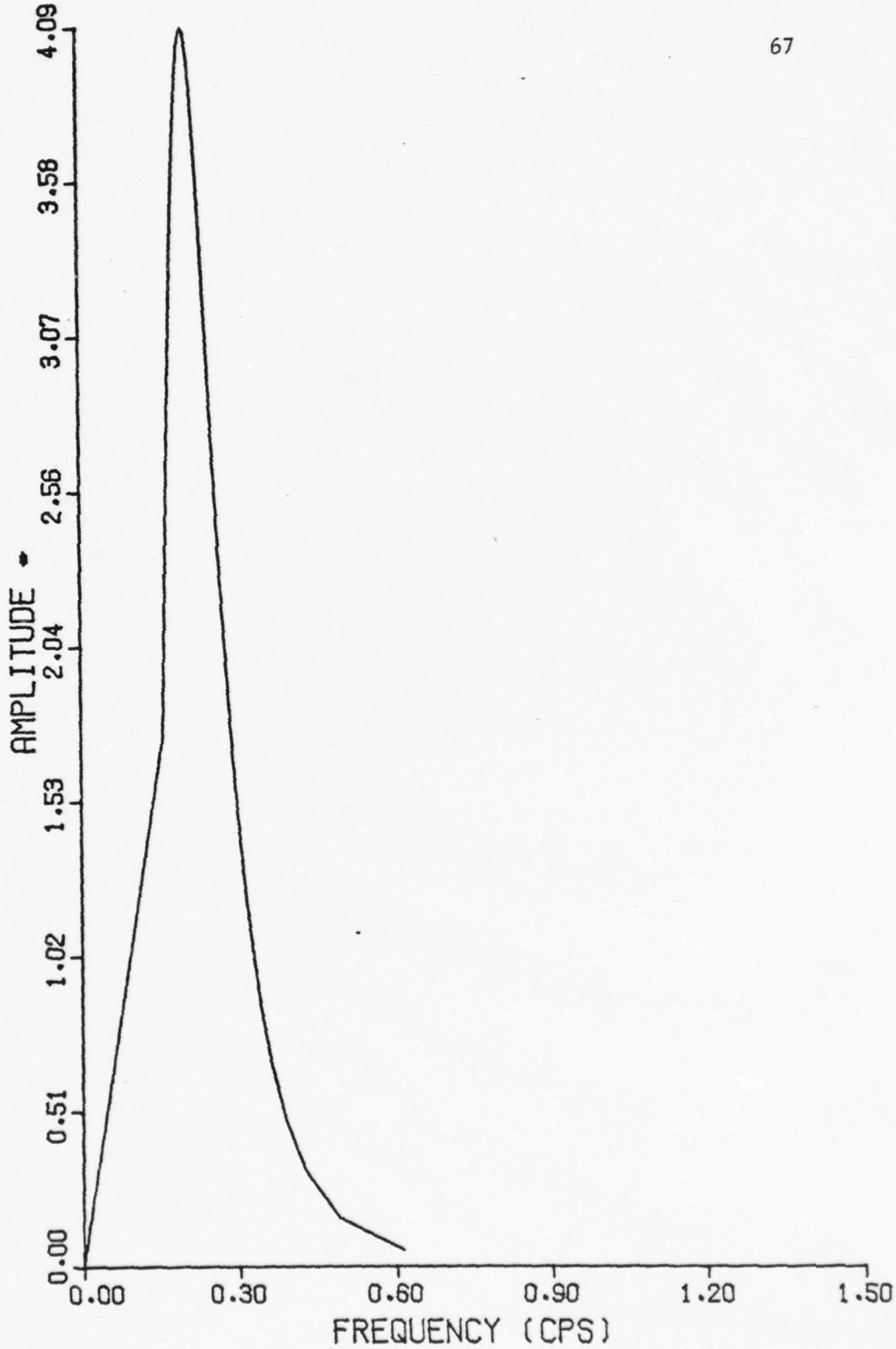

Figure 25. Original P-M Spectral Model

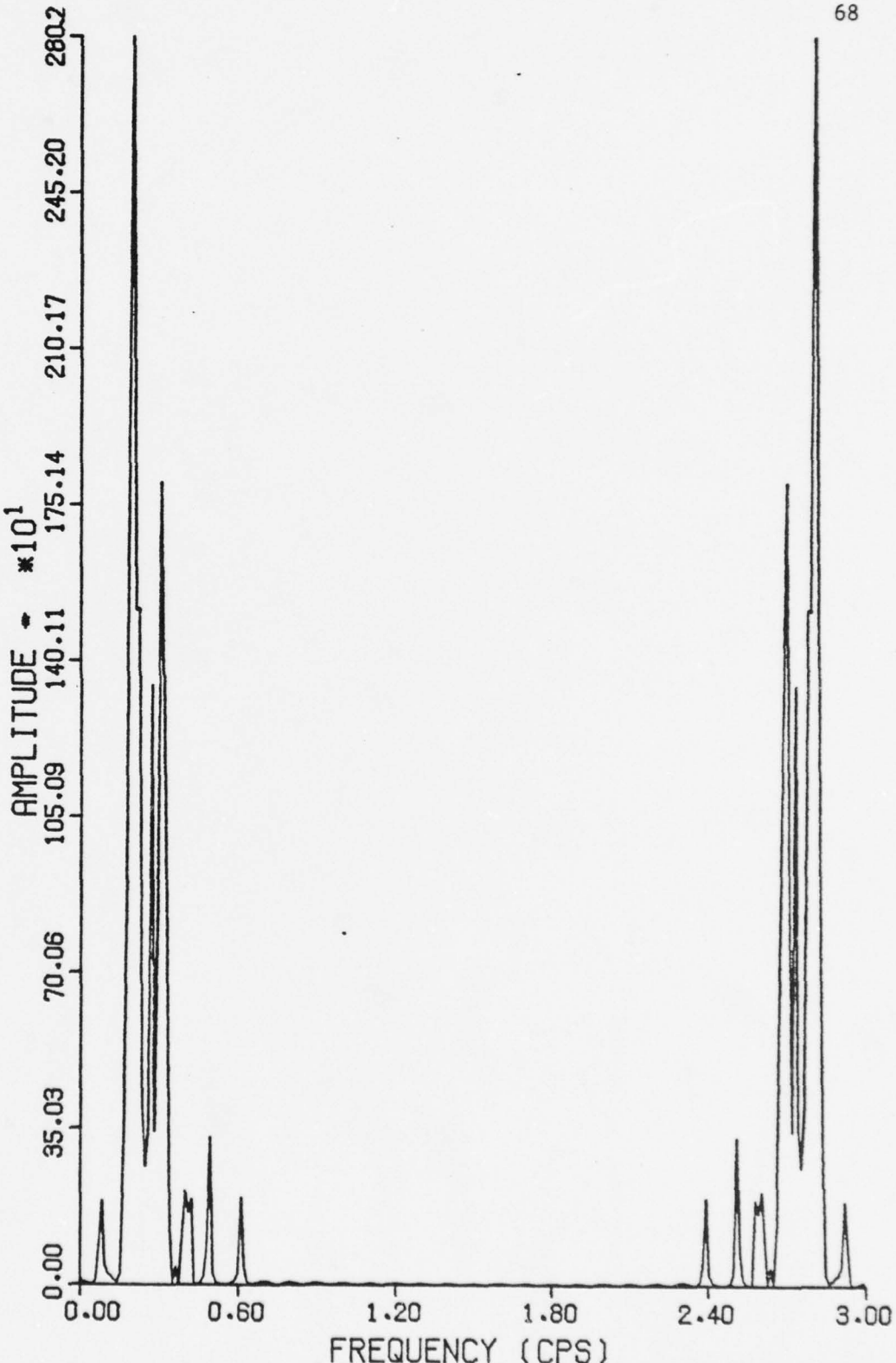

Figure 26. Raw Spectrum of Pulse-Shifted Combined P-M Generated Wave

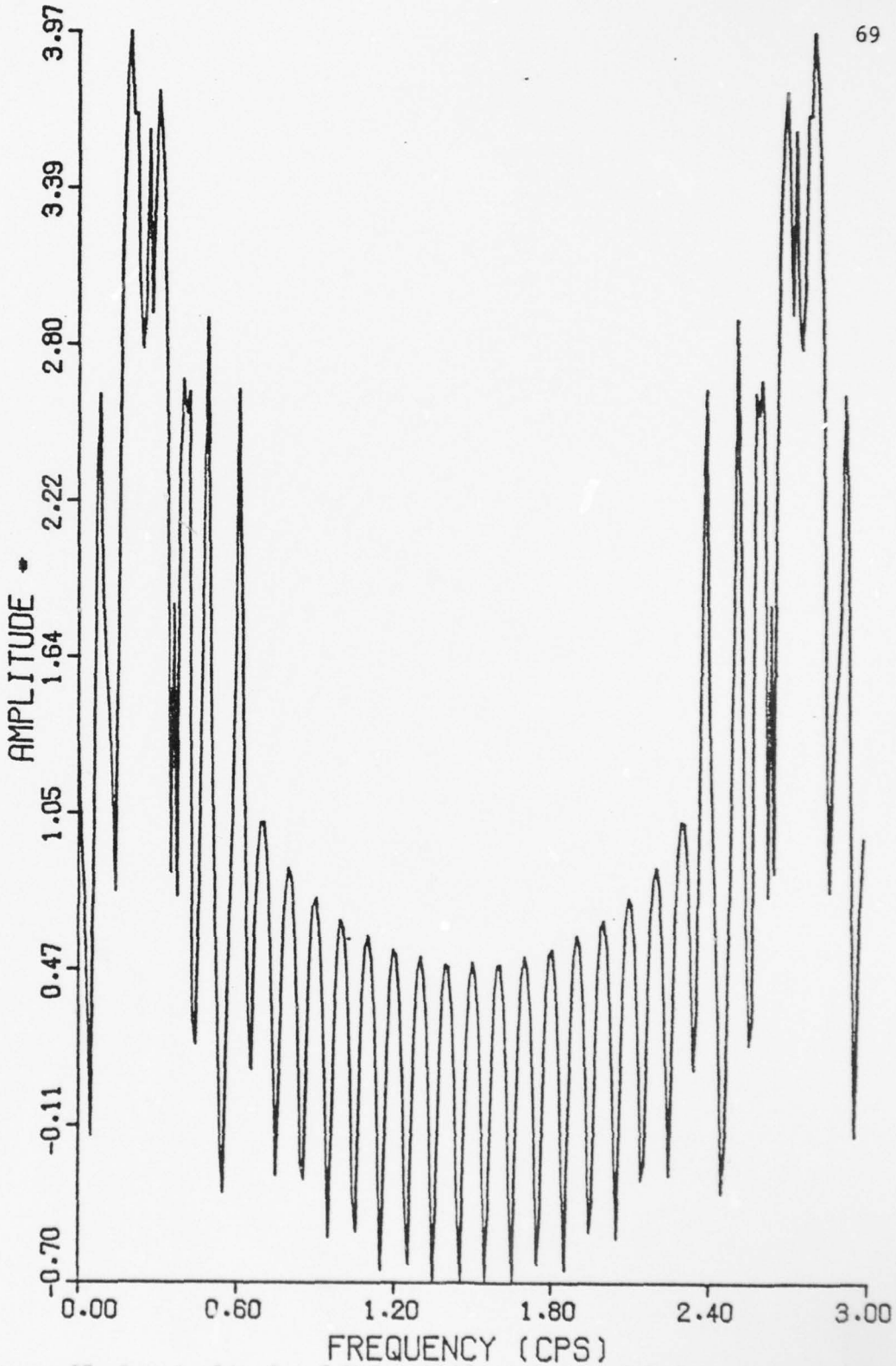

Figure 27. Log Amplitude of Pulse-Shifted Combined P-M Generated Wave

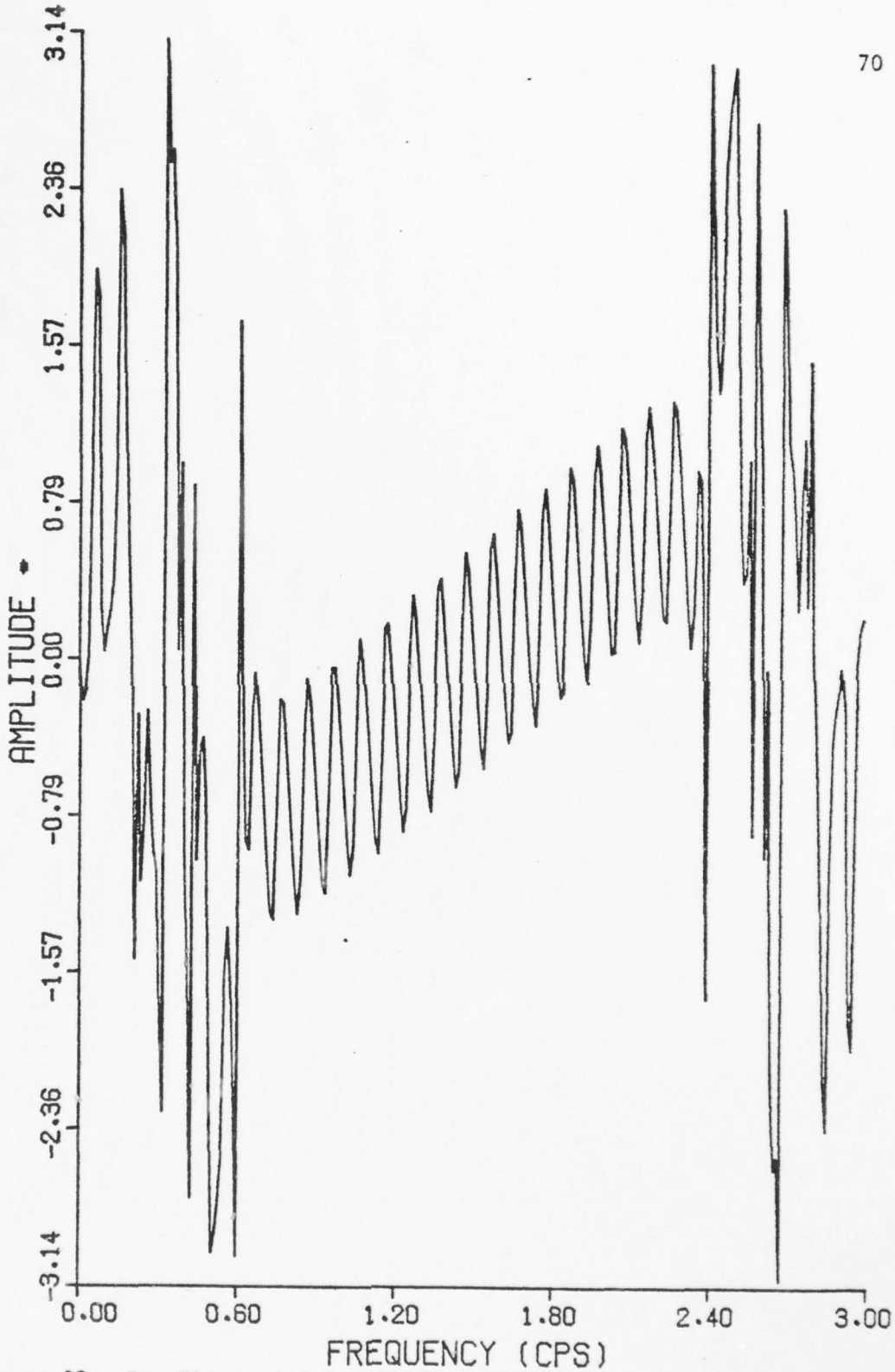

Figure 28. Raw Phase of Pulse-Shifted Combined P-M Generated Wave

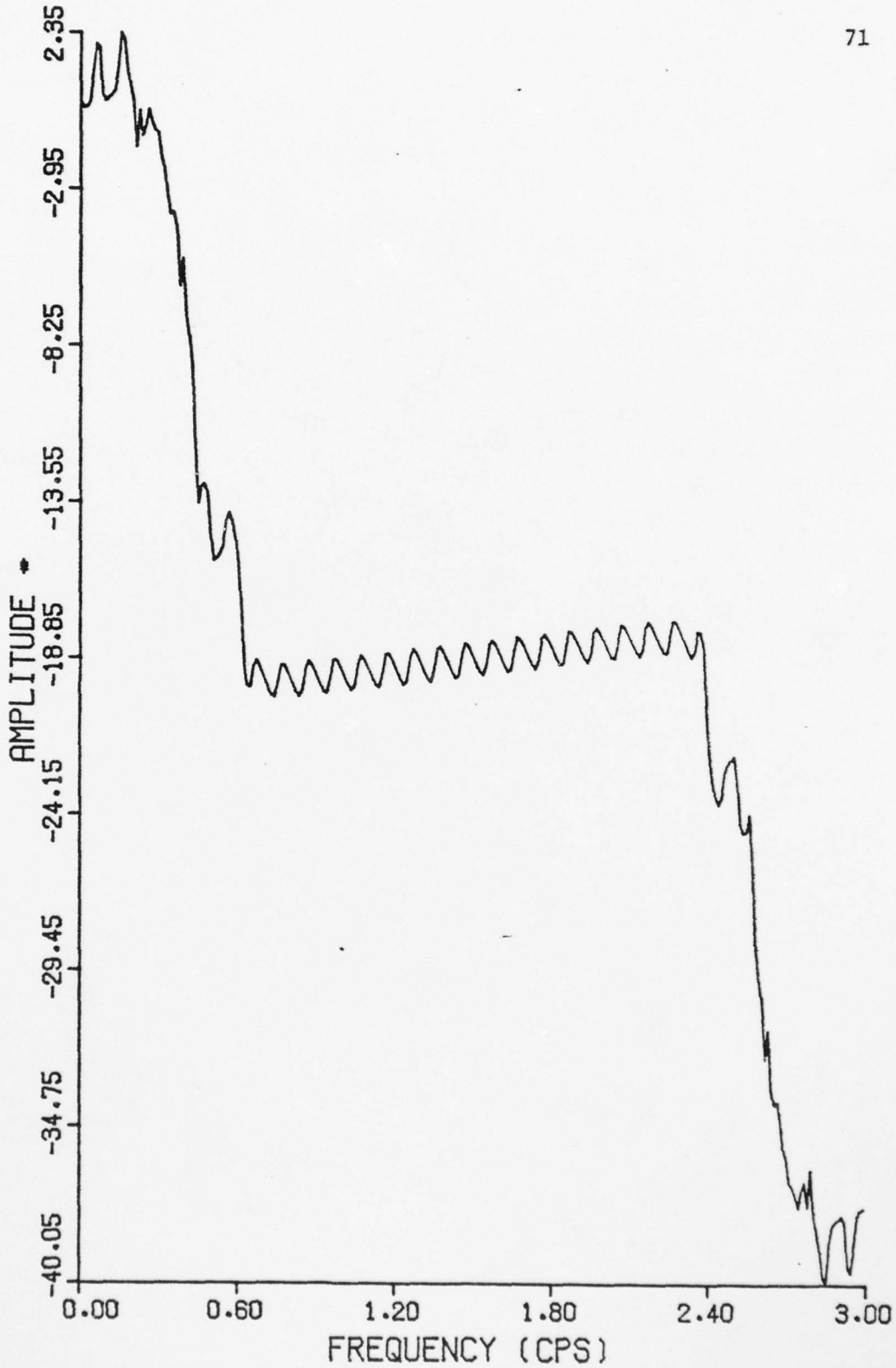

Figure 29. Unwrapped Phase of Pulse-Shifted Combined P-M Generated Wave

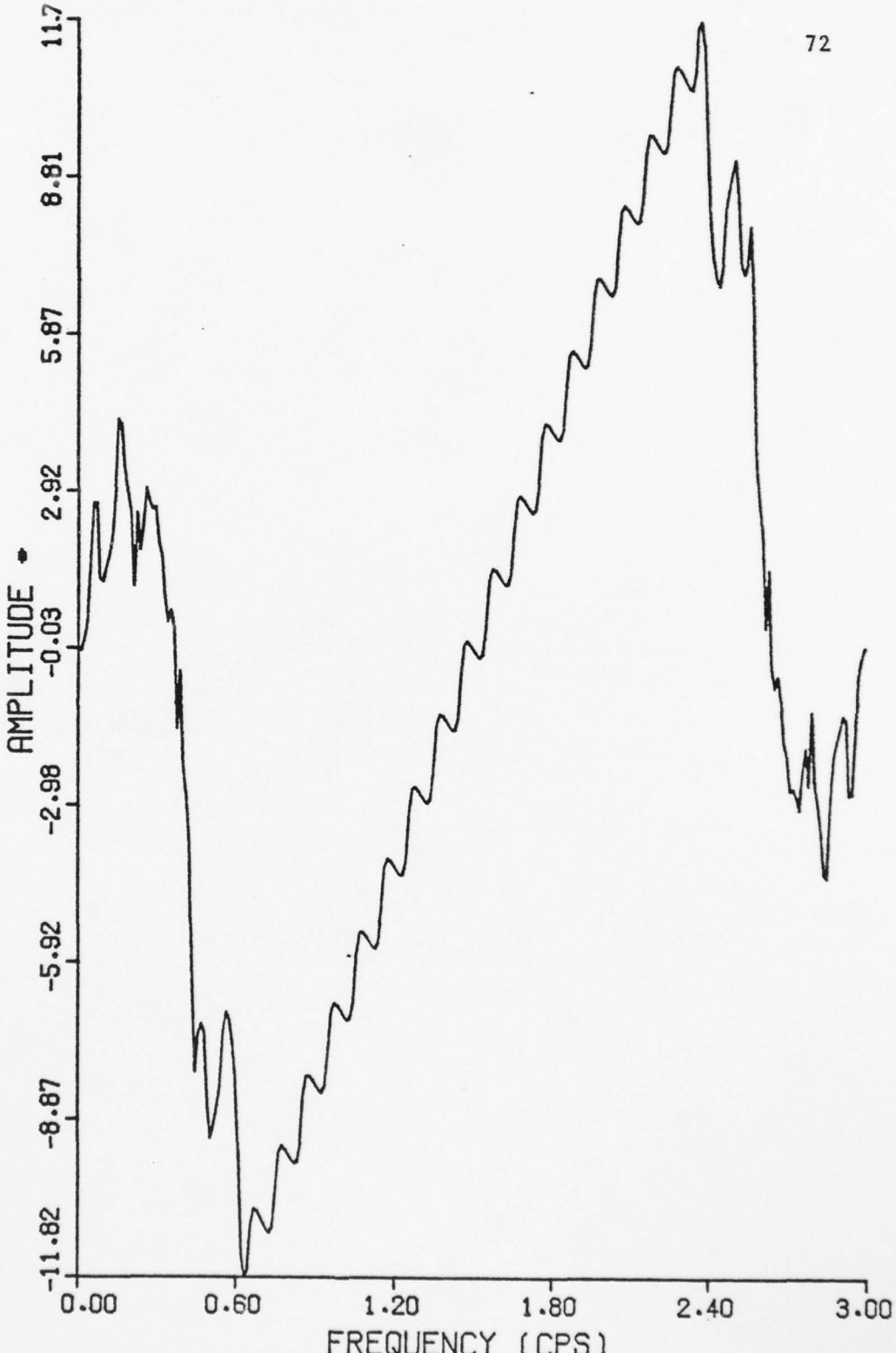

Figure 30. Unwrapped Phase with Linear Trend Removed of Pulse-Shifted Combined P-M Generated Wave

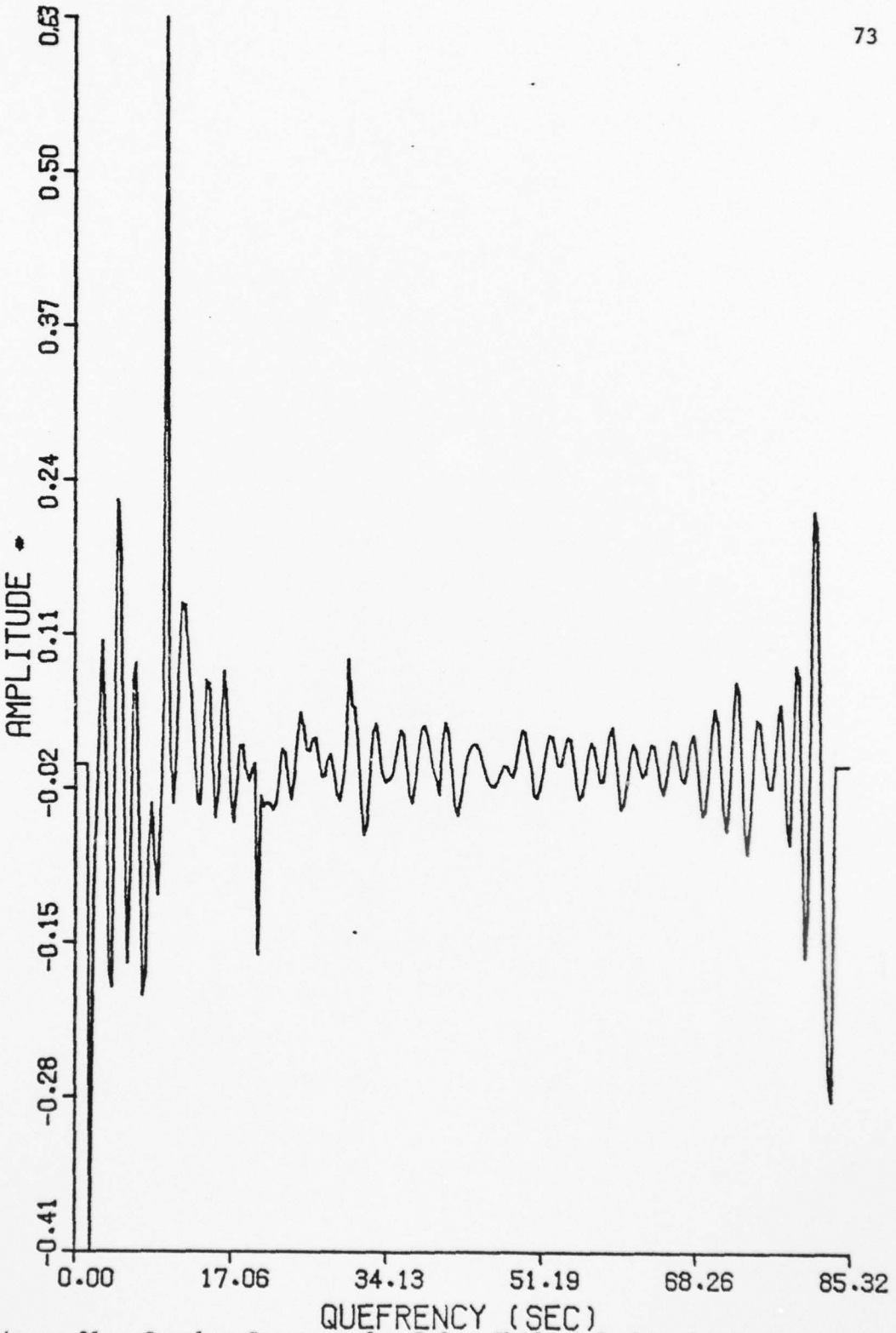

Figure 31. Complex Cepstrum for Pulse-Shifted Combined P-M Generated Wave

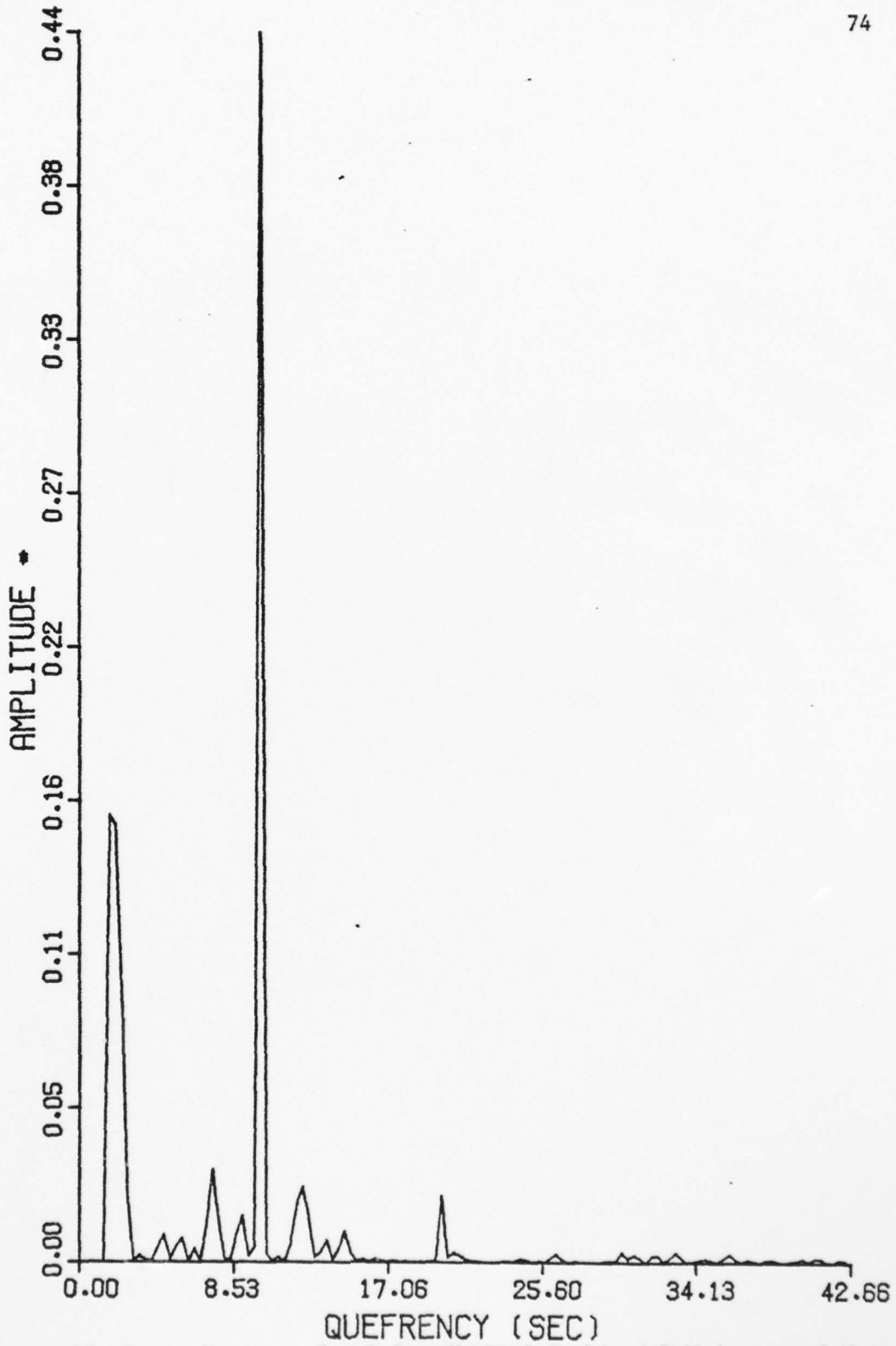

Figure 32. Power Cepstrum for Pulse-Shifted Combined P-M Generated Wave

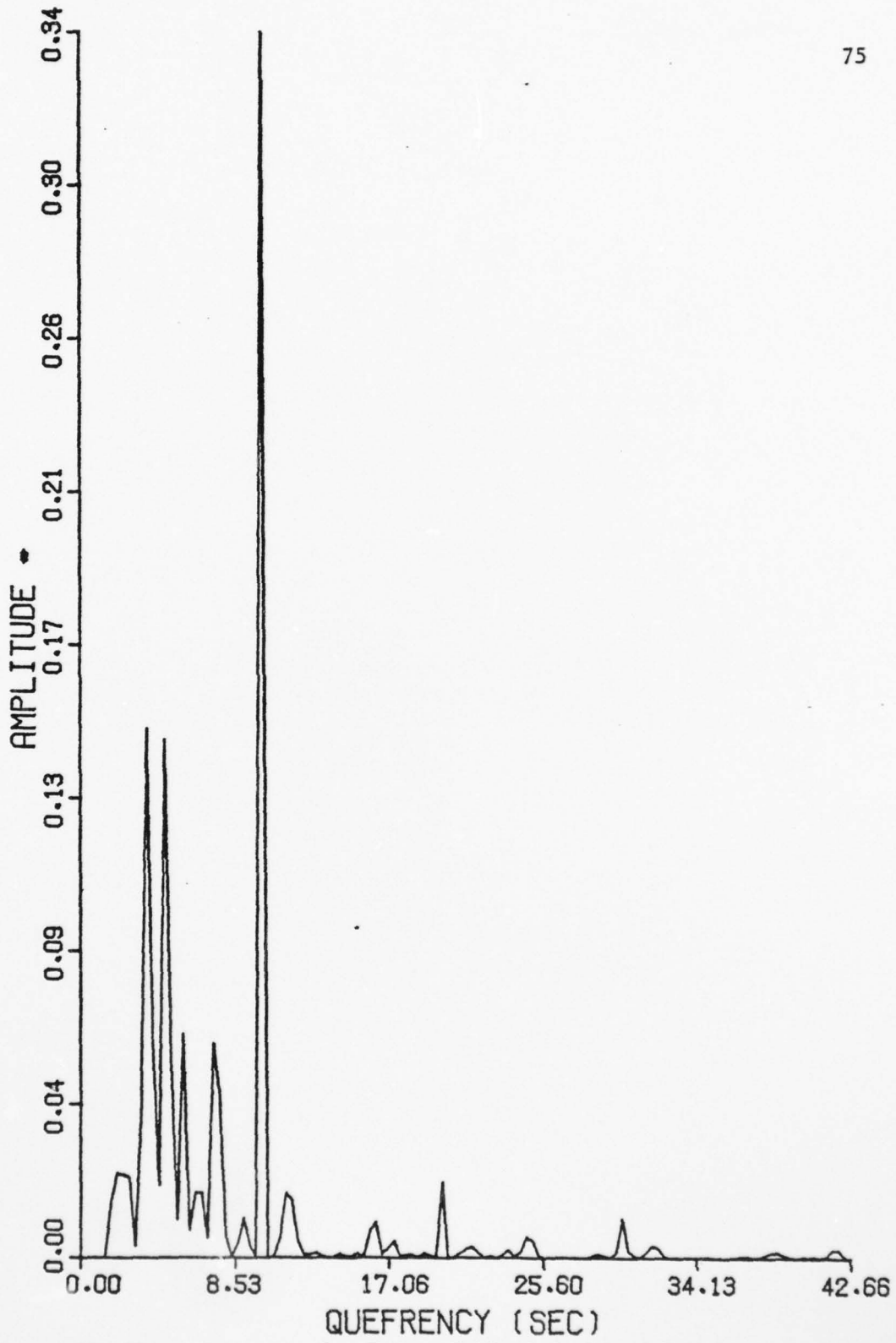

Figure 33. Phase Cepstrum for Pulse-Shifted Combined P-M Generated Wave

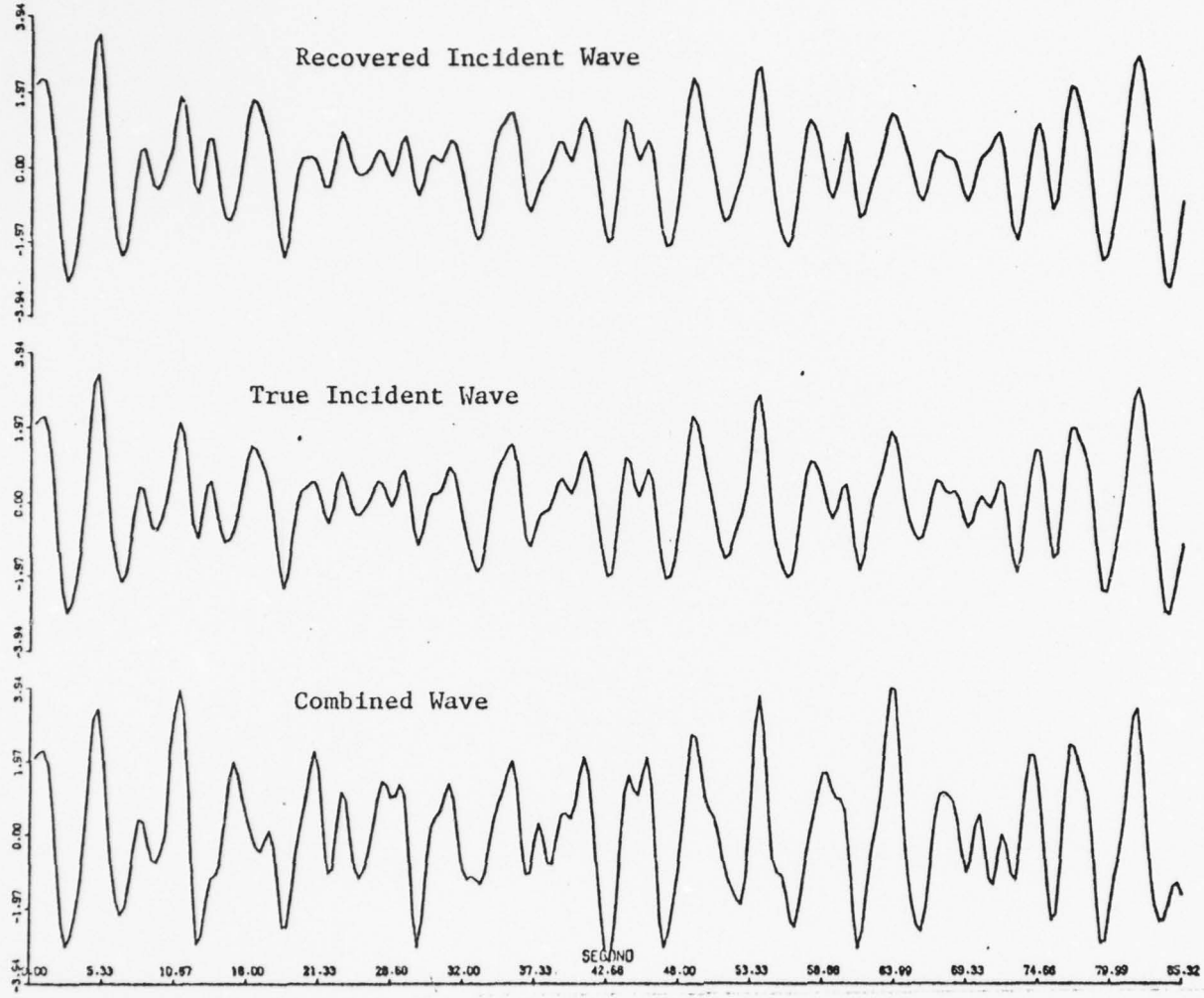

Figure 34. Recovered Incident, True Incident and Combined Wave Time Series for Pulse-Shifted P-M Generated Wave

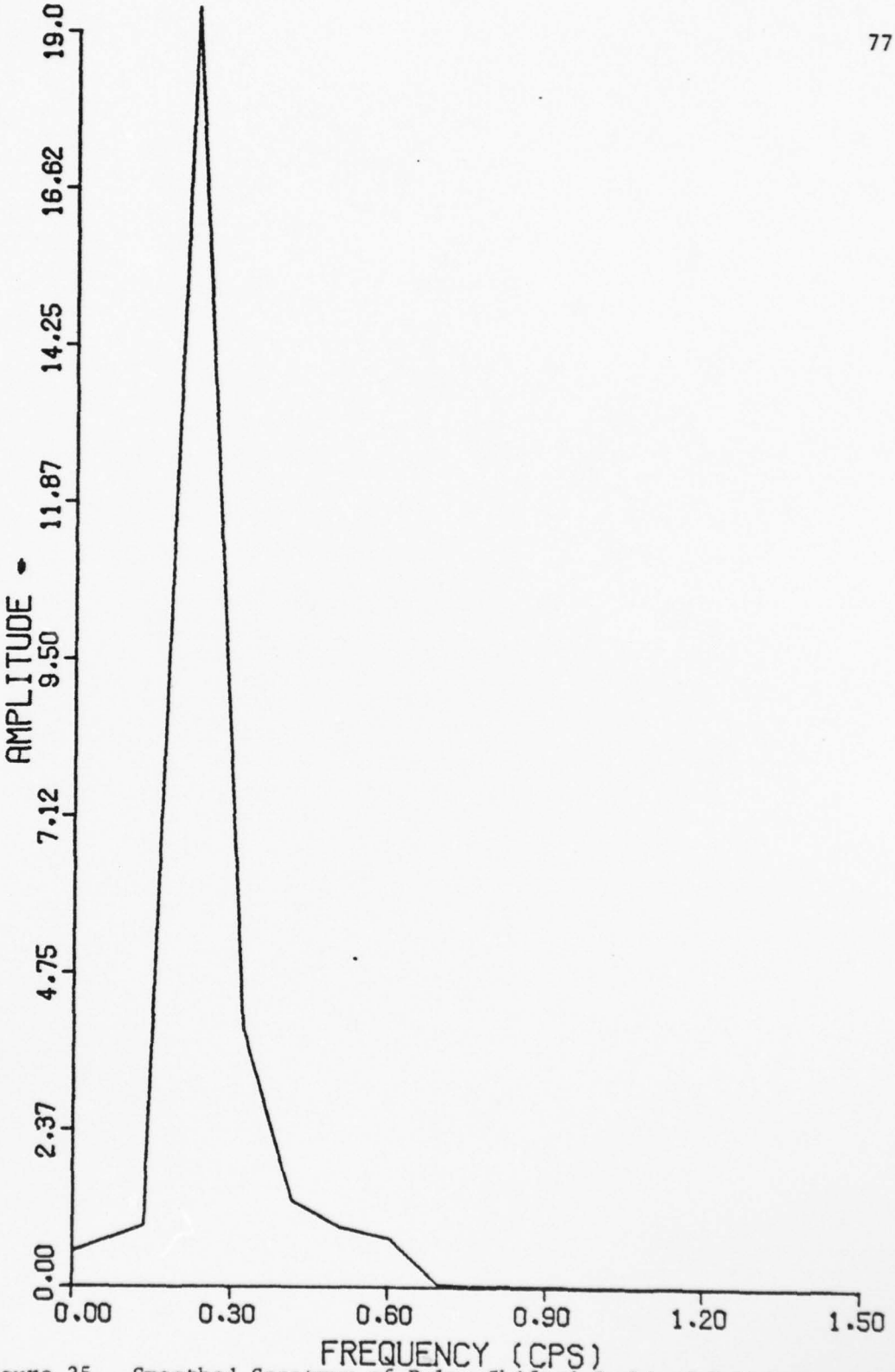

Figure 35. Smoothed Spectrum of Pulse-Shifted Combined P-M Generated Wave

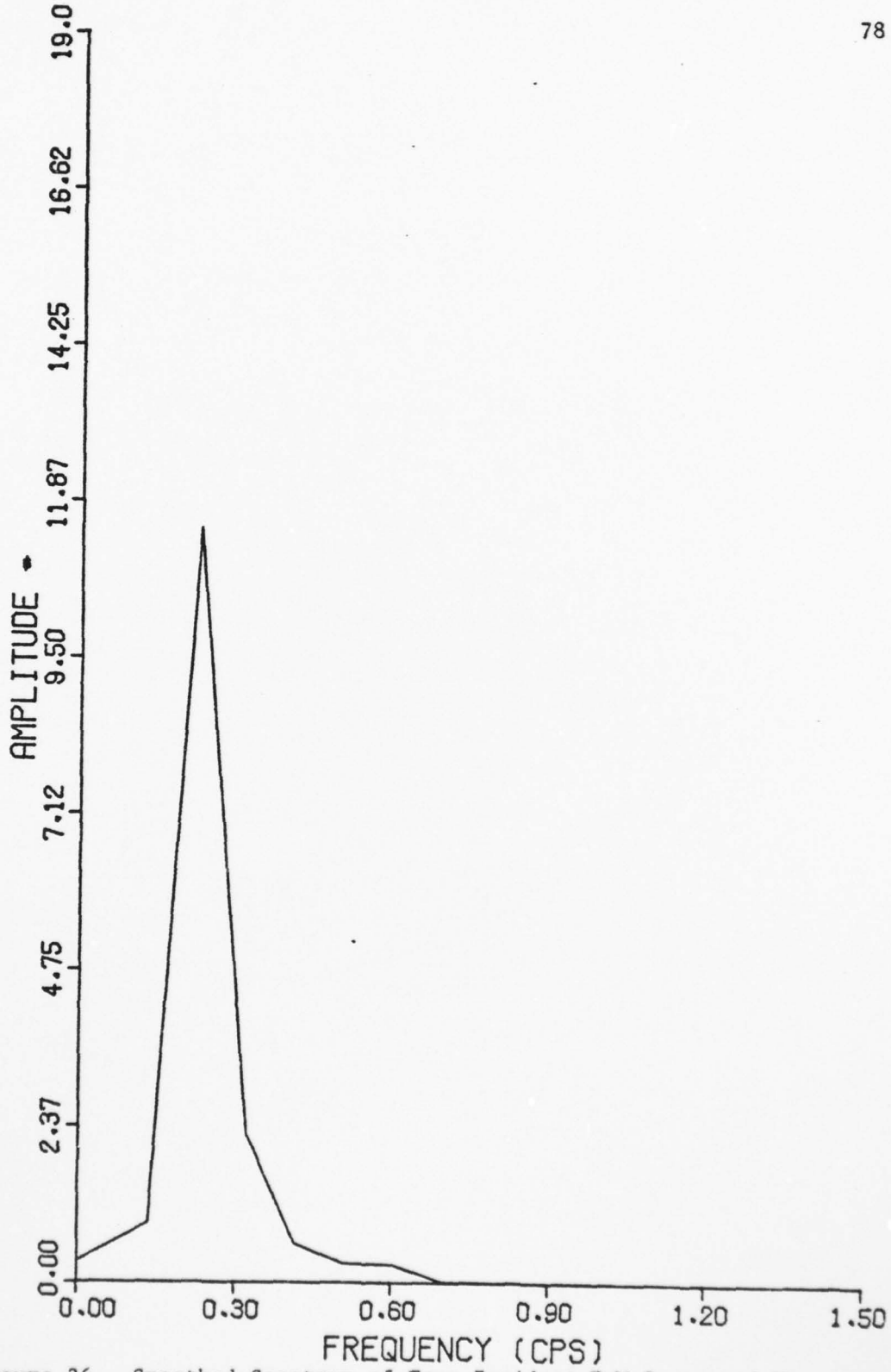

Figure 36. Smoothed Spectrum of True Incident P-M Generated Wave

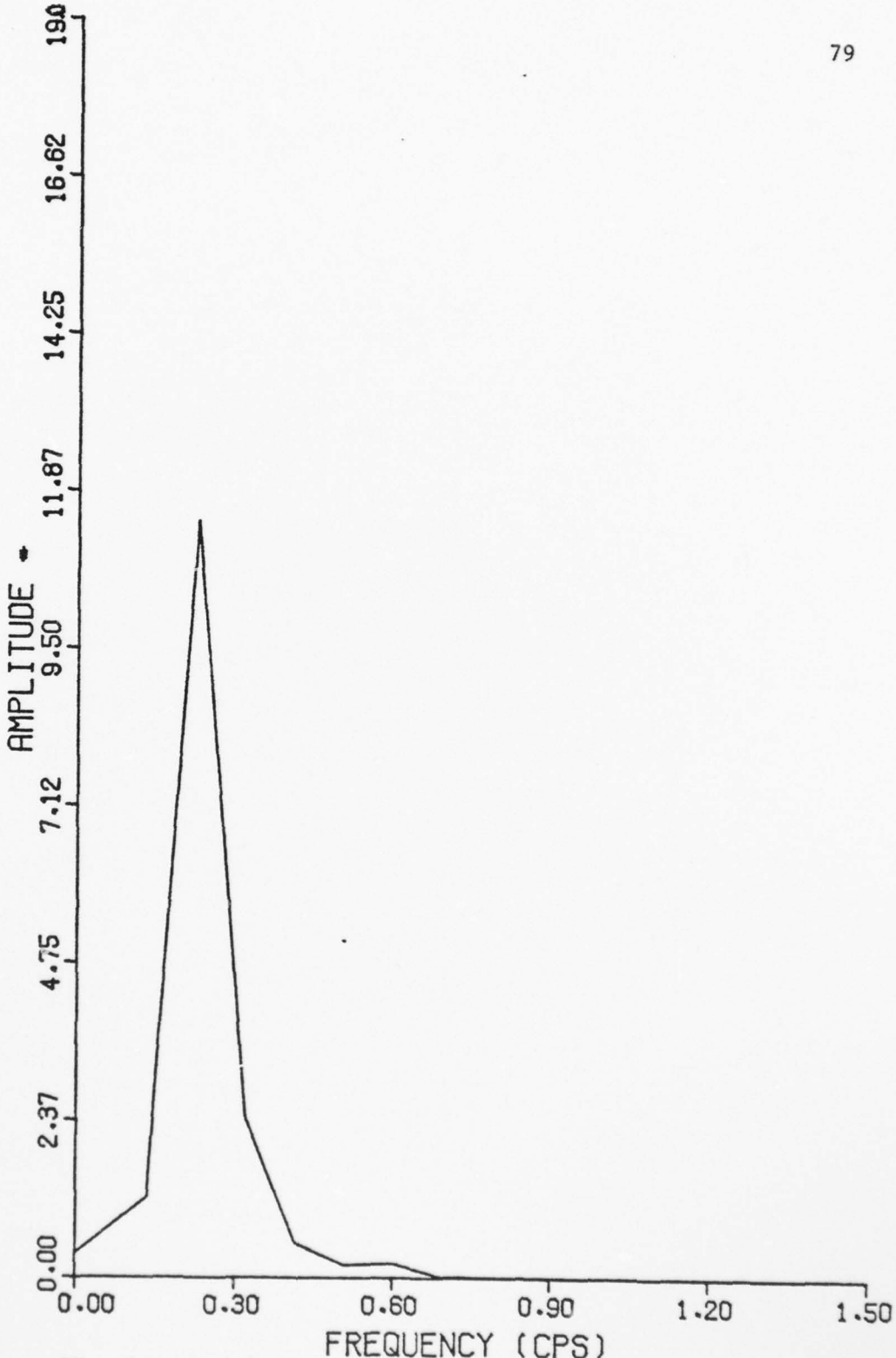

Figure 37. Smoothed Spectrum of Recovered Incident P-M Generated Wave from Pulse-Shifted Combined P-M Generated Wave

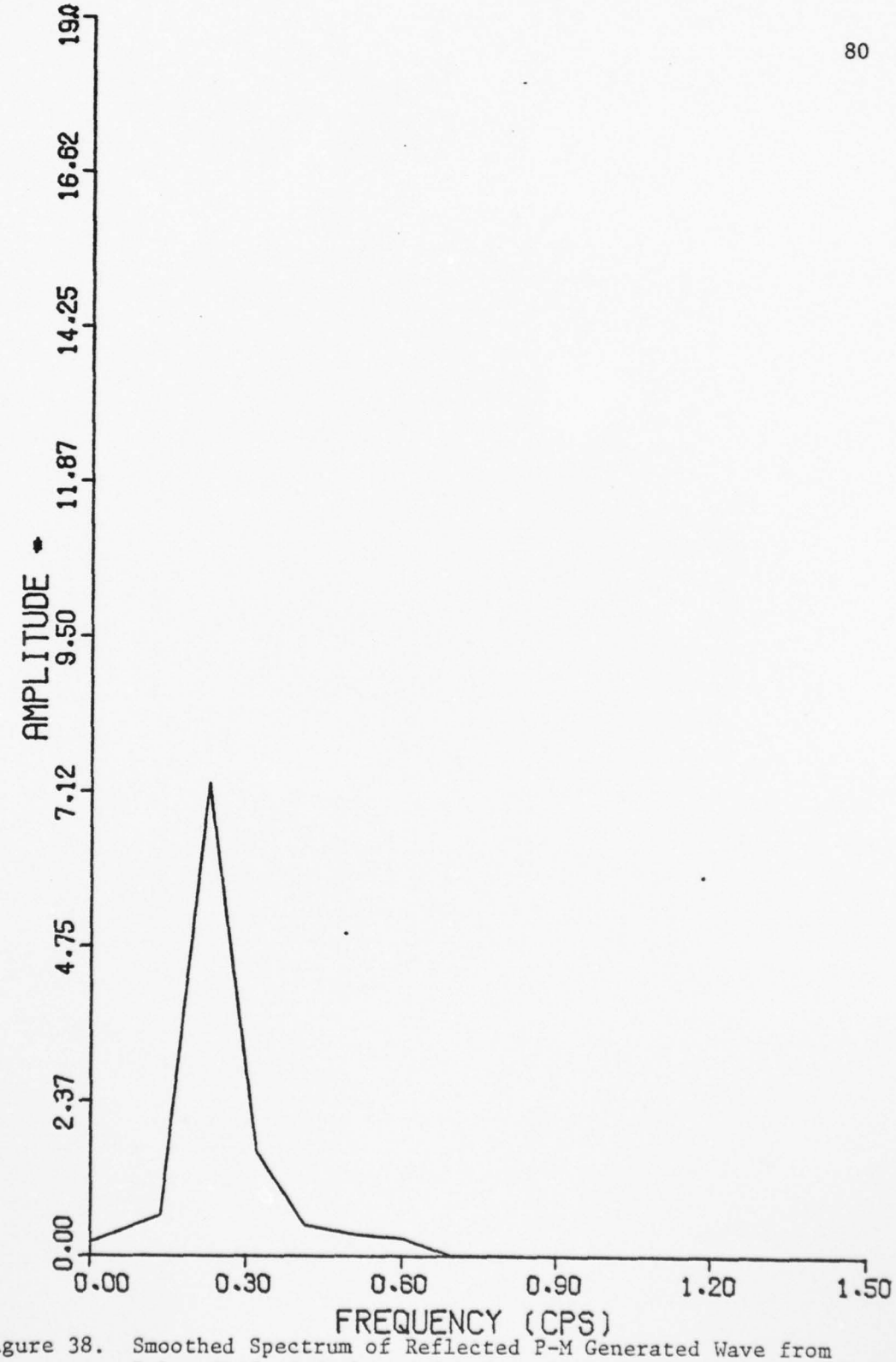

Figure 38. Smoothed Spectrum of Reflected P-M Generated Wave from Pulse-Shifted Combined P-M Generated Wave

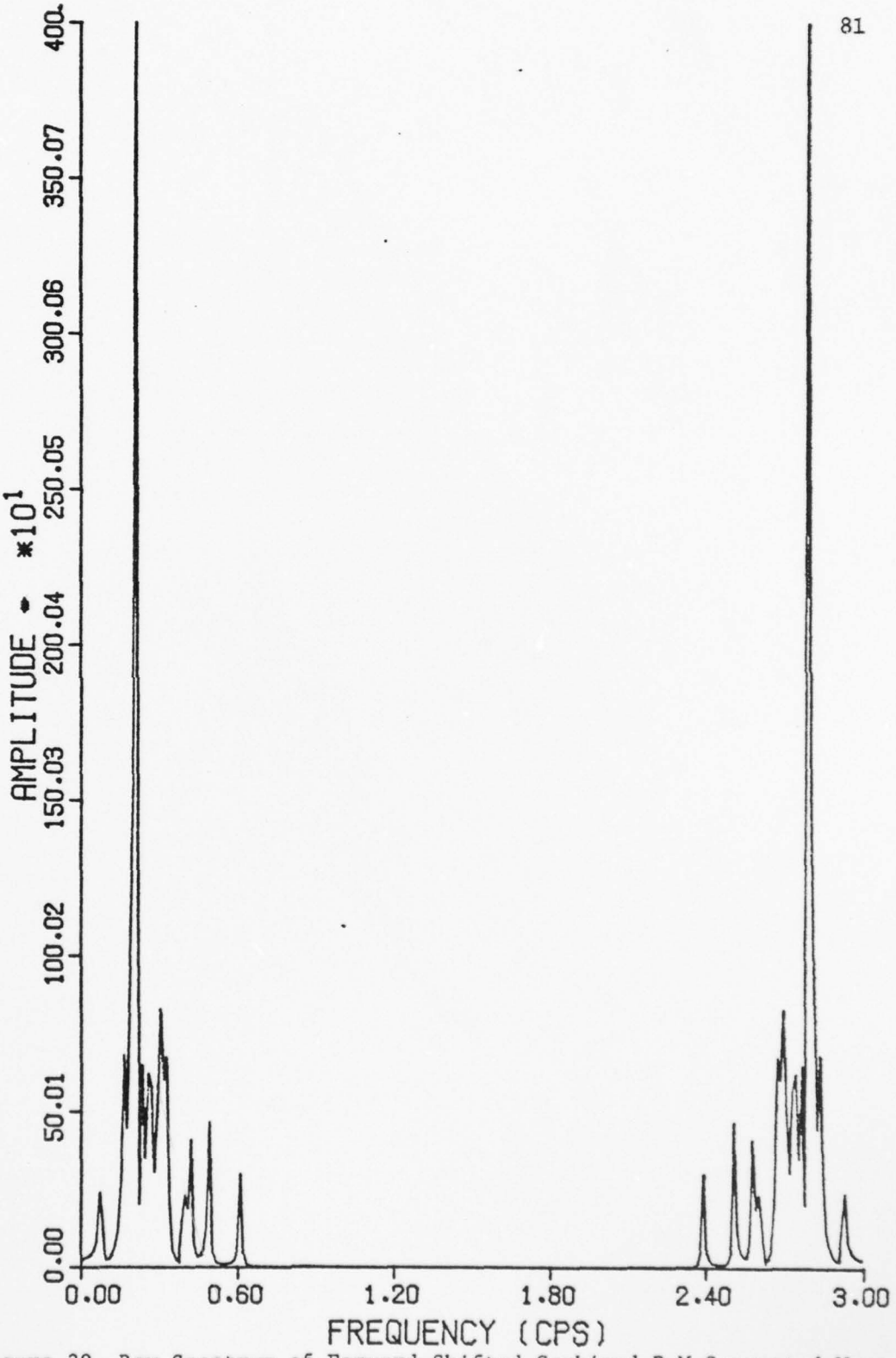

Figure 39. Raw Spectrum of Forward-Shifted Combined P-M Generated Wave

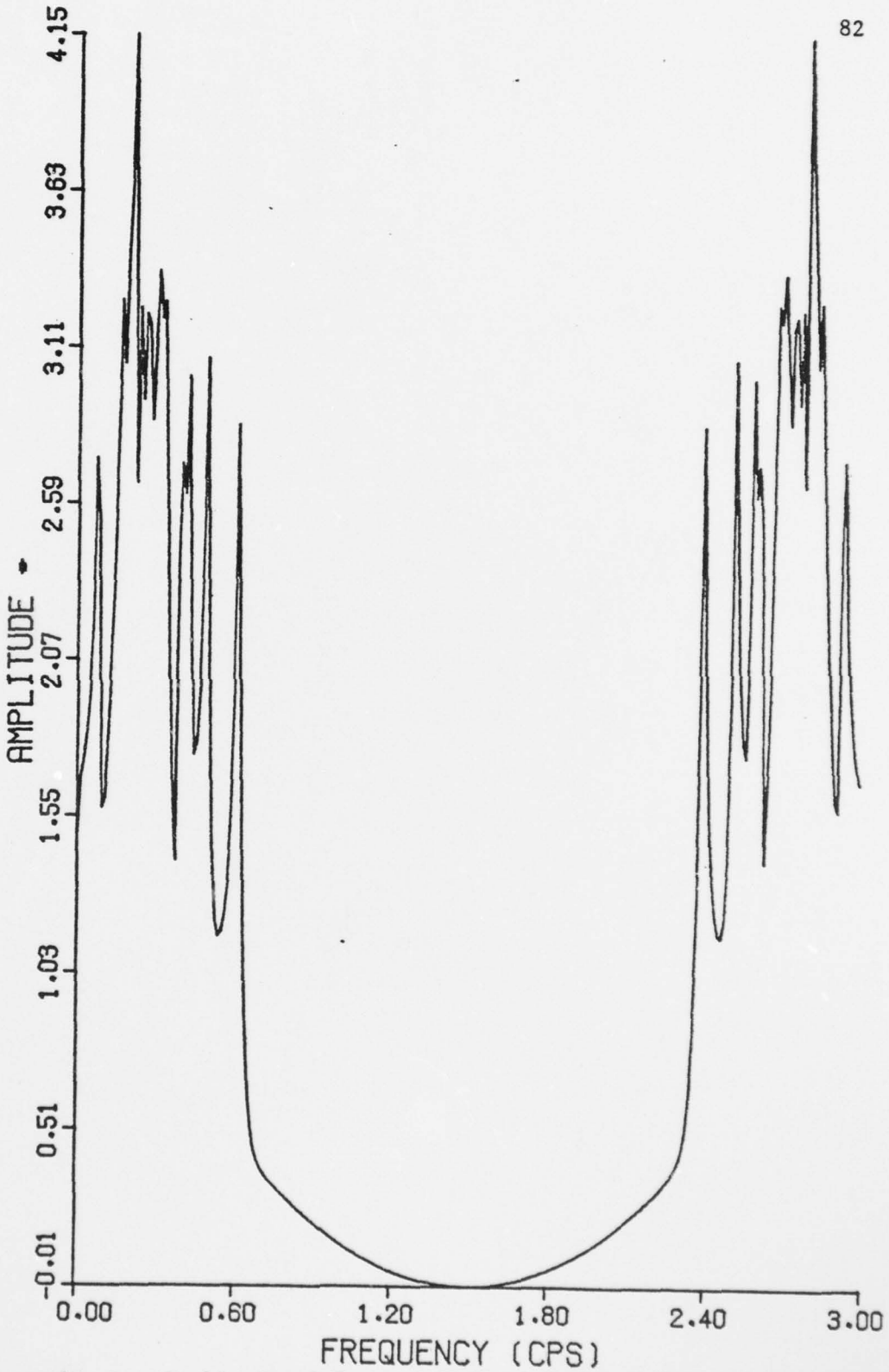

Figure 40. Log Amplitude of Forward-Shifted Combined P-M Generated Wave

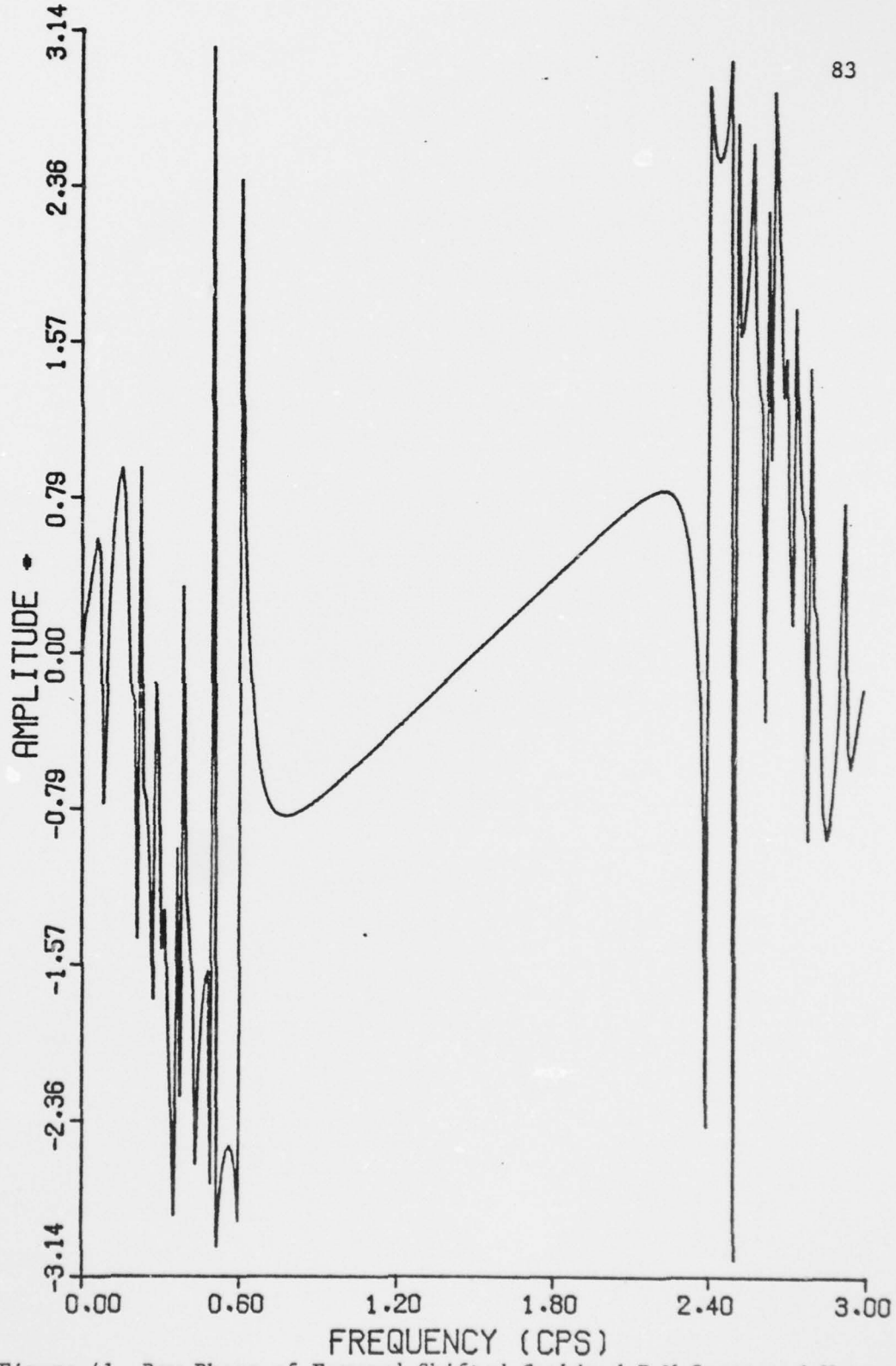

Figure 41. Raw Phase of Forward-Shifted Combined P-M Generated Wave

AD-A072 740 NAVAL POSTGRADUATE SCHOOL MONTEREY CA F/G 8/3
AN INVESTIGATION INTO THE USE OF CEPSTRAL ANALYSIS IN THE DECOM--ETC(U)
APR 78 D E MORRIS

UNCLASSIFIED NL

2 OF 2
ADA
072740

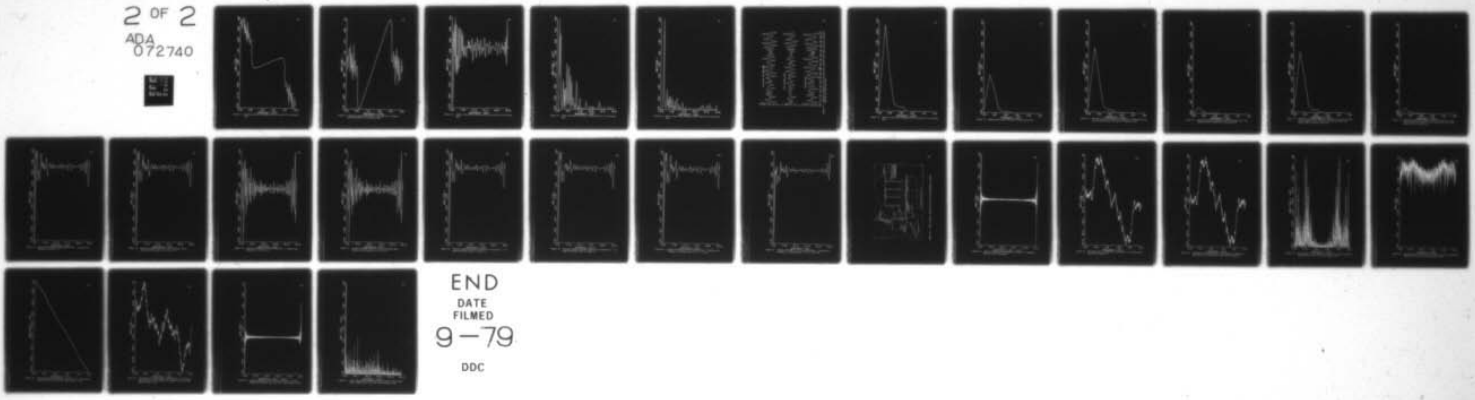

END
DATE
FILMED
9-79
DDC

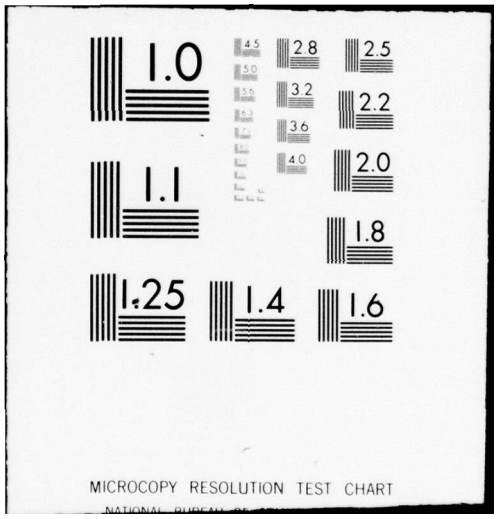
1.0
1.1
1.25
1.4
1.6
1.8
2.0
2.2
2.5
2.8
3.2
3.6
4.0
4.5
5.0
MICROCOPY RESOLUTION TEST CHART

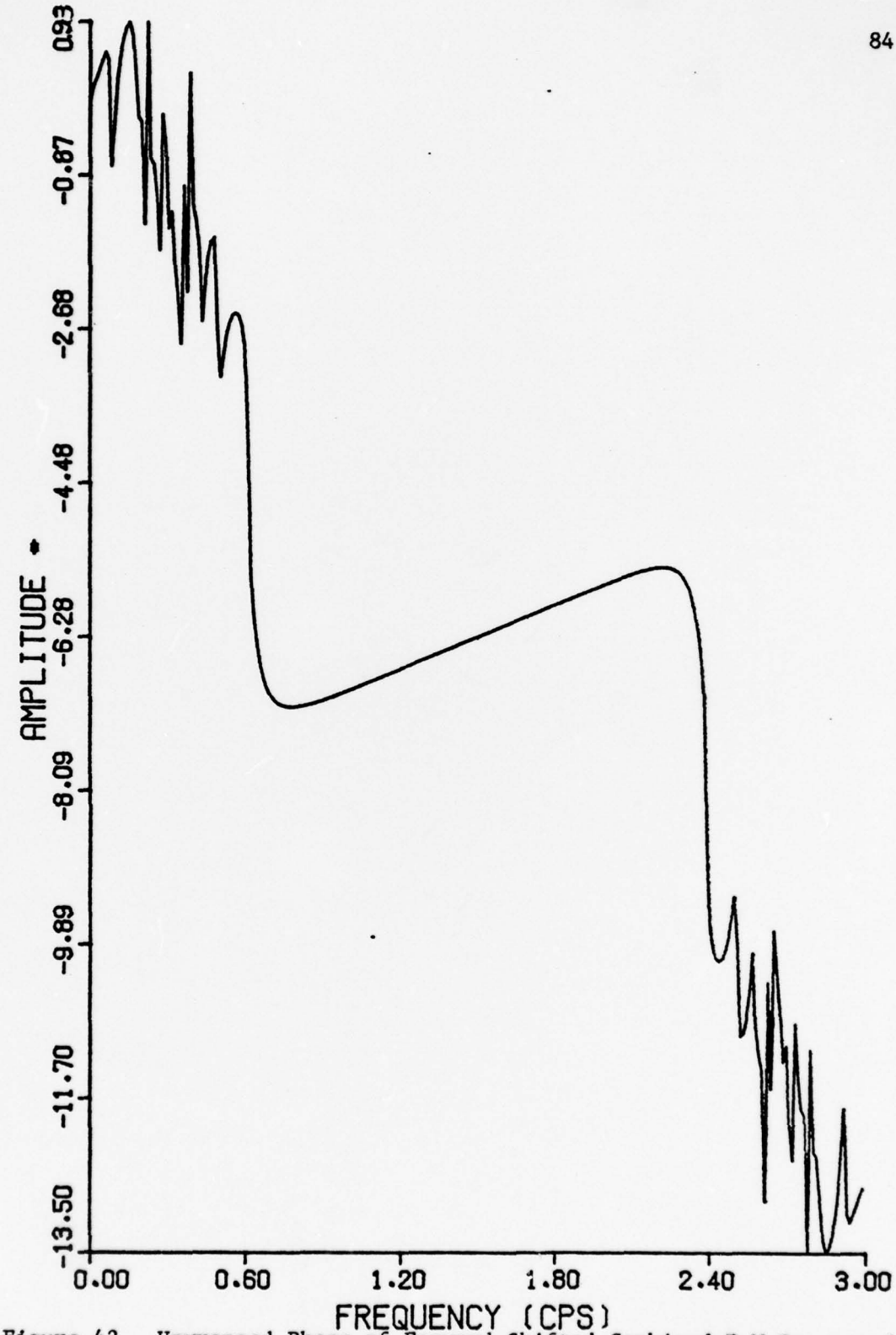

Figure 42. Unwrapped Phase of Forward-Shifted Combined P-M Generated Wave

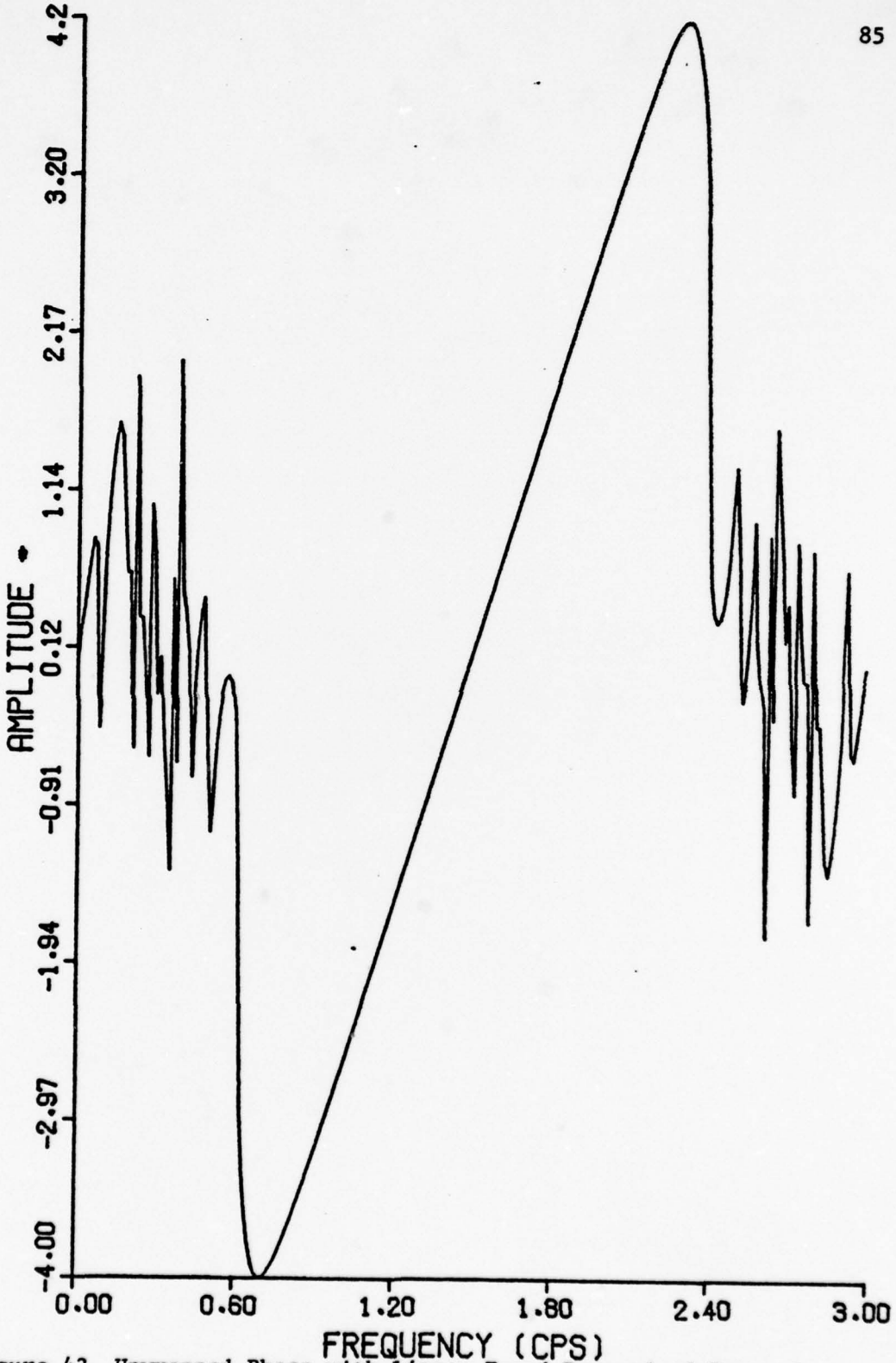

Figure 43. Unwrapped Phase with Linear Trend Removed of Forward-Shifted Combined P-M Generated Wave

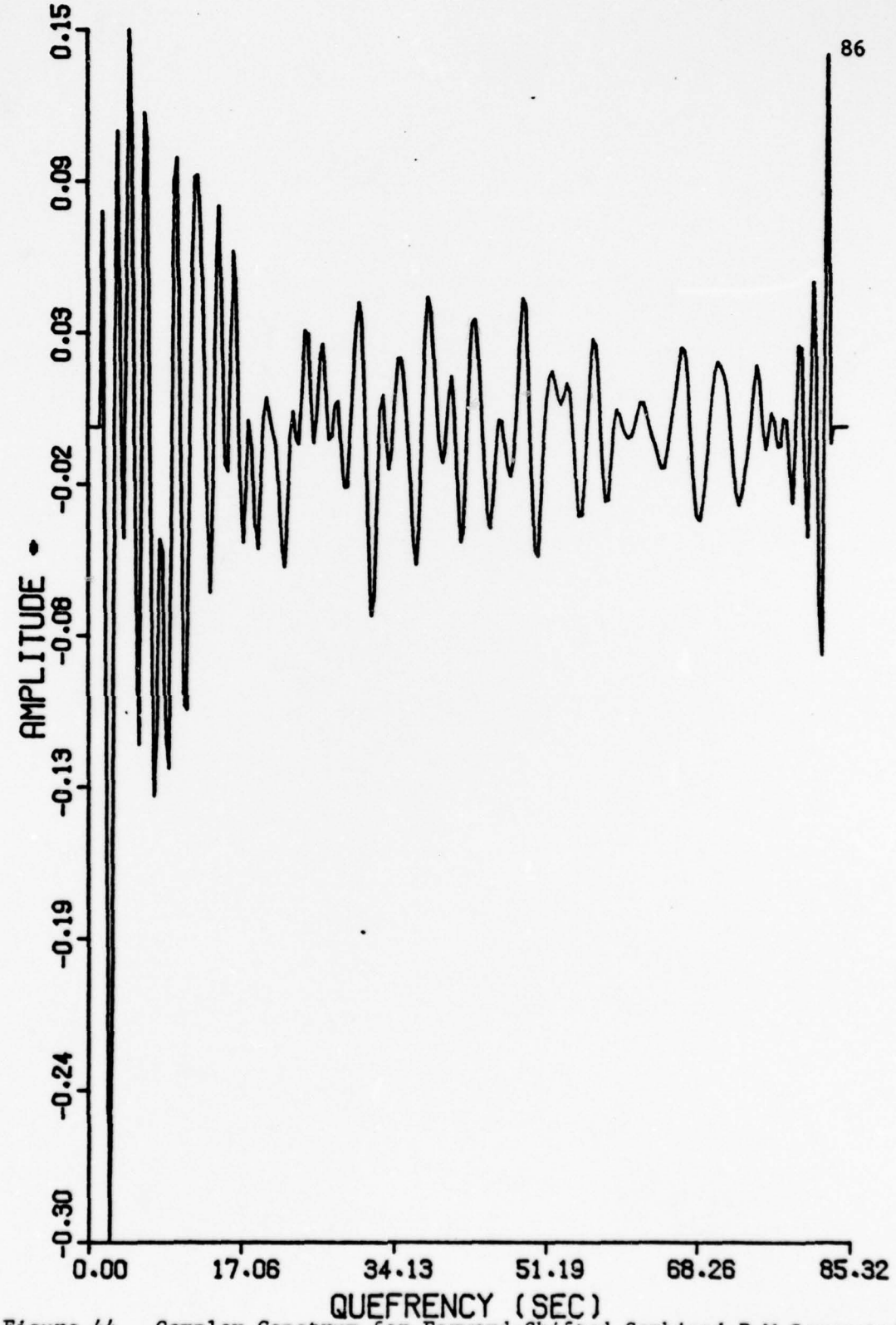

Figure 44. Complex Cepstrum for Forward-Shifted Combined P-M Generated Wave

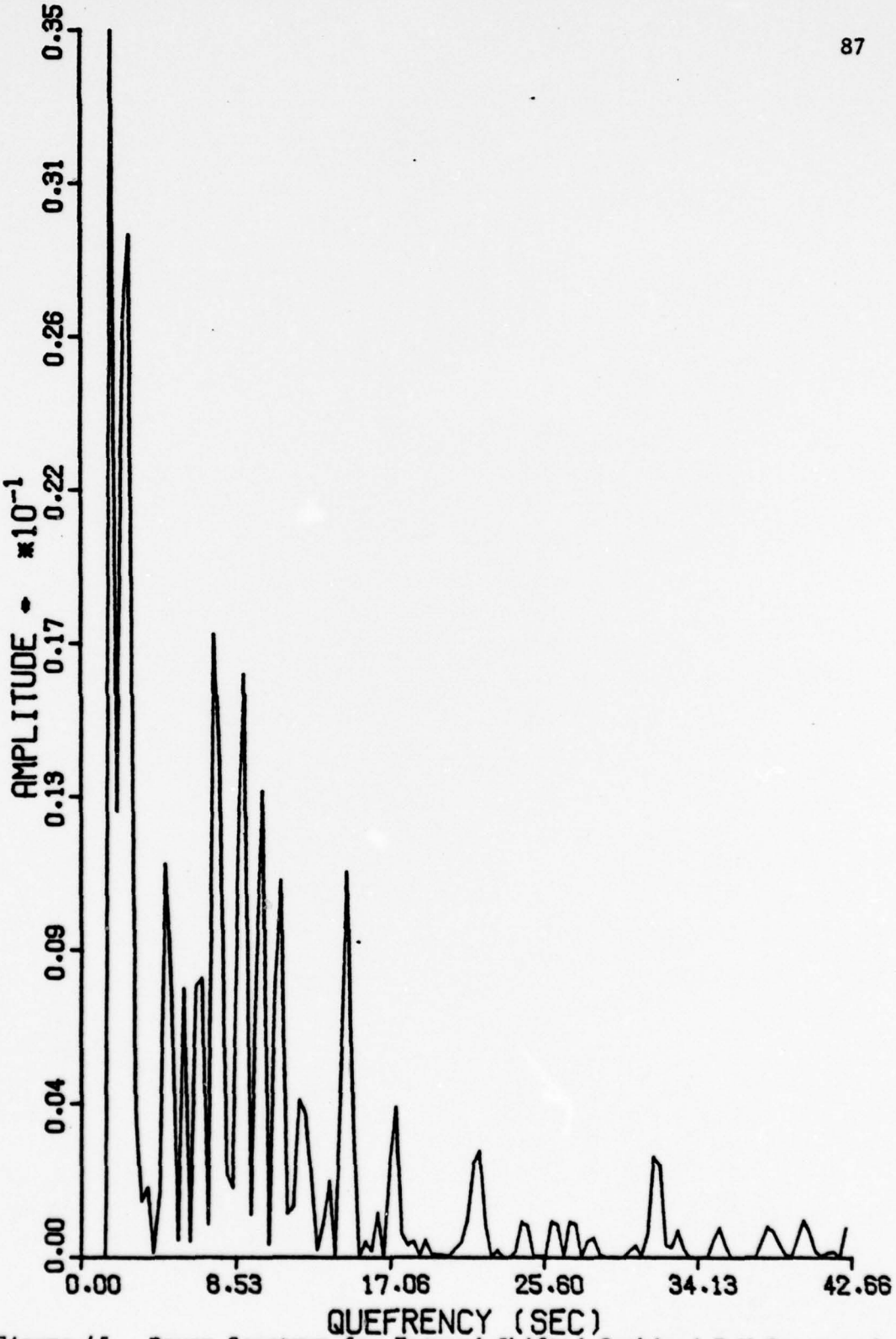

Figure 45. Power Cepstrum for Forward-Shifted Combined P-M Generated Wave

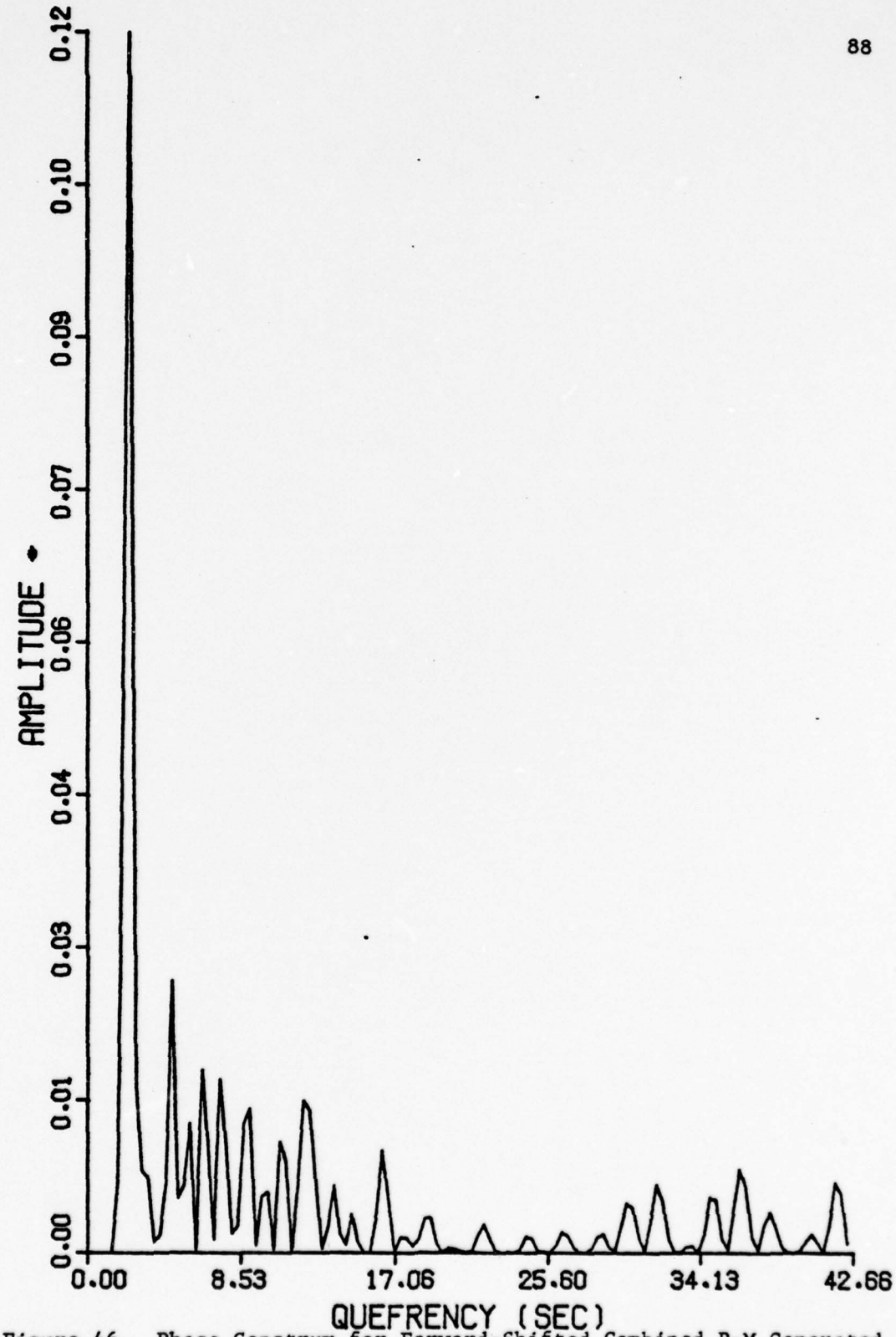

Figure 46. Phase Cepstrum for Forward-Shifted Combined P-M Generated Wave

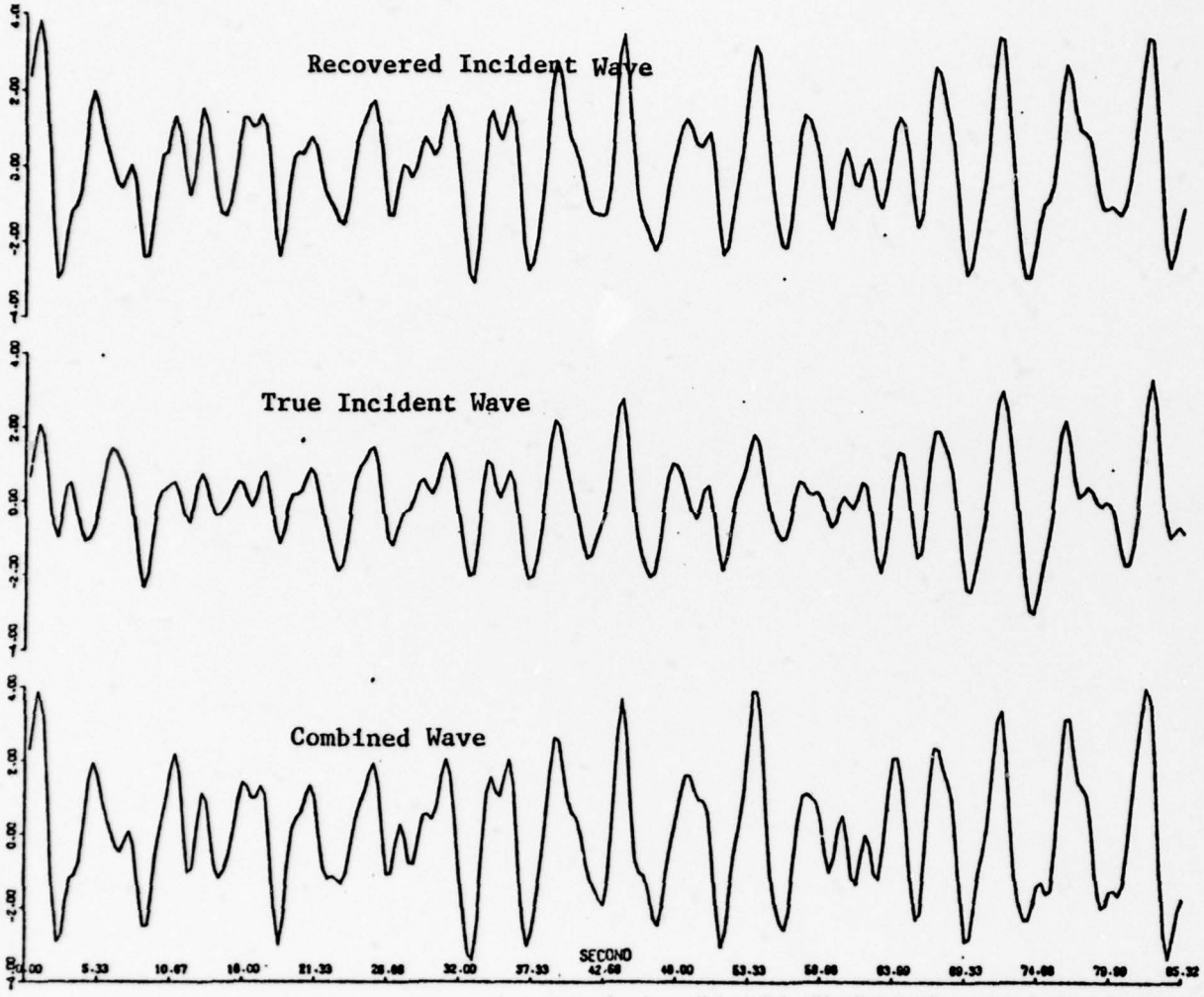

Figure 47. Recovered Incident, True Incident and Combined Wave Time Series for Forward-Shifted P-M Generated Wave

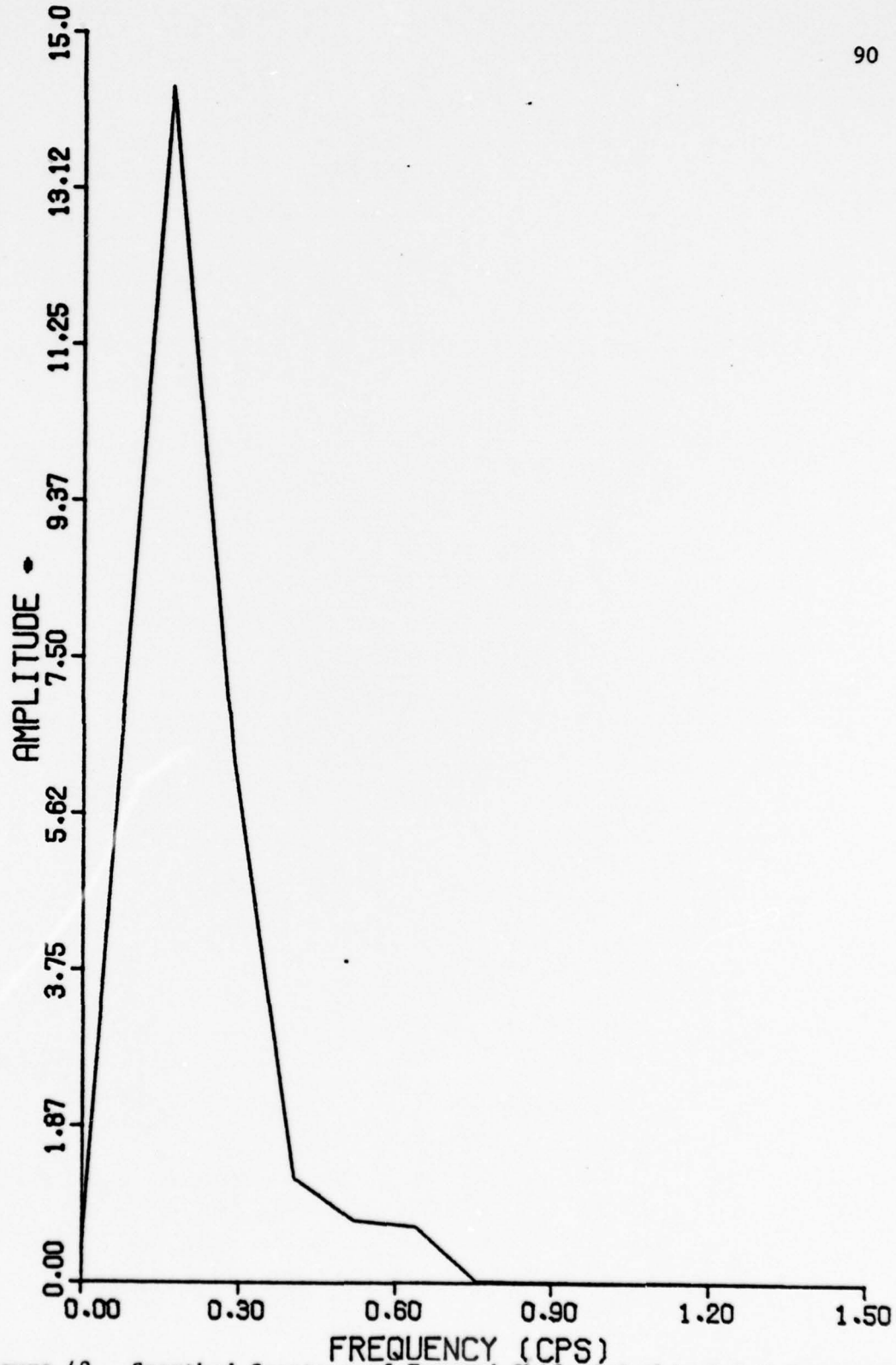

Figure 48. Smoothed Spectrum of Forward-Shifted Combined P-M Generated Wave

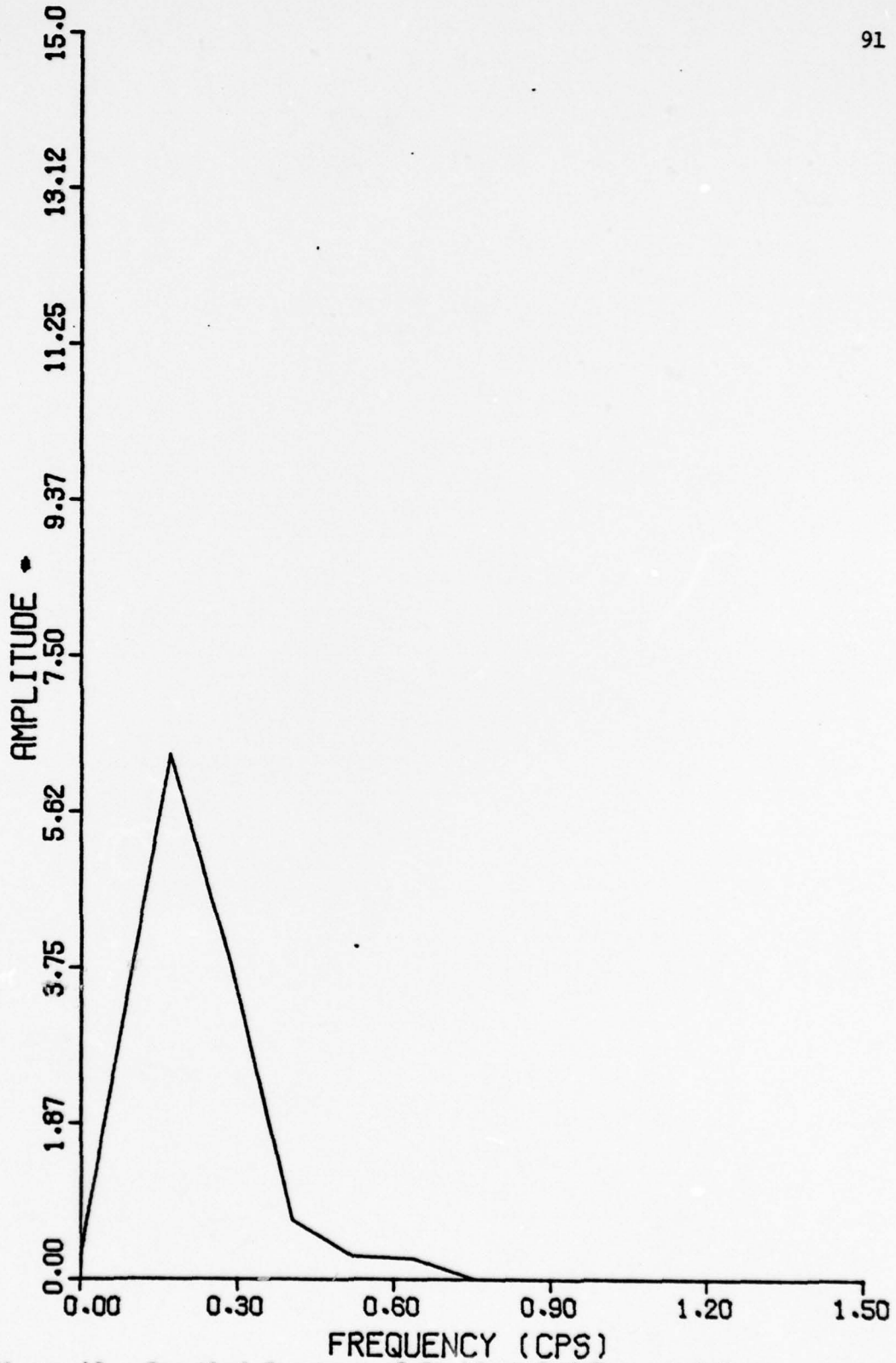

Figure 49. Smoothed Spectrum of Incident P-M Generated Wave

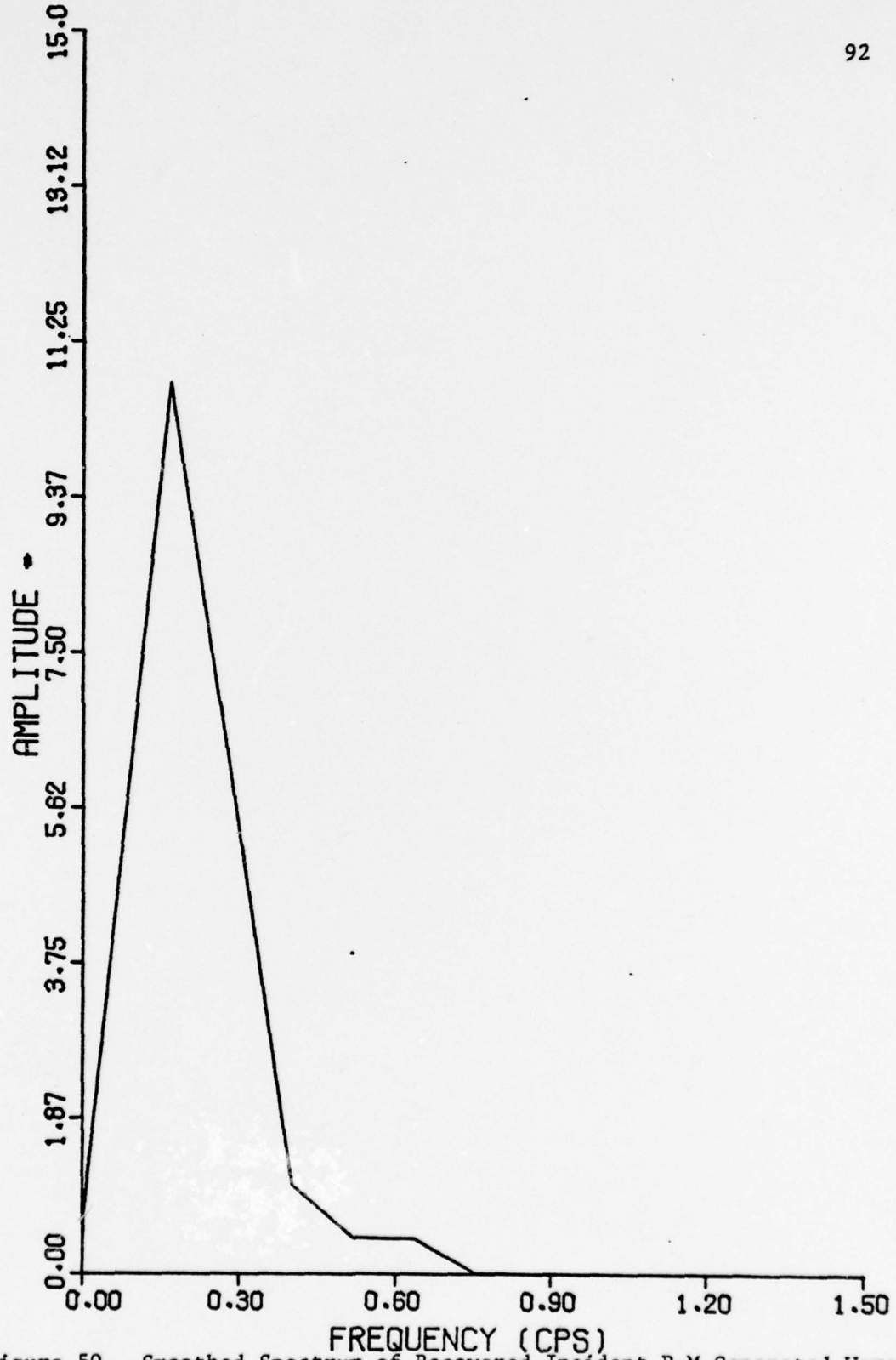

Figure 50. Smoothed Spectrum of Recovered Incident P-M Generated Wave from Forward-Shifted Combined P-M Generated Wave

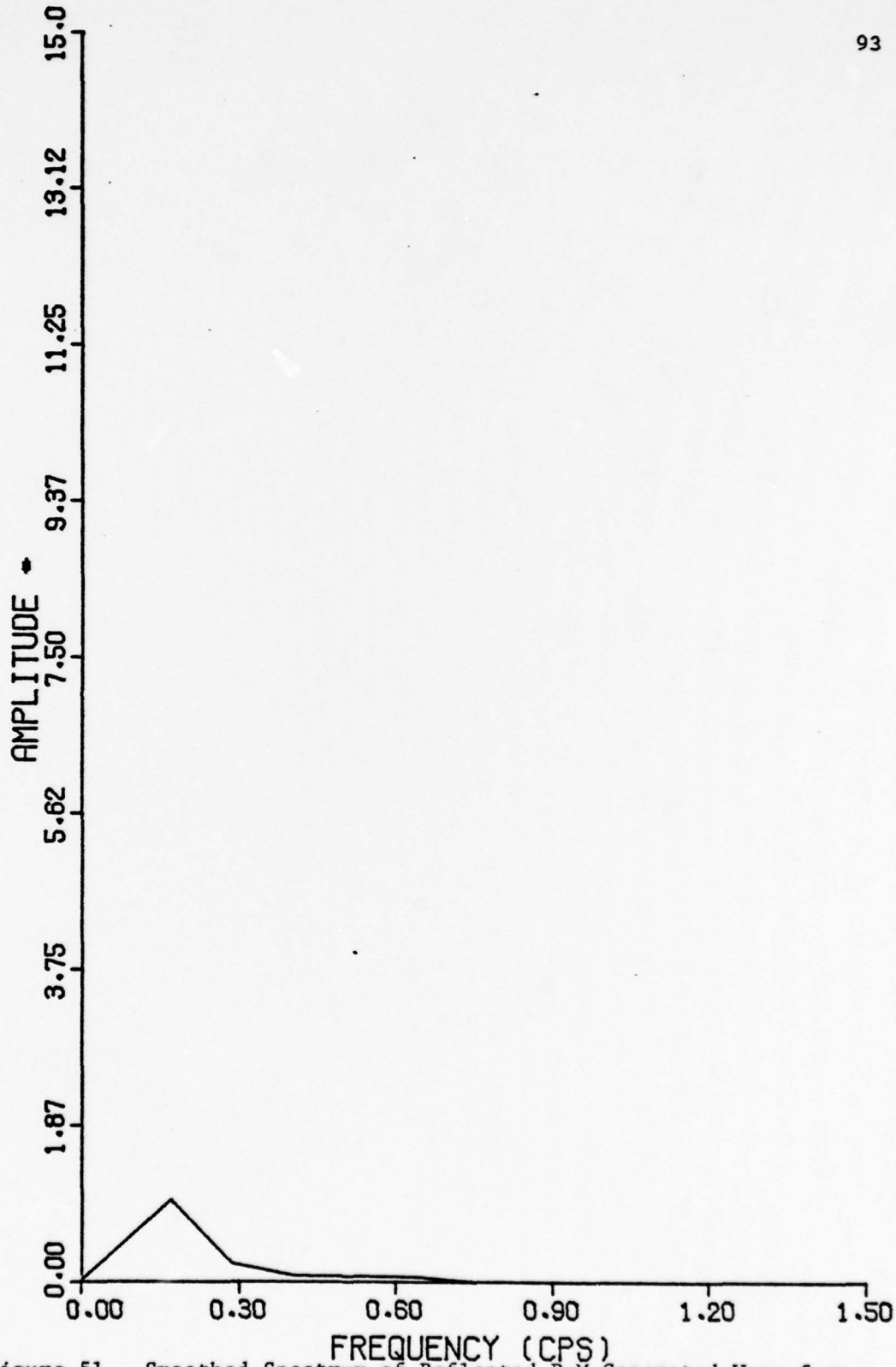

Figure 51. Smoothed Spectrum of Reflected P-M Generated Wave from Forward-Shifted Combined P-M Generated Wave

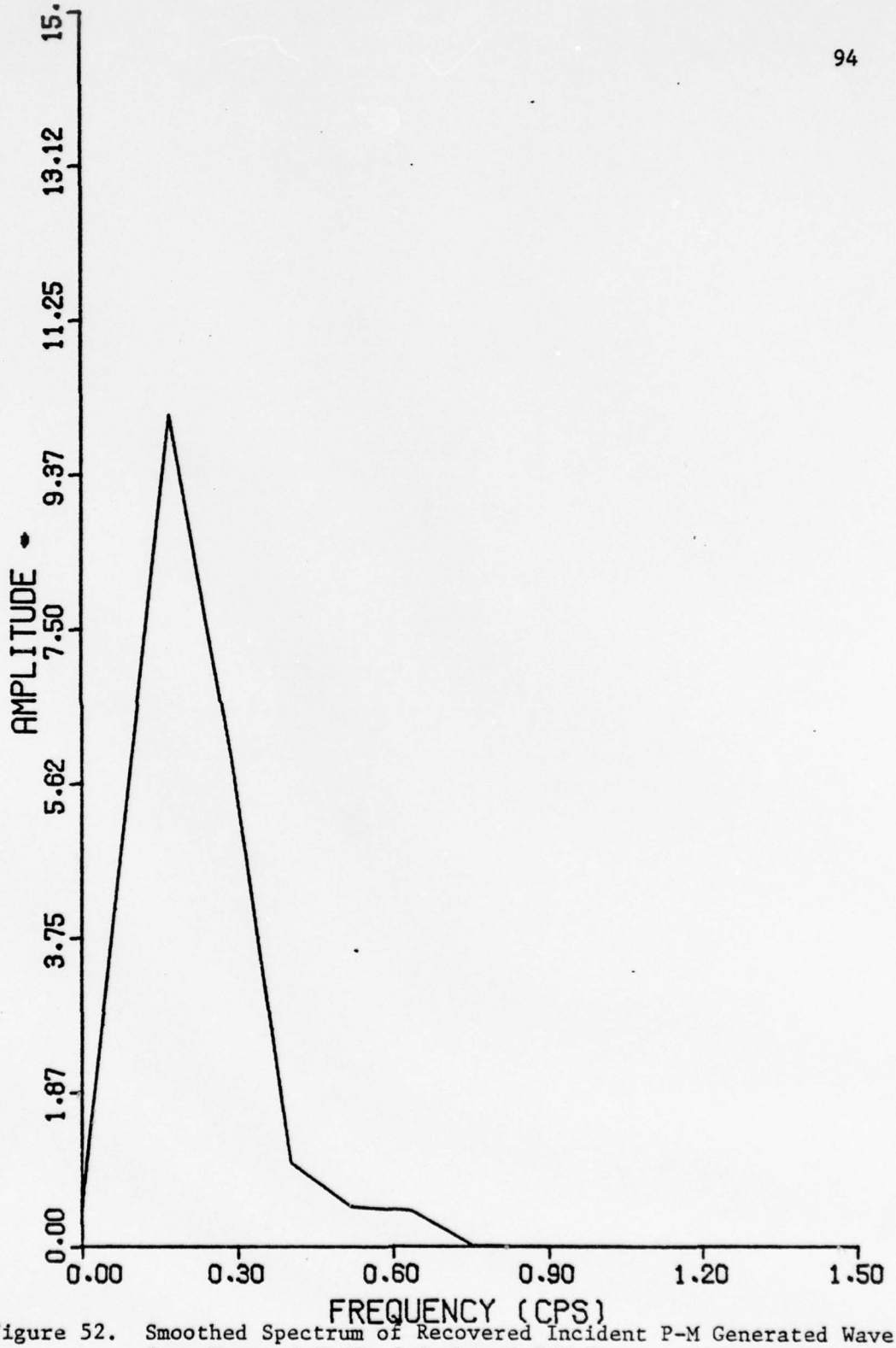

Figure 52. Smoothed Spectrum of Recovered Incident P-M Generated Wave from Forward-Shifted Combined P-M Generated Wave with Zeroes Added to End of Input Data

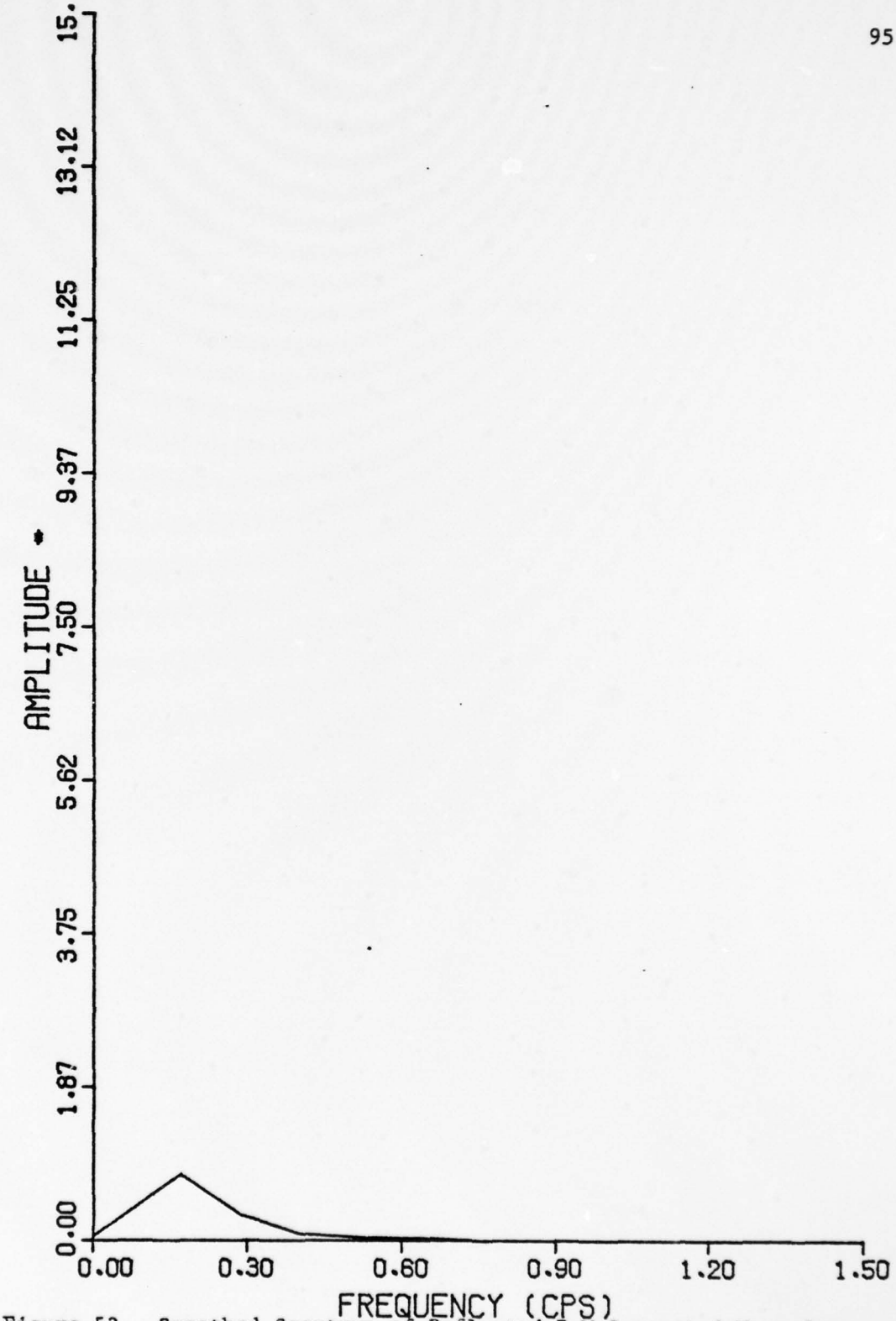

Figure 53. Smoothed Spectrum of Reflected P-M Generated Wave from Forward-Shifted Combined P-M Generated Wave with Zeroes Added to End of Input Data

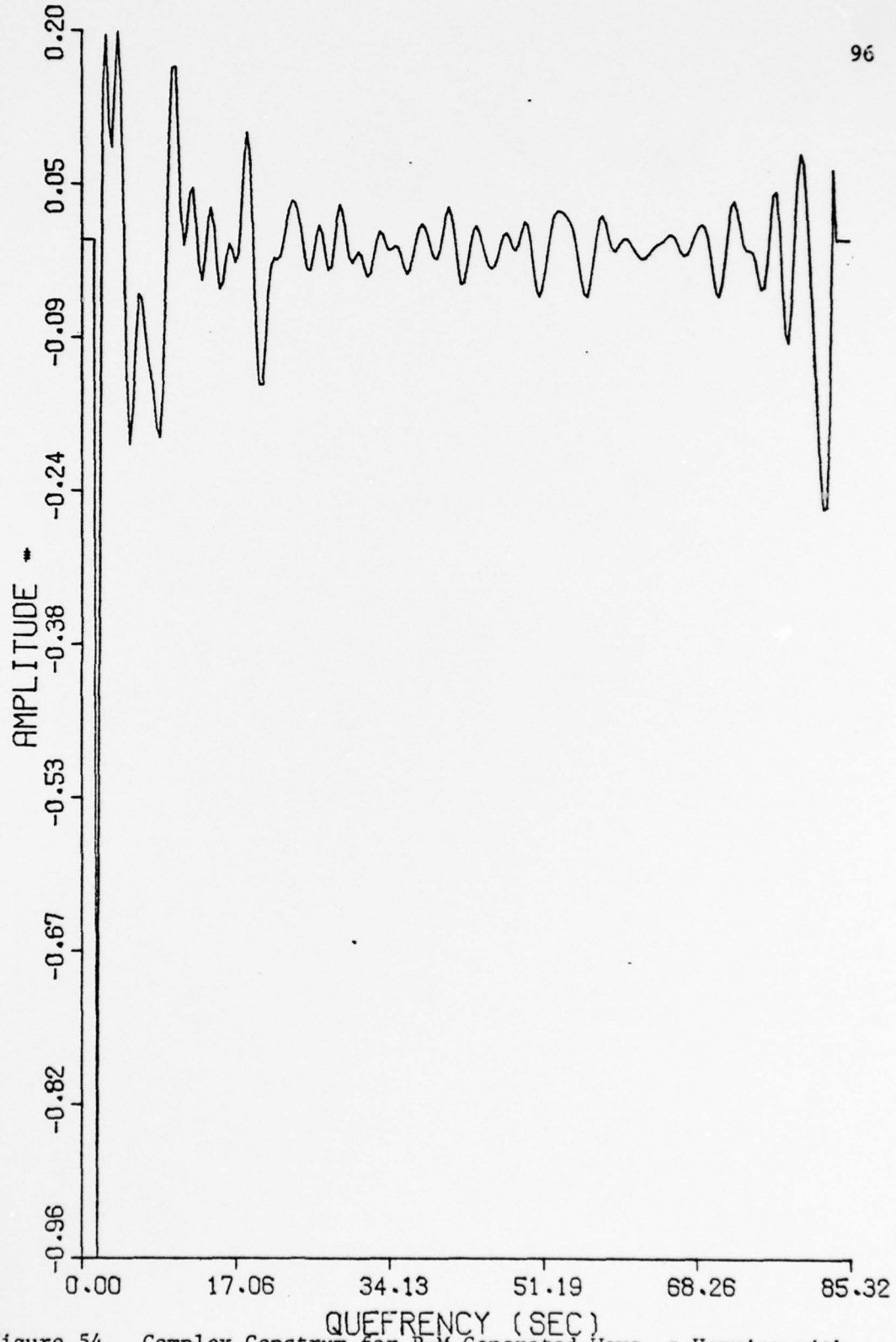

Figure 54. Complex Cepstrum for P-M Generated Wave, τ Varying with Frequency, $\Delta t=.333$, $\alpha=.5$

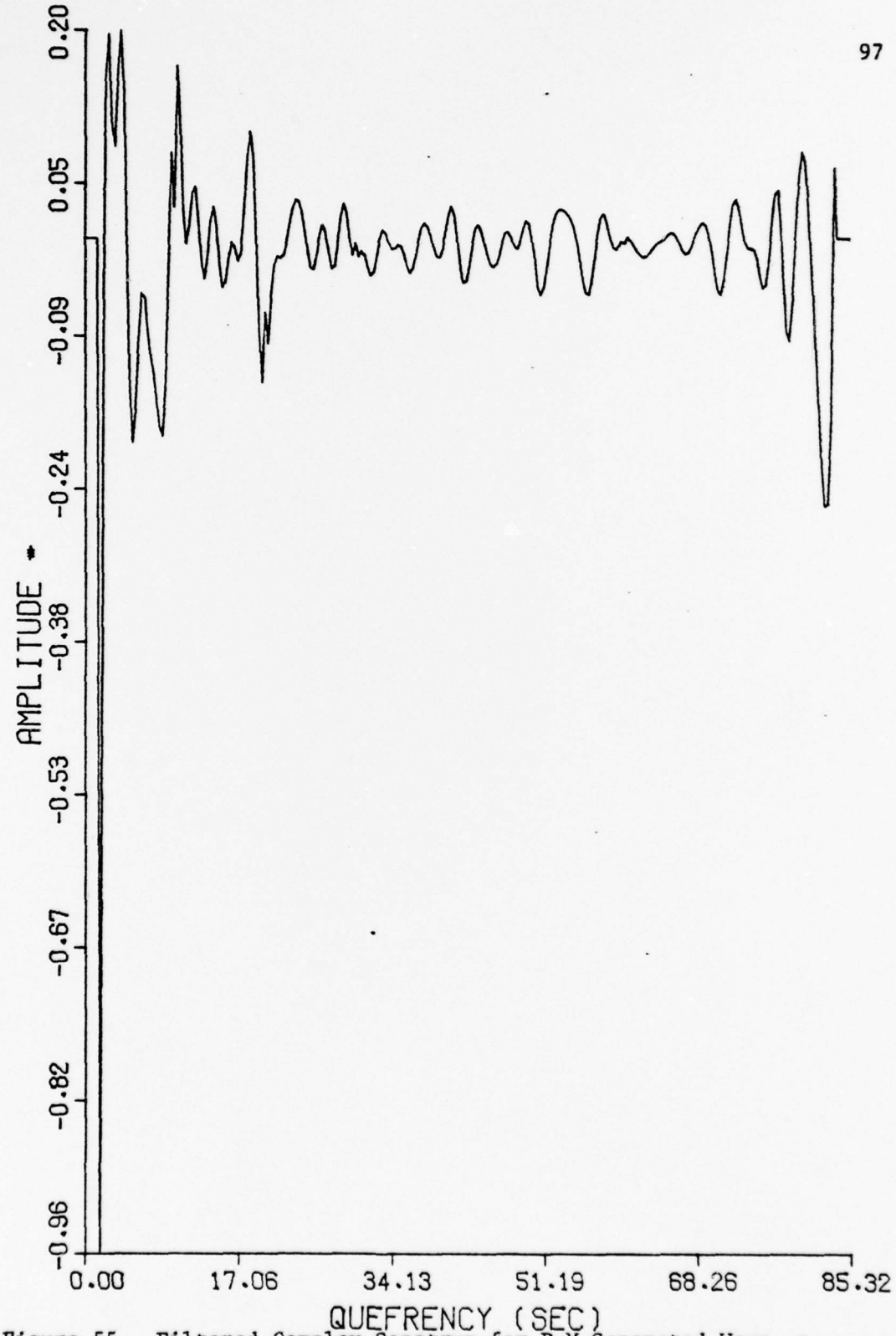

Figure 55. Filtered Complex Cepstrum for P-M Generated Wave, τ Varying with Frequency, $\Delta t=.3333$, $\alpha=.5$

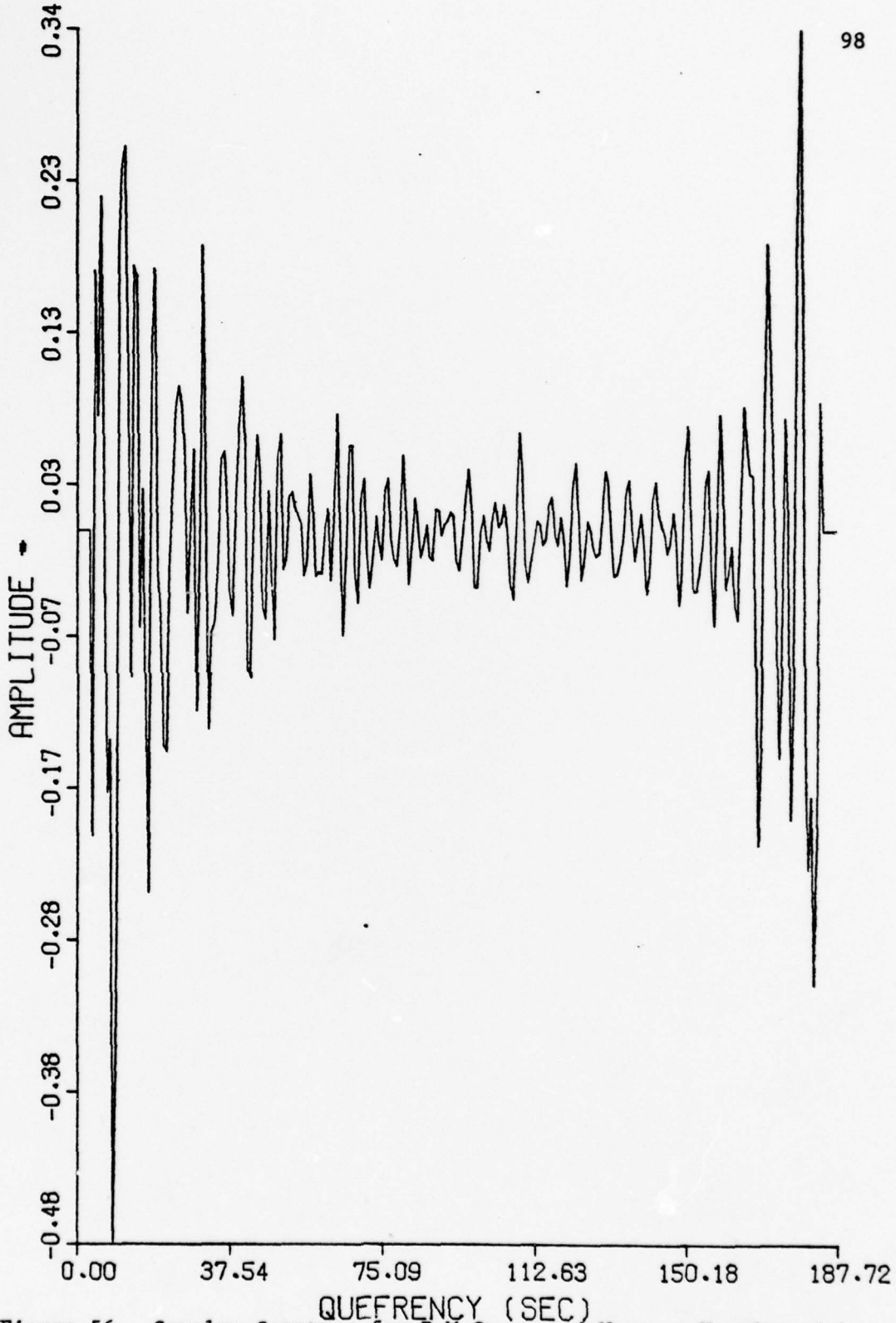

Figure 56. Complex Cepstrum for P-M Generated Wave, τ Varying with Frequency, $\Delta t = .7333$, $\alpha = .5$

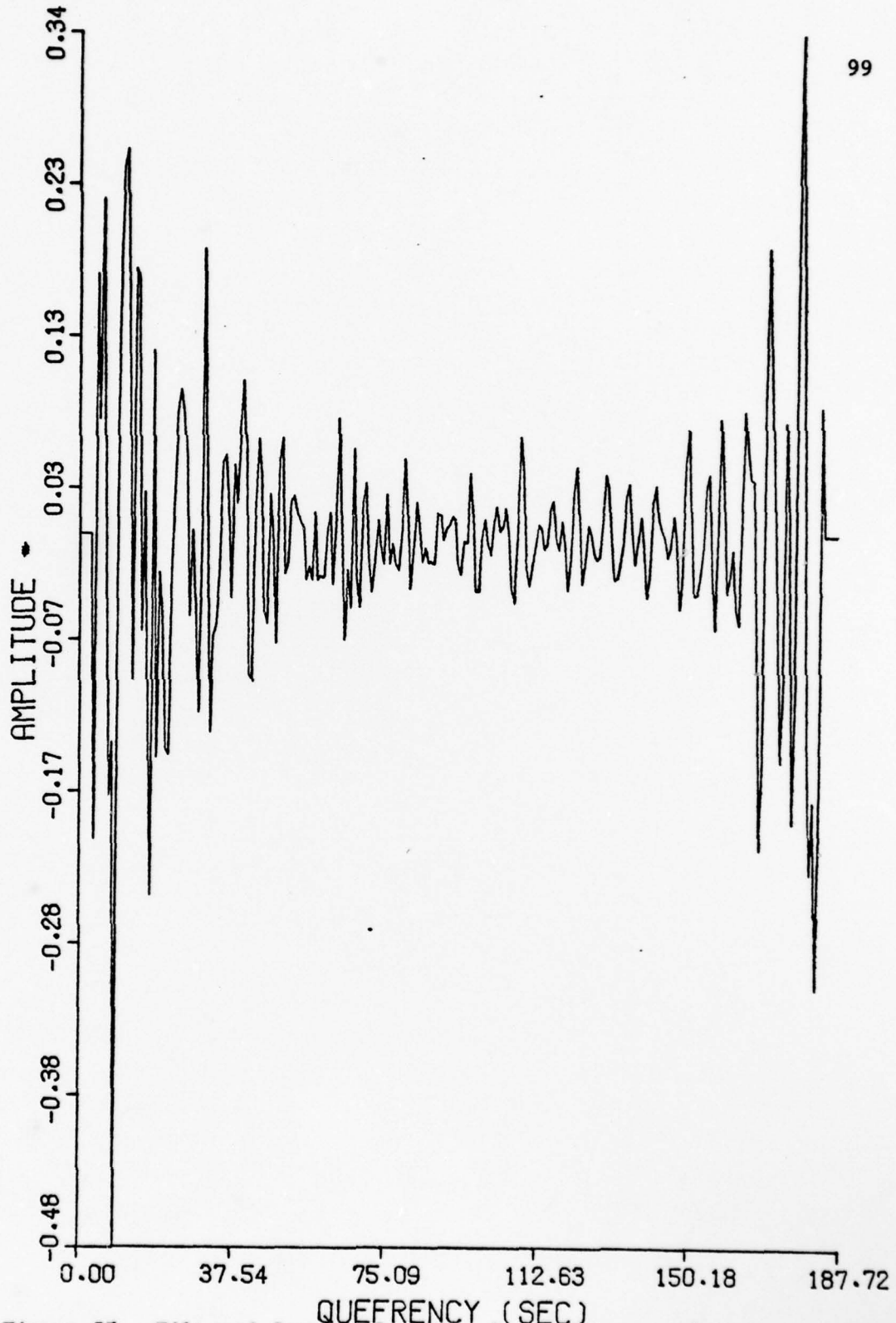

Figure 57. Filtered Complex Cepstrum for P-M Generated Wave, τ Varying with Frequency, $\Delta t = .7333$, $\alpha = .5$

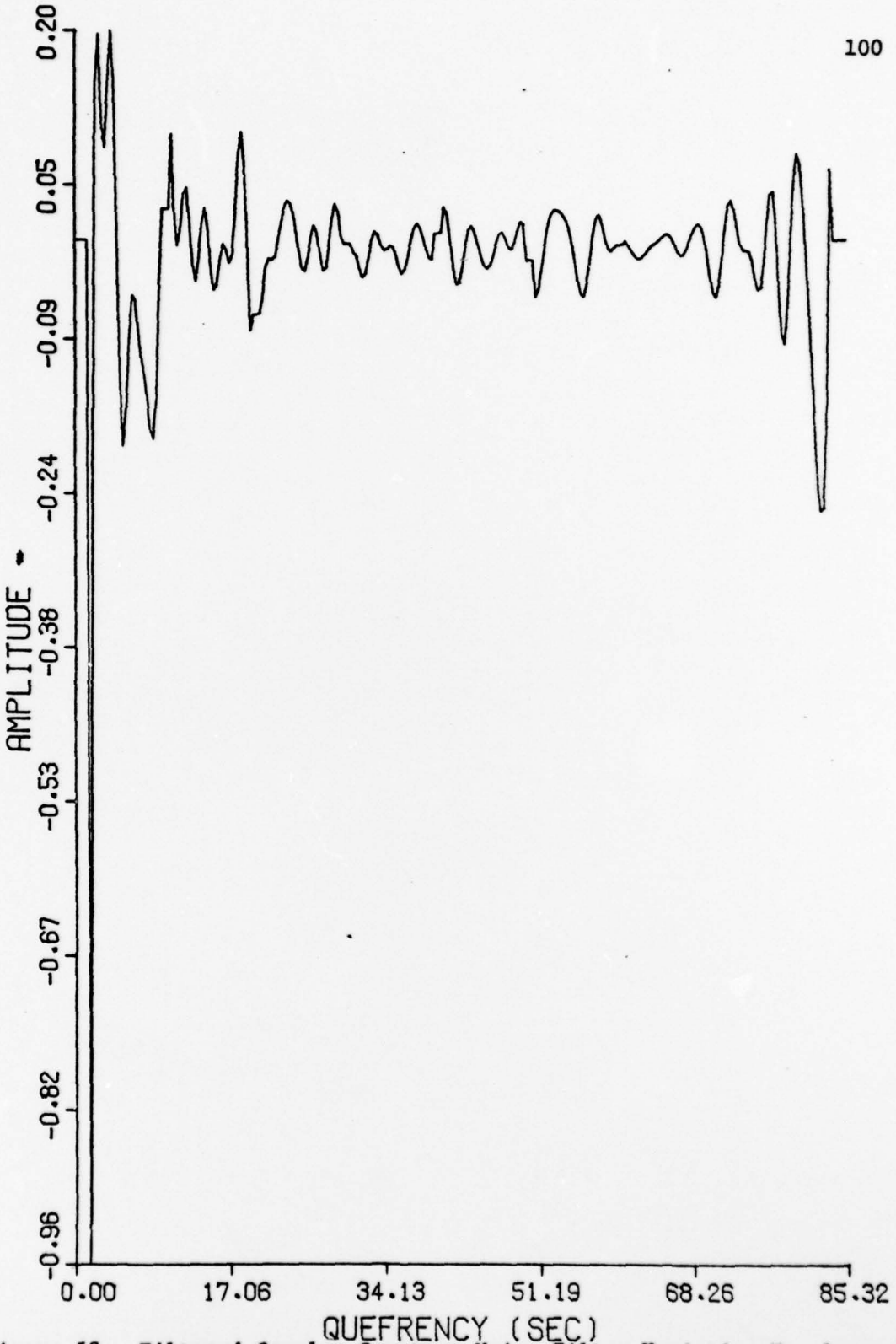

Figure 58. Filtered Complex Cepstrum Using Filter Variation No. 1 on Complex Cepstrum Shown in Figure 54

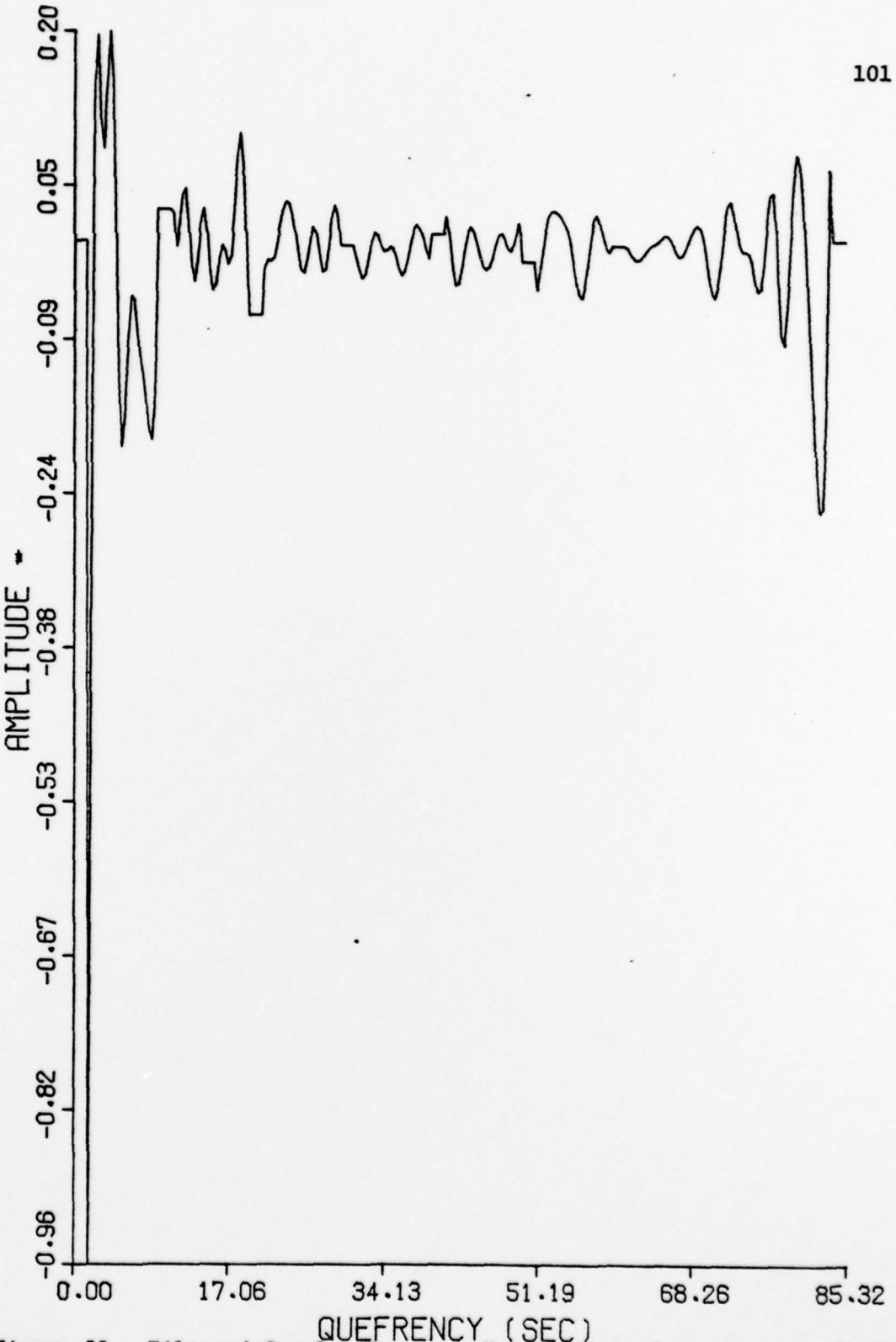

Figure 59. Filtered Complex Cepstrum Using Filter Variation No. 2 on Complex Cepstrum Shown in Figure 54

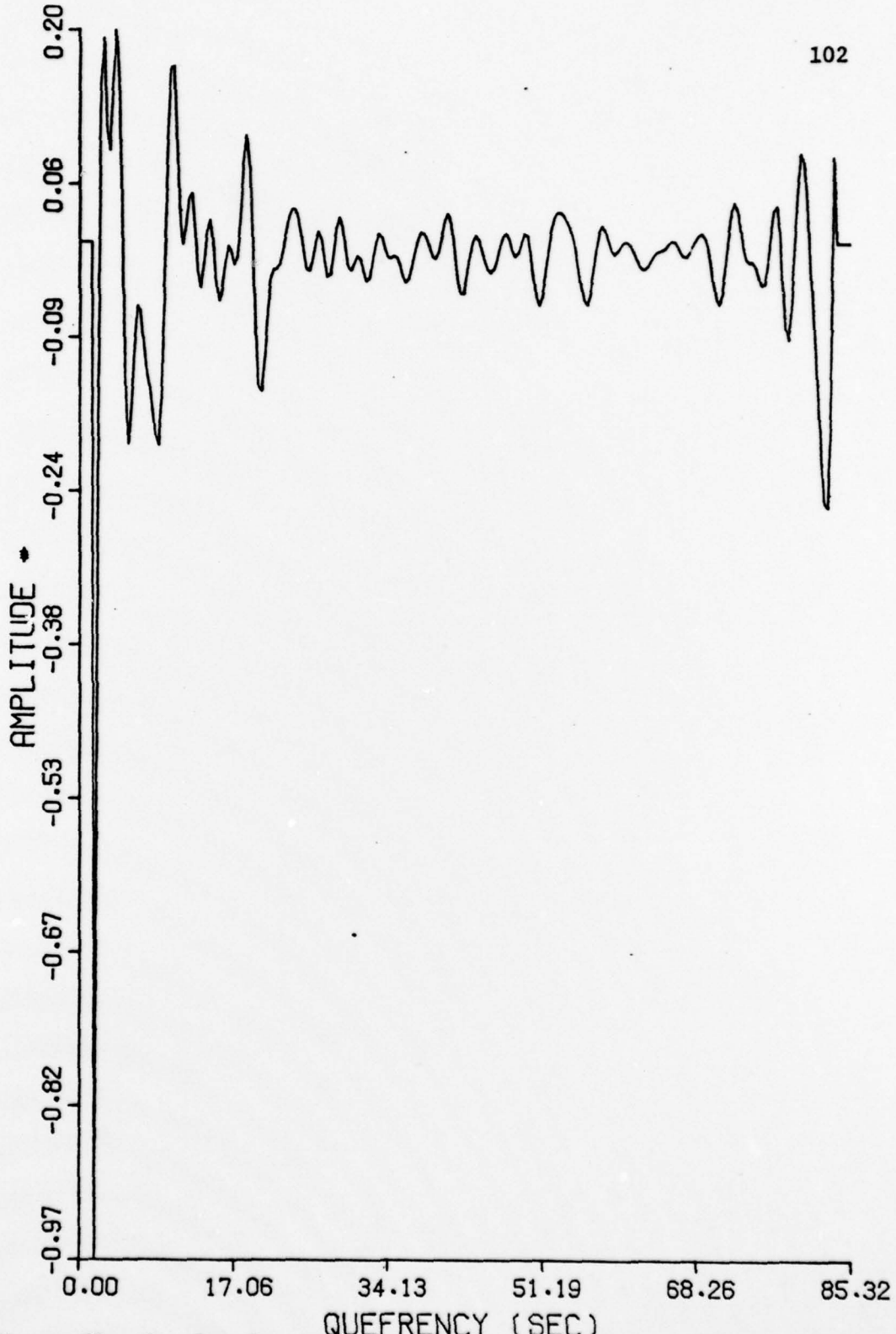

Figure 60. Complex Cepstrum for P-M Generated Wave, τ Varying with Frequency, α Varying from .4 to .6, Δt=.3333

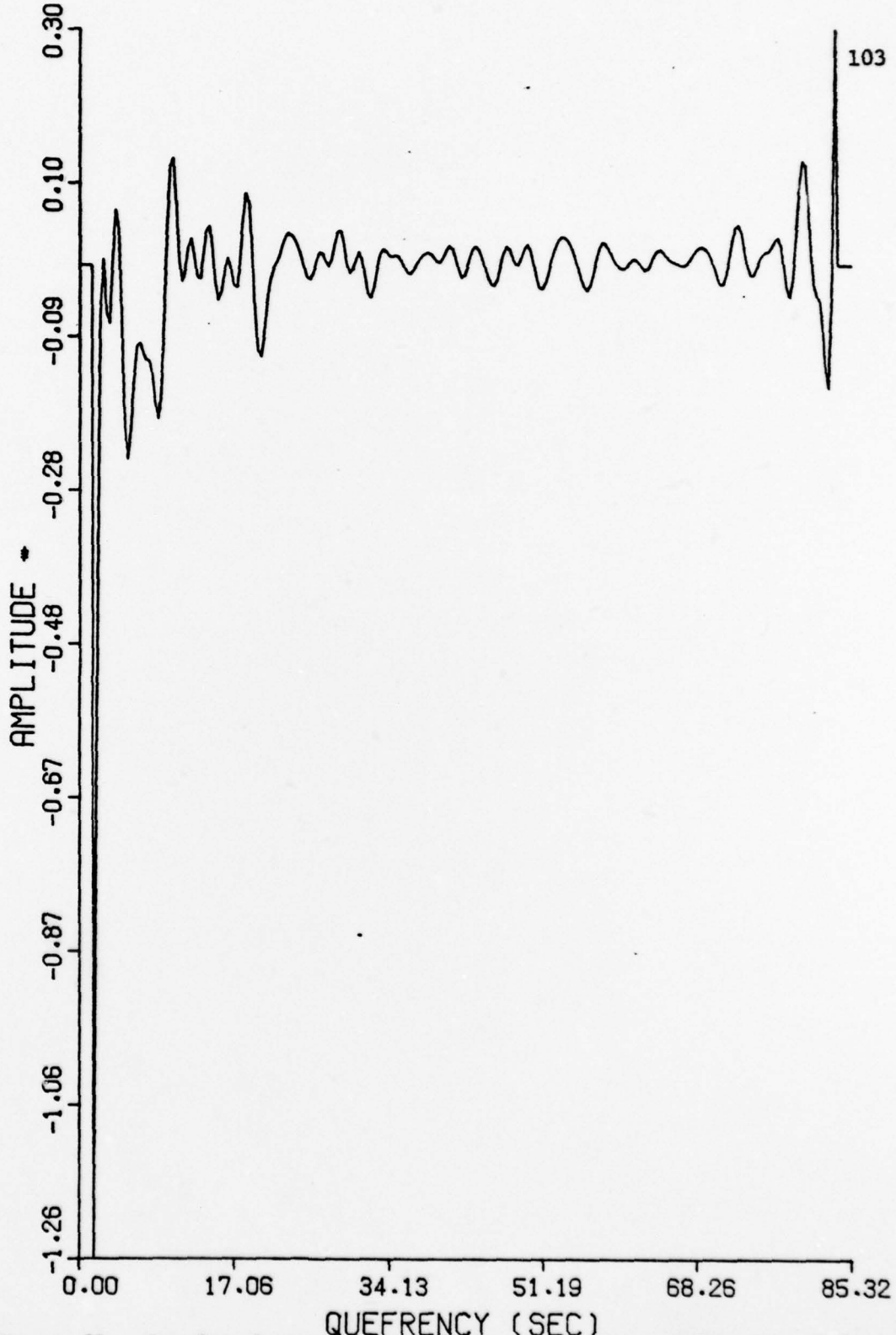

Figure 61. Complex Cepstrum for P-M Generated Wave, τ Varying with Frequency, α Varying from .7 to .9, Δt=.3333

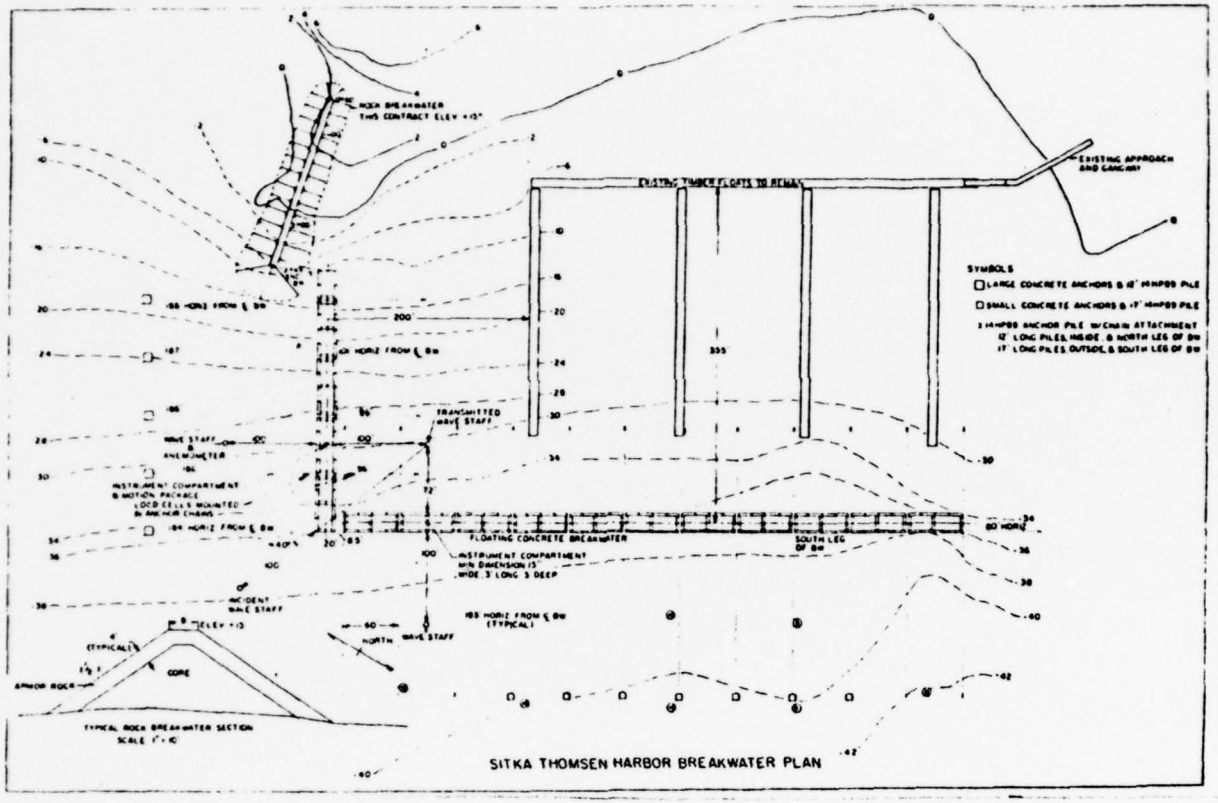

Figure 62. Sitka, Alaska, Breakwater Plan and Instrumentation Layout

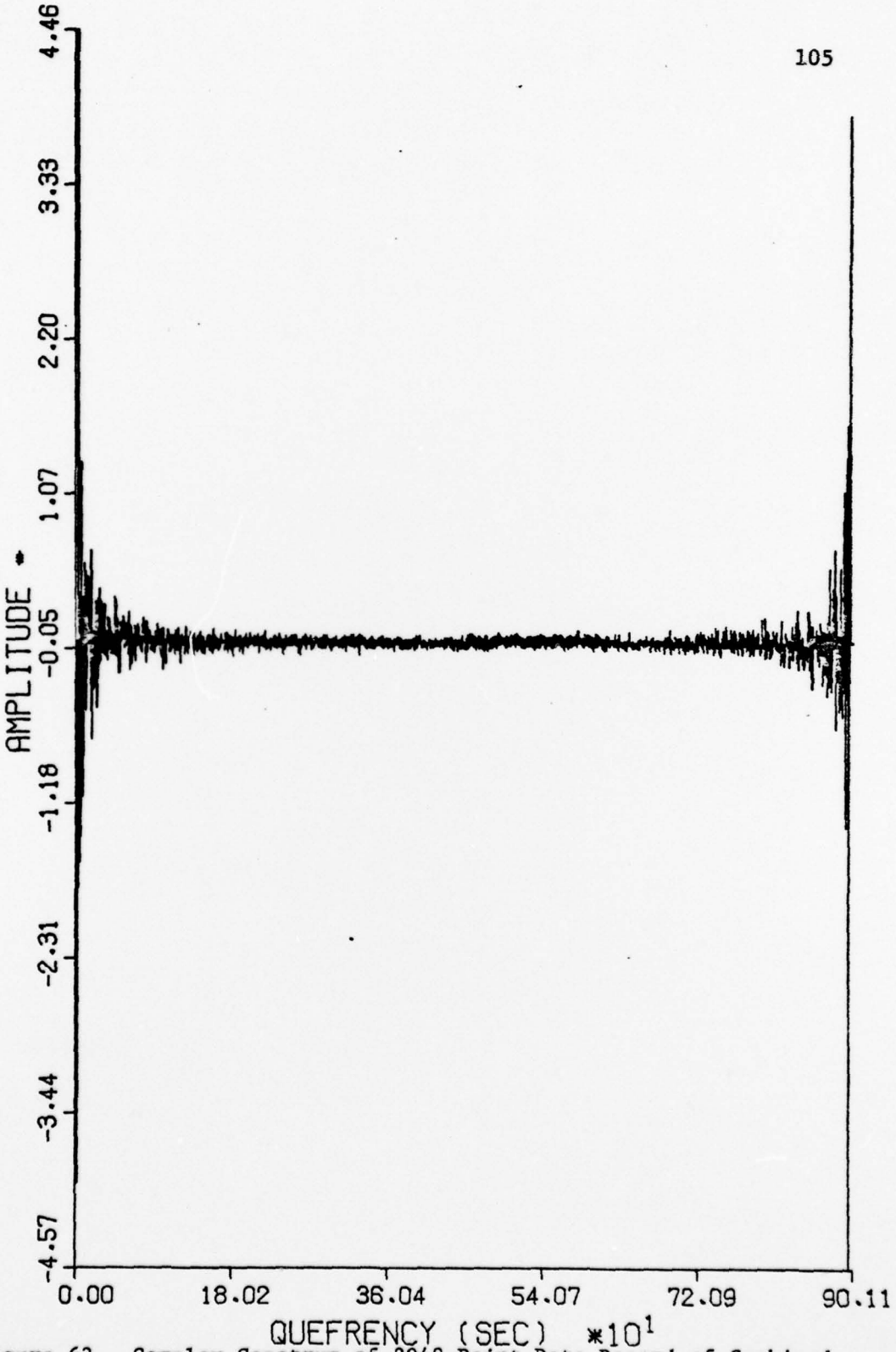

Figure 63. Complex Cepstrum of 2048-Point Data Record of Combined Wave from Sitka Breakwater

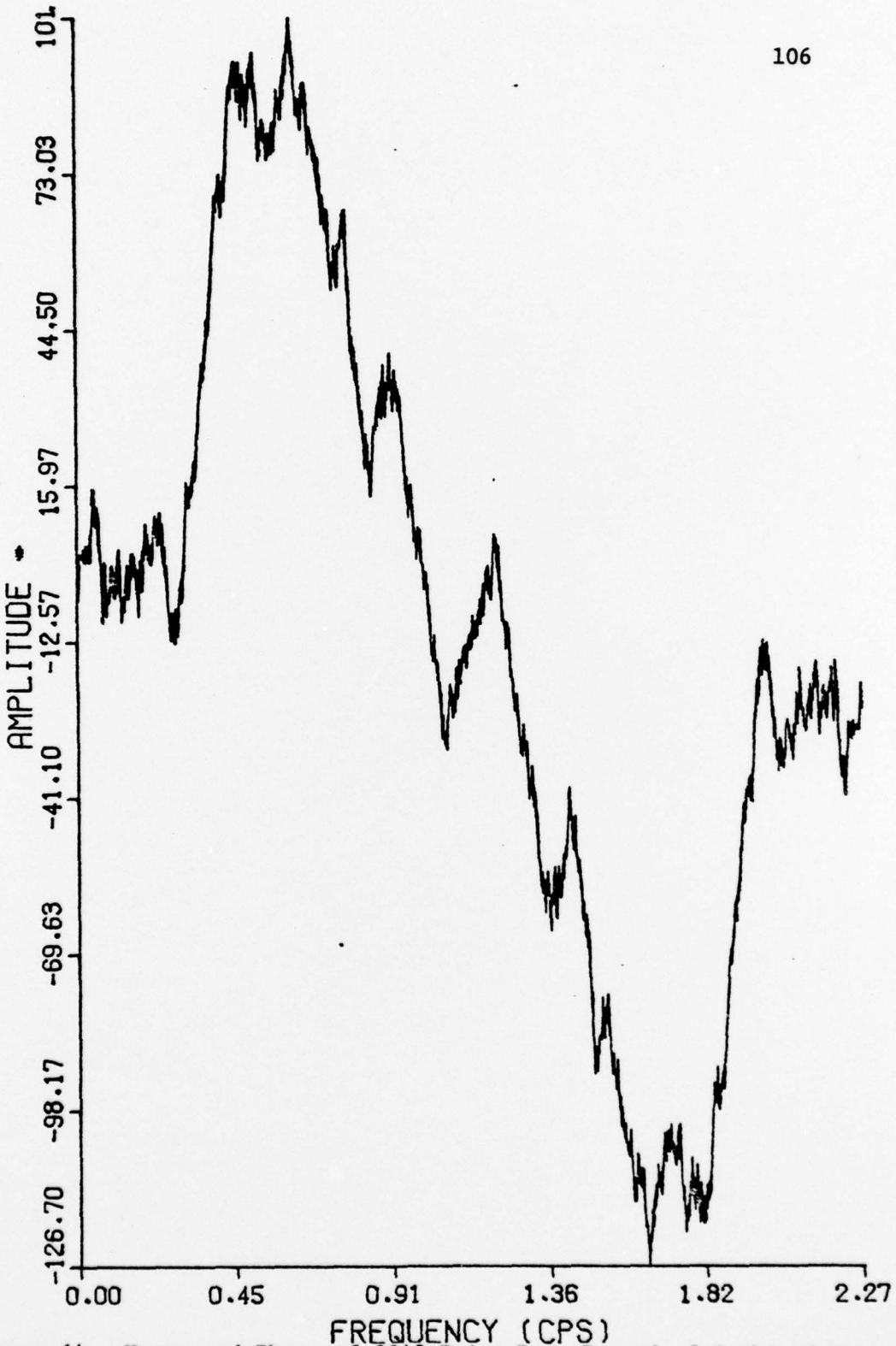

Figure 64. Unwrapped Phase of 2048-Point Data Record of Combined Wave From Sitka Breakwater

Figure 65. Unwrapped Phase with Linear Trend Removed of 2048-Point Data Record of Combined Wave from Sitka Breakwater

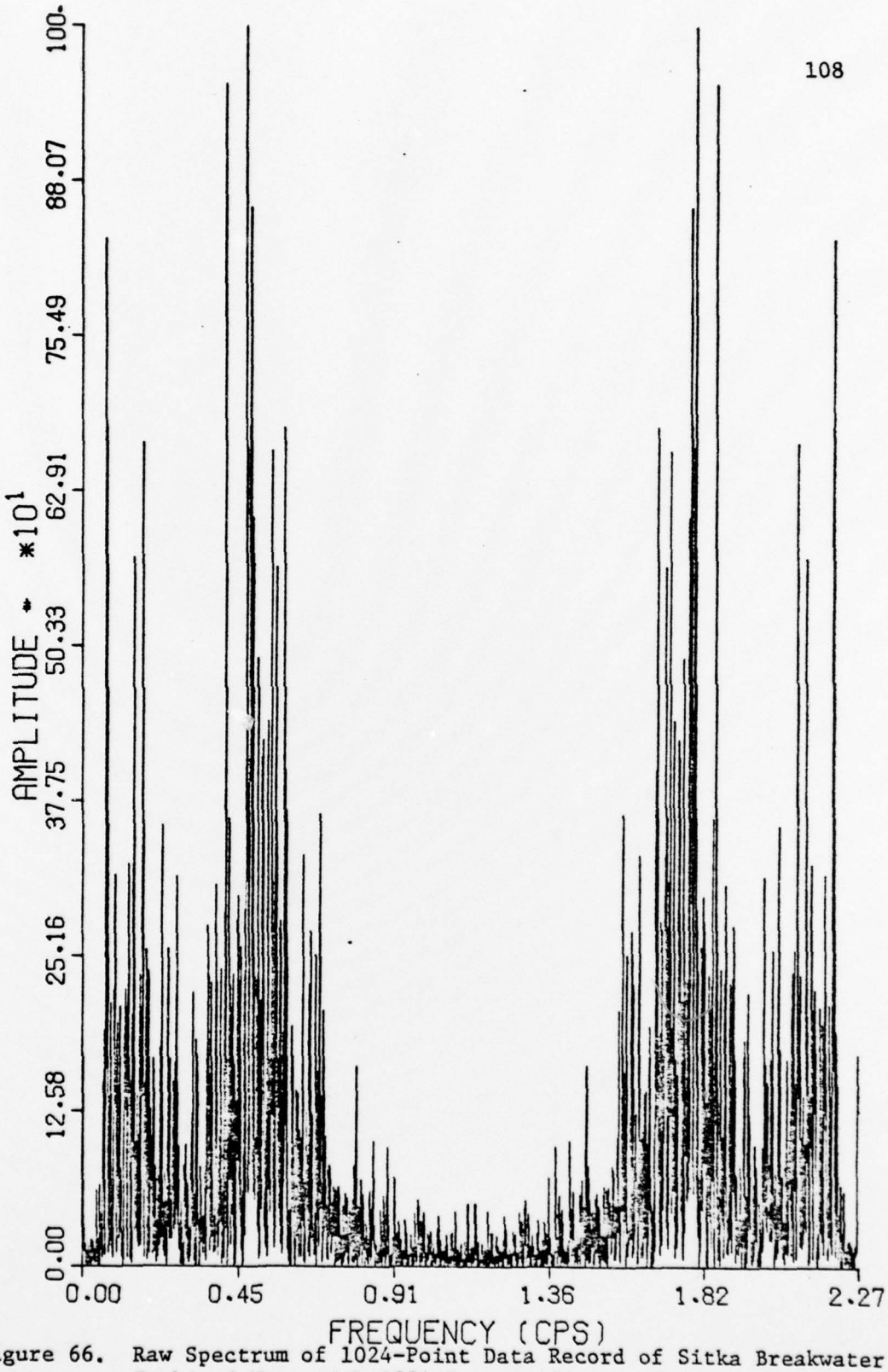

Figure 66. Raw Spectrum of 1024-Point Data Record of Sitka Breakwater Combined Wave with 1024 Zeroes Added to End

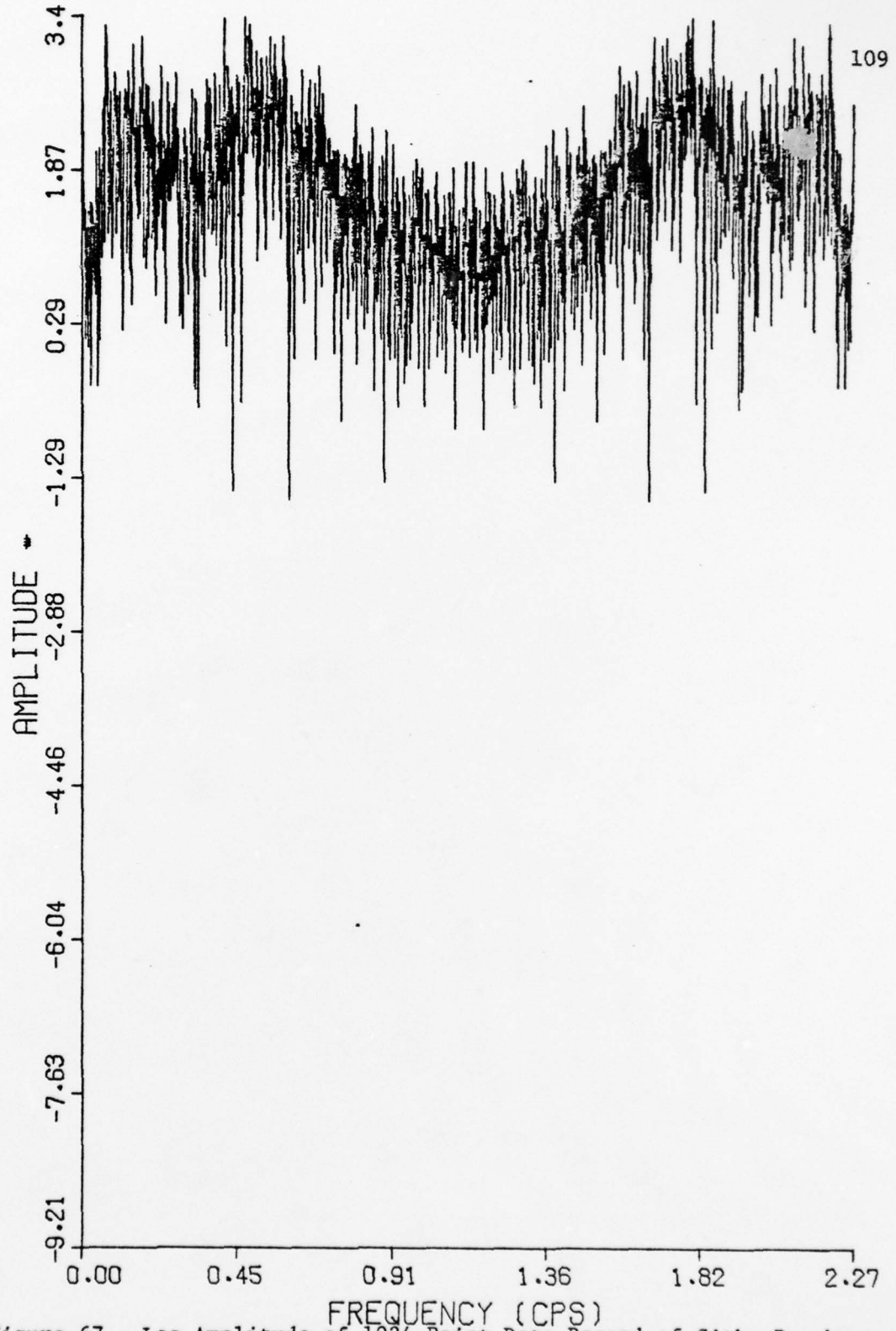

Figure 67. Log Amplitude of 1024-Point Data Record of Sitka Breakwater Combined Wave with 1024 Zeroes Added to End

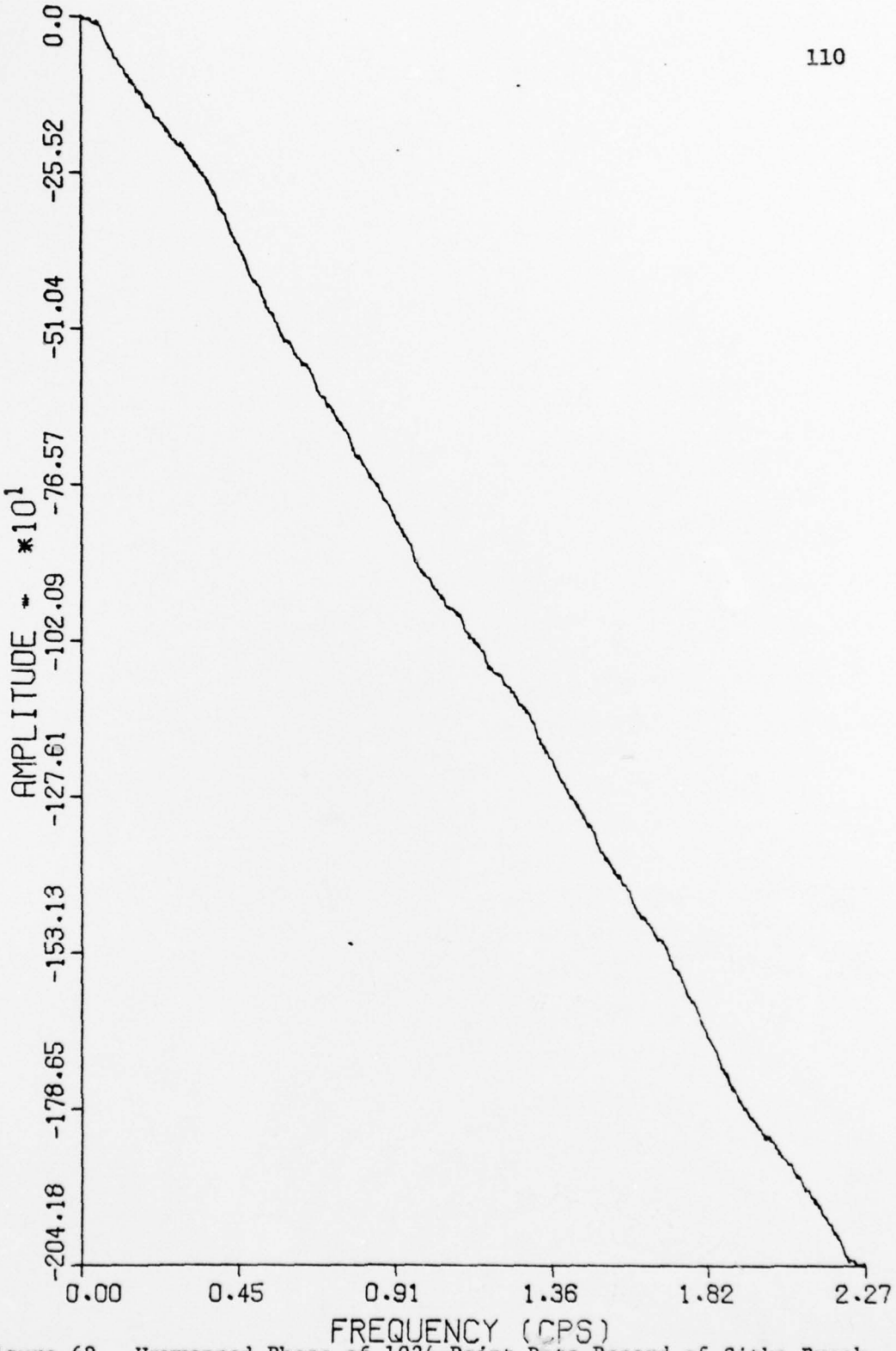

Figure 68. Unwrapped Phase of 1024-Point Data Record of Sitka Breakwater Combined Wave with 1024 Zeroes Added to End

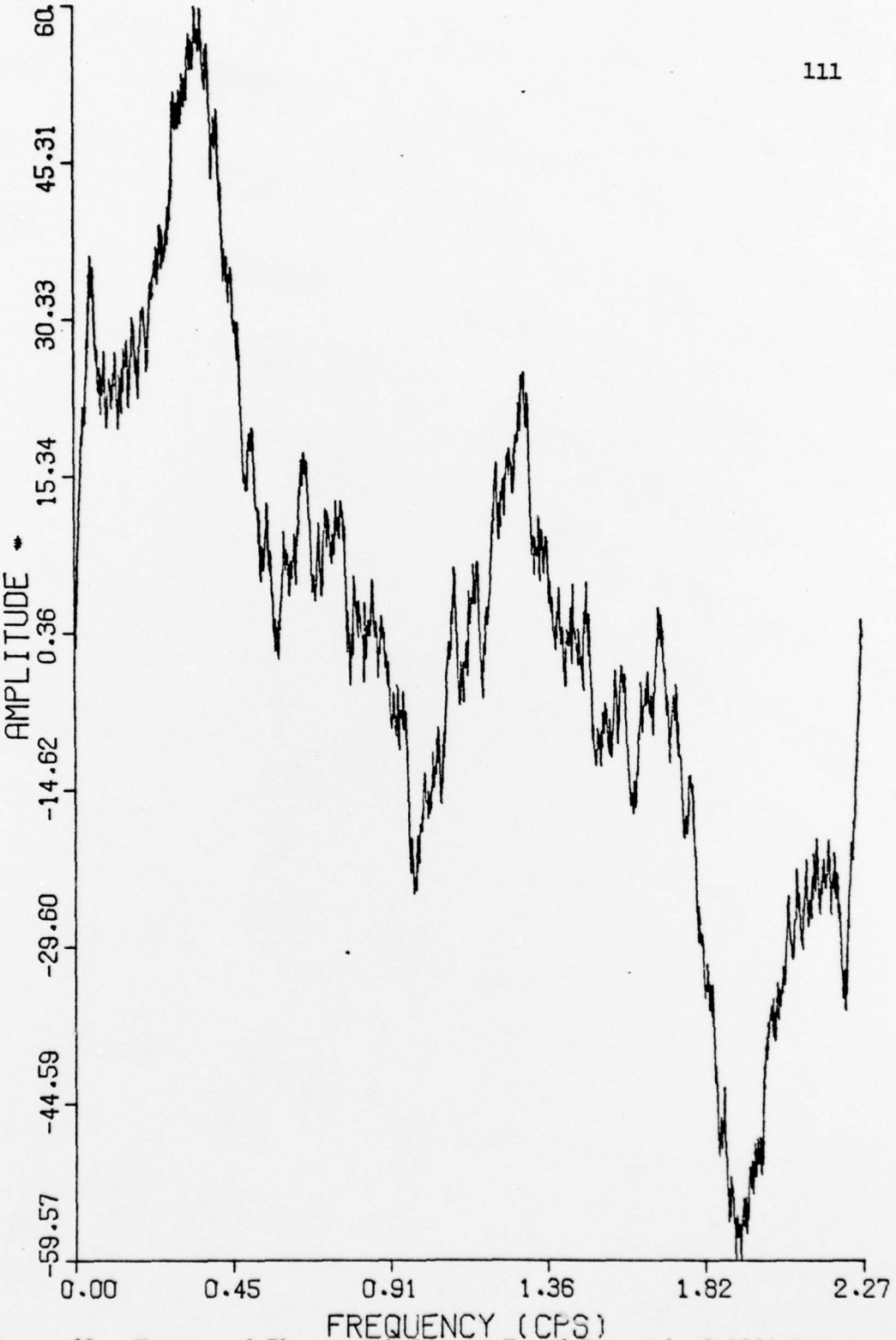

Figure 69. Unwrapped Phase with Linear Trend Removed of 1024-Point Data Record of Sitka Breakwater Combined Wave with 1024 Zeroes Added to End

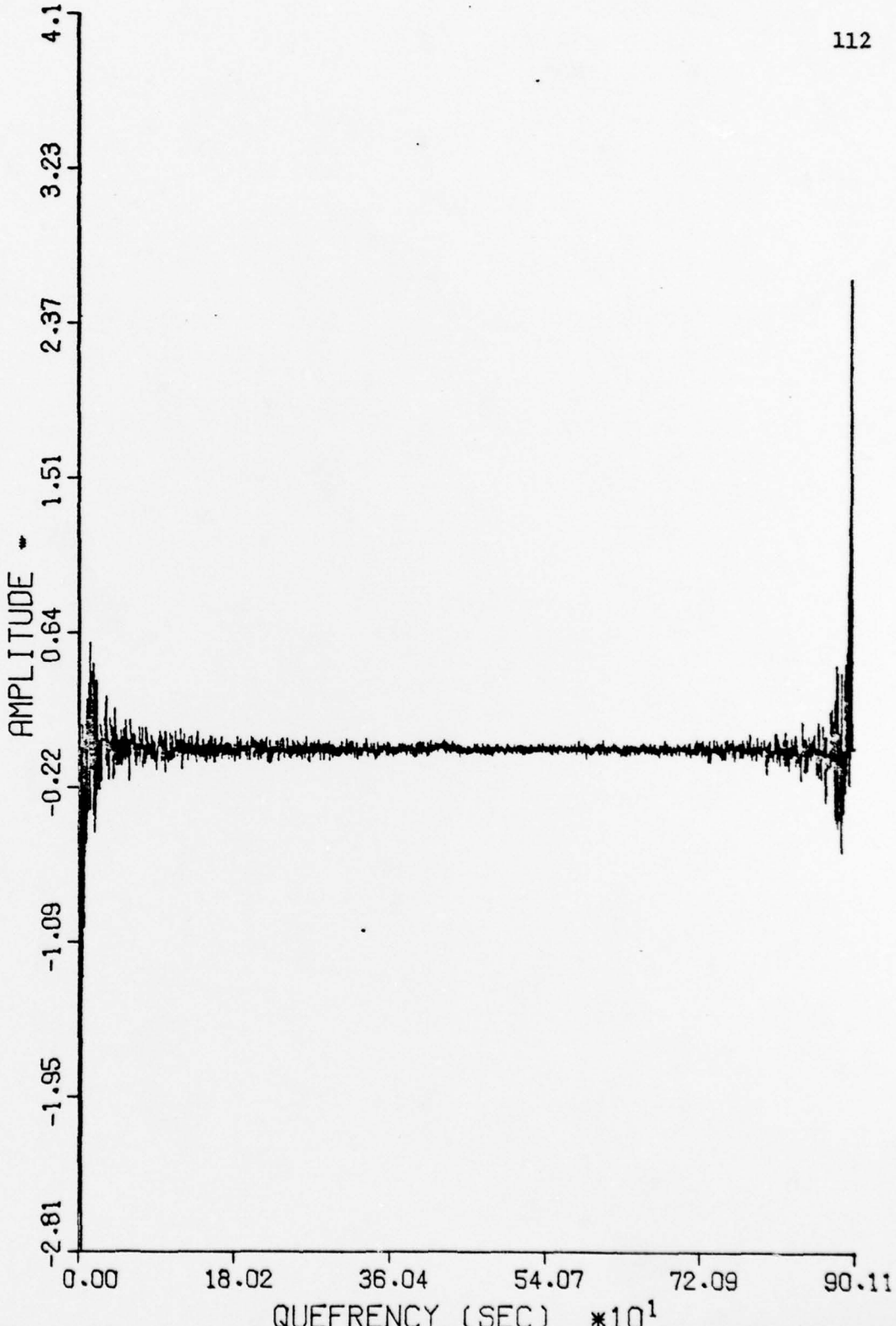

Figure 70. Complex Cepstrum of 1024-Point Data Record of Sitka Breakwater Combined Wave with 1024 Zeroes Added to End

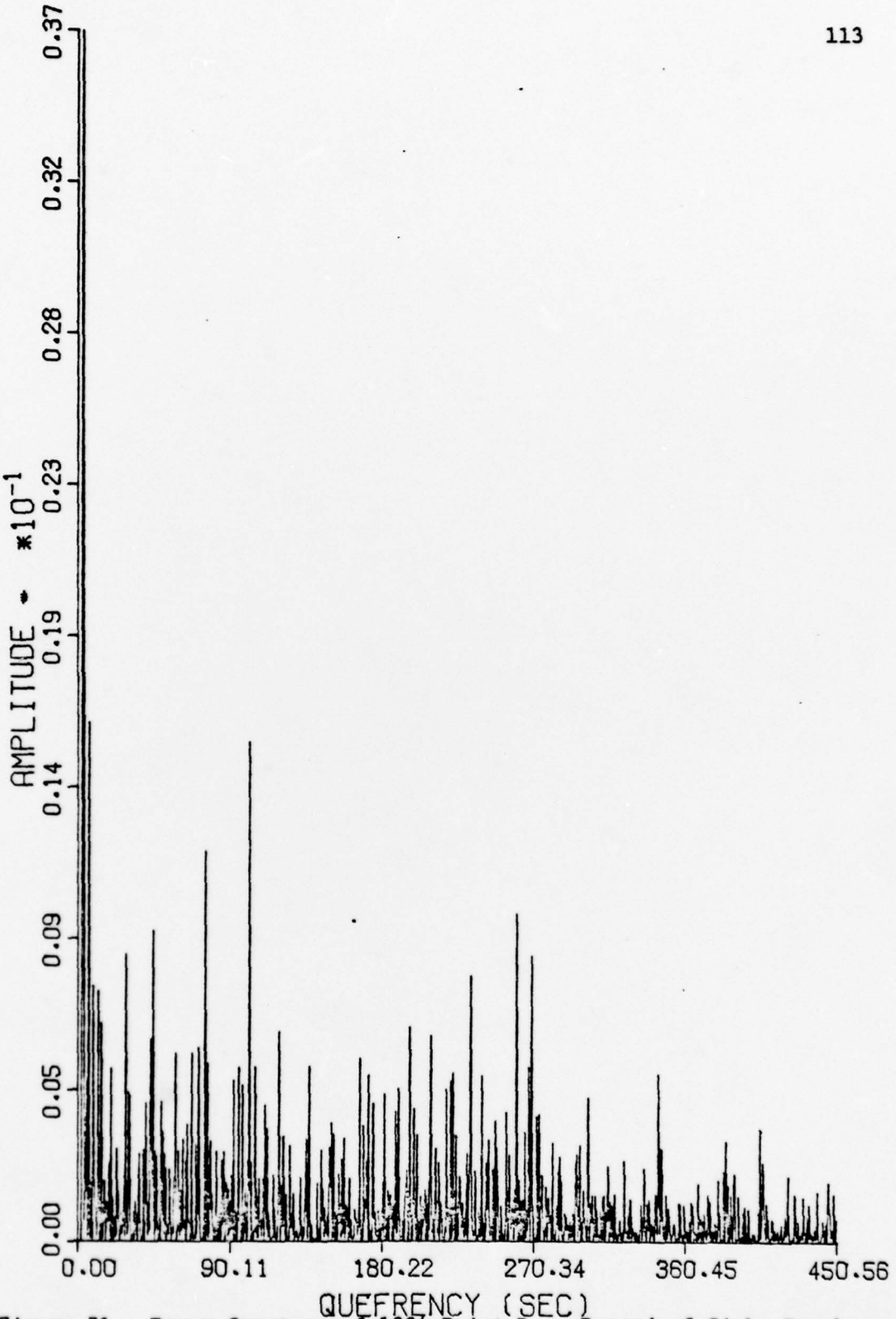

Figure 71. Power Cepstrum of 1024-Point Data Record of Sitka Breakwater Combined Wave with 1024 Zeroes Added to End